UNIVERSITÉ DU QUÉBEC

THÈSE PRÉSENTÉE À
L'UNIVERSITÉ DU QUÉBEC À CHICOUTIMI
COMME EXIGENCE PARTIELLE
DU DOCTORAT EN INGÉNIERIE

Par

Defen Yu

STUDY OF ELECTRIC DISCHARGE AND SPACE CHARGE FORMATION PHENOMENA IN THE AIR GAPS OF AN ICE-COVERED INSULATOR USING AN ICICLE/ICE-COVERED PLATE ELECTRODE SYSTEM

ÉTUDE DES PROCESSUS DES DÉCHARGES ÉLECTRIQUES ET FORMATION DE CHARGES D'ESPACE DANS LES INTERVALLES D'AIR D'UN ISOLATEUR RECOUVERT DE GLACE À L'AIDE D'UNE CONFIGURATION D'ÉLECTRODES GLAÇON/PLAQUE RECOUVERTE DE GLACE

JUNE, 2007

Bibliothèque
Paul-Émile-Boulet

UQAC
Université du Québec
à Chicoutimi

Mise en garde/Advice

Afin de rendre accessible au plus grand nombre le résultat des travaux de recherche menés par ses étudiants gradués et dans l'esprit des règles qui régissent le dépôt et la diffusion des mémoires et thèses produits dans cette Institution, **l'Université du Québec à Chicoutimi (UQAC)** est fière de rendre accessible une version complète et gratuite de cette œuvre.

Motivated by a desire to make the results of its graduate students' research accessible to all, and in accordance with the rules governing the acceptation and diffusion of dissertations and theses in this Institution, the **Université du Québec à Chicoutimi (UQAC)** is proud to make a complete version of this work available at no cost to the reader.

L'auteur conserve néanmoins la propriété du droit d'auteur qui protège ce mémoire ou cette thèse. Ni le mémoire ou la thèse ni des extraits substantiels de ceux-ci ne peuvent être imprimés ou autrement reproduits sans son autorisation.

The author retains ownership of the copyright of this dissertation or thesis. Neither the dissertation or thesis, nor substantial extracts from it, may be printed or otherwise reproduced without the author's permission.

ABSTRACT

In cold climate regions, ice accumulation on insulators decreases their insulating strength, sometimes resulting in flashover faults and the consequent power outages. This problem has been paid great attention by many researchers and a large number of publications and reports have been available. It was found that one of the most common evidence on ice-covered energized insulators is the presence of air gaps along the ice surface due to corona discharge activities.

The corona discharge at the icicle tips in the air gap is the first stage of the flashover process. During these corona discharge activities, a large number of space charges, including the positive and negative ions, are generated and, in turn, they influence the electric field distribution in the air gap and the consequent sequential discharge activities. However, due to its invisible properties and its complexity, the influence of the space discharge on the electric field distribution and on the flashover process is generally ignored in previous studies.

This present thesis aims to study the fundamental and initial processes of electric discharge in the air gap on the ice-covered insulators, within the framework of the NSERC/Hydro-Quebec Industrial Chair on Atmospheric Icing of Power Network Equipment (CIGELE) and the Canada Research Chair on Atmospheric Icing Engineering of Power Network (INGIVRE), at the Université du Québec à Chicoutimi in collaboration with The Key Laboratory of High Voltage Engineering and Electrical New Technology of the Ministry of Education at Chongqing University (CQU). In order to simplify the study, a physical model, an icicle/iced-plate electrode system, is introduced based on numerous previous investigations to simulate the icicle tip and ice-covered insulator surface on real ice-covered insulators. Experimental investigations

are systematically carried out in an artificial climate chamber in the High-Voltage Lab of CQU. Using a measurement system consisting of a ultra-violet camera, CoroCAM IV+, and a special-designed pulse current sensor, the corona discharge characteristics such as the corona inception voltage (V_{inc}), the discharge volume at V_{inc}, the repetition rate of discharge pulses, and the current pulse waveform are investigated in detail under different parameters. These parameters include the gap distance, the environmental temperature, the freezing water conductivity, the atmospheric pressure and the voltage polarities as well as the voltage types. Subsequently, the statistic analysis is applied to the experimental results and the influence of these parameters on the discharge current pulse characteristics is determined.

In order to reveal the physical mechanism underlying the corona discharge and determine the influence of space charge on the consequent discharge processes, a dynamic physics process of space charge is proposed to analyze this discharge phenomenon. A mathematical model is established to simulate the drift and diffusion process of the space charge clouds. From this model, the critical time of space charge clouds are calculated and are validated with the experimental results. Finally, the possible influences of space charge on the flashover of iced-covered insulators are analyzed and discussed.

The study results give a better understanding of the corona discharge at the tip of icicles on the ice-covered insulators. However, due to the time limitation and the complexity of this phenomenon, further studies are necessary to complete the model and theory. Several recommendations are proposed for future studies.

RÉSUMÉ

Dans les régions au climat froid, les accumulations de glace sur les isolateurs diminuent leur performance électrique, résultant parfois en contournements et pannes d'électricité. Ce problème a attiré l'attention de nombreux chercheurs et a amené à la publication de nombreux articles et rapports. On a découvert que l'un des signes les plus courants associés aux isolateurs recouverts de givre est la présence d'intervalles d'air le long de la surface de glace, causés par l'activité des décharges couronne.

La décharge couronne à la pointe des glaçons dans l'intervalle d'air est la première étape du processus de contournement. Durant ces activités de décharges de couronne, un grand nombre de charges d'espace, incluant les ions positifs et négatifs, sont générés, ce qui influence la distribution du champ électrique dans les intervalles d'air ainsi que les activités de décharges séquentielles conséquentes. Cependant, dû aux propriétés invisibles et à la complexité des décharges d'espace, son influence sur la distribution du champ électrique et sur le processus de contournement a été généralement ignorée dans les études antérieures.

Cette thèse de doctorat vise à étudier les processus fondamentaux et initiaux des décharges électriques dans les intervalles d'air des isolateurs recouverts de givre. Ce travail a été effectué dans le cadre des activités de la Chaire industrielle NSERC/Hydro-Québec/UQAC sur le givrage atmosphériques des équipements des réseaux électriques (CIGELE) et de la Chaire du Canada sur l'ingénierie du givrage des réseaux électriques (INGIVRE) à l'Université du Québec à Chicoutimi, en collaboration avec le Key Laboratory of High Voltage Engineering and Electrical New Technology of the Ministry of Education à l'Université de Chongqing. Dans le but de simplifier l'étude, un modèle physique, un système d'électrode recouvert de glace, a été conçu sur la base de nombreuses investigations antérieures pour simuler la pointe des glaçons et la surface glacée d'isolateurs réels recouverts de glace. À cette fin, des tests systématiques ont été

effectués dans une chambre climatique du laboratoires de haute tension de l'Université de Chongqing. Utilisant un système d'acquisition de données consistant en une caméra à ultraviolets CoroCam IV^{+} et un détecteur de pulsations de courant spécialement conçu à cette fin, les caractéristiques des décharges de couronne tel que la tension de seuil de la décharge couronne, le volume d'apparition de couronne, le taux de répétition des impulsions de décharge et de variation du courant ont été analysés en détail selon différents paramètres. Ces paramètres incluent les intervalles d'air, la température ambiante, la conductibilité de l'eau de congélation, la pression atmosphérique et la polarité du voltage ainsi que les types de voltages. Par la suite, les résultats expérimentaux ont été soumis à l'analyse statistique et l'influence de ces paramètres sur les caractéristiques des pulsations de décharge a été déterminée.

Dans le but de mettre en lumière le mécanisme physique sous-jacent les décharges couronne et de déterminer l'influence des charges d'espace sur les processus de décharge induits, un modèle physique de charges d'espace dynamique a été proposé pour analyser le phénomène de décharge. Un modèle mathématique a été élaboré pour simuler le processus de dérivation et de diffusion des nuages de charge d'espace. Ce modèle permet de calculer et de valider le temps critique des charges d'espace. Finalement, les influences possibles des charges d'espace sur le contournement des isolateurs recouverts de glace sont discutées.

Les résultats de l'étude donnent une meilleure compréhension des décharges de couronne à la poine des glaçons accumulés sur les isolateurs recouverts de glace. Cependant, dû à la limite de temps et à la complexité de ce phénomène, des études plus approfondies seront nécessaires pour compléter le modèle et la théorie. Plusieurs recommandations ont été proposées pour de futures études.

ACKNOWLEDGEMENTS

This work was carried out within the framework of the NSERC/Hydro-Québec/UQAC Industrial Chair on Atmospheric Icing of Power Network Equipment (CIGELE) at the University of Québec in Chicoutimi, in collaboration with Chongqing University, P.R.China.

I would like to take this opportunity to express my appreciation to those who helped me complete this thesis through their technical and moral support.

First, I would like to express my deepest gratitude to my director, Professor Masoud Farzaneh, for his supervision, support, patience and confidence during my PhD project; and my co-director, Prof. Caixun Sun, for precious discussions and guidance during tests in China.

I want to express my gratitude and respect to Dr. J.Zhang, not only for his scientific but also his human qualities. I am especially thankful to him for his sincere and unstinting support, which were essential in realizing this project.

I am also grateful to Prof. I. Fofana, and Dr. J.Li for the valuable advice and worthwhile discussions and help. In addition, I should also remember some Chinese friends such as Prof. H. Lu, Dr P.Fu etc. for their support and encouragement in getting through the difficult times.

Finally, I would like to thank my parents for their constant moral support and all the energy they put into my education, which enabled me to get to the point where I am today. I would like to express my especial appreciation to my wife Ms Bai Xue, for her eternal love and understanding during my past four years' study in Canada.

TABLE OF THE CONTENT

LIST OF FIGURES

LIST OF TABLES

DEFINITION OF TERMS

Arc: A continuous luminous discharge of electricity across an insulation medium, usually accompanied by the partial discharge volatilization of the electrodes, or a discharge of electricity through a gas, normally characterized by a voltage drop in the immediate vicinity of the cathode approximately equal to the ionization potential of the gas.

Background Noise: The total of all sources of interference in a system used for the production, detection, measurement, or recording of a signal, independent of the presence of the signal.

Breakdown: the abrupt transition of the gap resistance from a practically infinite value to a relatively low value.

Corona (Air): A luminous discharge due to ionization of the surrounding a conductor caused by a voltage gradient exceeding a certain critical value.

Corona Inception Voltage (CIV): The lowest voltage at which continuous corona of specified pulse amplitude occurs at the applied voltage is gradually increased. Where the applied voltage is sinusoidal, the CIV is expressed as $1/\sqrt{2}$ of the peak voltage.

Corona Pulse: A voltage or current pulse which occurs as some designated location in a circuit as a result of corona discharge.

Electric field strength: At a given point in space, the ration of force on a positive test charge placed at the point to the magnitude of the test charge, in the limit that the

magnitude of the test charge goes to zero. The electric field strength at a point in space is a vector defined by its components along three orthogonal axes.

Flashover: A disruptive discharge through air around or over the surface of solid or liquid insulation, between parts of different potential or polarity, produced by the application of voltage wherein the breakdown path becomes sufficiently ionized to maintain an electric arc.

Glow Discharge: a discharge of electricity through gas characterized by: a change of space potential, in the immediate vicinity of the cathode, that is much higher than the ionization potential of the gas; a low, approximately constant, current density at the cathode, and a low cathode temperature.

Leakage Current: The total detector current flowing at the operating bias in the absence of radiation.

Partial Discharge (PD): An electric discharge which only partially bridges the insulation between conductors, and which may or may not occur adjacent to a conductor.

Space Charge: A net excess of charge of one sign distributed throughout a specified volume.

Test Object: an encapsulated stand-alone, executable test procedure.

LIST OF ABBREVIATIONS AND SYMBOLS

AC	Alternating current
CIGELE	NSERC/Hydro-Québec/UQAC Chair on Atmospheric Icing of Power Network Equipment
CQU	Chongqing University
D	Ddiffusion Coefficient of ions
D_T	Diffusion coefficient of ions in horizontal direction
D_L	Diffusion coefficient of ions in vertical direction
DC	Direct current
DC+	Positive DC voltage
DC-	Negative DC voltage
E	Electric field strength [kV/m]
E_{app}	Electric field strength from applied voltage
E_s	Electric field strength from space charge
E_{re}	Electric field strength of re-inception
E_{mean}	The mean Electric field strength in the air gap system
E_{max}	The maximum Electric field strength in the air gap system
E_{arc}	Voltage gradient along arc
E_{ws}	The maximum withstand strength

E_{cr}	The critical electric field strength of corona discharge
F	The form factor of gap space,
HV	High voltage
K	Boltzmann constant
N	Air density
NaCl	Sodium Chloride
P_0	Standard atmospheric pressure
P	Atmospheric pressure
Q	Corona discharge magnitude (pC)
S_{in}	The inner curve surface of critical volume
S_{out}	The outer curve surface of critical volume
T	Temperature (°C)
UQAC	University of Québec at Chicoutimi,
V_{arc}	Voltage drop along arc
V_{inc}	Corona inception voltage (kV)
V_{app}	Applied voltage
V_0	Corona inception voltage at standard atmospheric pressure
X	The boundary of critical volume
d	Air gap distance (cm)
d_c	The distance in radial direction from the central axis of corona channel

d_r	Distance between point and electrode tip along radial direction
e	Electronic charge
k	Mobility of ions
k^+	Mobility of positive ions
k_m	Effect parameter of atmospheric pressure on V_{inc}
m	The mass of the particle
n	Ion density
r	The radius of the space charge cloud
t	Time
t_c	Critical time interval
ρ	Distance of space charge sphere away from icicle electrode
x_c	Critical arc length
x	The length of the avalanche
Δt	Time interval of discharge pulse
δV	Ripple factor
α	First Townsend coefficient
η	The ionization efficiency
v	Drift velocity of ions
ε	Permittivity of free space
μ_1	The expectant value of discharge magnitude for the first peak
μ_2	The expectant value of discharge magnitude for the second peak

σ^2	Variances of discharge magnitude
σ	Freezing water conductivity
δ	Standard deviation

LIST OF PAPERS PUBLISHED FROM THIS PH.D THESIS WORK

[1]. M. Farzaneh, D. Yu, J. Zhang, L.Shu, W.Sima, and C.Sun. "Measurement of Corona Discharge in an Icicle/Iced-Plate Electrode System under Positive DC Voltage". ISH-2005, Aug.24-28, pp.D-05, Beijing.

[2]. Defen Yu, Jianhui Zhang, Masoud Farzaneh, Wenxia Sima, Lichun Shu, and Caixin Sun. "Analysis of DC positive corona discharge characteristics using an icicle to iced plate electrode system", April, 2-5 Seoul South Korea, CMD-2006.

[3]. M.Farzaneh, J.Zhang, D.Yu, C.Sun, W.Sima and L.Shu, "Characteristics of Corona Discharge in an Icicle /Iced-Plat Electrode System under Negative DC- Voltage", Jun. 26-30, Bali, Indonesia, ICPADM 2006.

[4]. D. Yu, M. Farzaneh, J. Zhang, L. Shu, W. Sima and C. Sun, "Properties of Corona Discharge under Positive DC Voltage at Low Atmospheric Pressure", CEIDP 2006 Annual Report Conference on Electrical Insulation and Dielectric Phenomena, October 2006, pp. 393-396, Kansas City, USA.

[5]. D. Yu, M.farzaneh, J.Zhang, L. Shu, W. Sima, and C. Sun, "Comparison of corona discharge characteristics of icicle/iced-plate electrode system between positive and negative DC voltage", Accepted by ISH-2007

[6]. W. Sima, J. Feng, D. Yu, J. Zhang, Q. Yang, X. Lai and M. Farzaneh, "DC Corona Discharge Test and Measurement in an Icicle to Iced-Plate Air Gas System", High Voltage Engineering of China, June 2006, vol. 32, No. 5, pp.1-3,34.

[7]. X. Lai, L. Shu, X. Jiang, D. Yu, J. Zhang and M. Farzaneh, "Investigation of the Characteristics of DC positive Corona Discharge in an Icicle/iced-plate Air Gap", Power System Technology of China. Vol.40, No.7, pp32-36, April, 2006.

[8]. W. Sima, J. Feng, Q. Yang, X. Lai, D. Yu., M. Faezaneh, J. Zhang, "The properties of Positive DC Corona Discharge in Iced Electrode System under Low Atmospheric Pressure", Accepted by Chinese Society of Electrical Engineers (In press).

[9]. D. Yu, M. Farzaneh, J. Zhang, L. Shu, W. Sima, and C. Sun, "Study to Effect of Space Charge on Discharge Process of Positive DC Icicle/Iced-Plate Electrode Air Gap", IEEE Transactions on Dielectrics and Electrical Insulation, Special Issue on Ice-Covered Insulators, Dec 2006 (accepted for publication)

CHAPTER 1

INTRODUCTION

CHAPTER 1

INTRODUCTION

1.1 INTRODUCTION

Continuous supply with electric power has become one of the major foundations of industrialized societies. Various technologies of modern life, such as communication, transportation, heating, cooking, health care etc., rely solely on electricity in order to work, and any outage will often cause major problems.

The first public power station was put into service in 1882 in London. Soon, a number of other public supplies for electricity followed in other developed countries. The early systems produced direct current at low-voltage, but their service was used mainly for electric lighting from Deptford to central London over 28 miles at 10kV. By 1890, the art in the development of an AC generator and transformer had been perfected to the point at which AC supply was becoming common, displacing the earlier DC system. From the earliest days of electricity it was realized that, to make full use of economic generation, the transmission network must be tailored to production with increased interconnection for pooling of generation in the integrated system. In addition, the development of hydroelectric power needs to carry that power over long distances to the centers of

consumption were recognized, which makes the insulation components in electrical equipments, in particular various insulators, play an increasingly important role in the operation of power systems.

Insulators are the devices which are used in power networks to support, separate or contain conductors at high voltage. They function to electrically separate and mechanically connect two conductors with different electric potentials. Normally, most insulators are used on high-voltage overhead transmission lines and substations. They are called outdoor insulators and required to withstand extreme changes in environmental conditions, and their properties directly determine the safety of power systems.

1.2 DEFINITION OF PROBLEM

In the cold-climate regions of the world, during the winter, overhead transmission lines and their substations are subjected to atmospheric ice and snow accretion, both of which may cause mechanical damage or electrical failures to power systems.

Mechanical damage is caused by external load to the towers, transmission lines and substation hardware which are too heavily loaded to collapse the lines with dramatic consequences. The second is a change in the insulators' performance that sometimes may result in flashover faults and the consequent power outages. Both of them cause trouble in national economic and daily life [1] [2] [3] [4]. Such events have been reported by many authors in various countries such as Canada [5] [6] [7] [8], the United States [9] [10] [11], Japan [12], Norway [13], China [14], England [15] and Finland [16].

A typical example of insulator flashover incidents in Canada occurred on March 9-10, 1986, within the Ontario Hydro network [8]. Due to freezing rain and fog, the surface of the insulators accumulated ice and short icicles, which resulted in 57 successive flashovers. Of these, 27 involved transmission line insulators local to the area just west of Toronto. Most of the 500 kV transmission systems in southern Ontario were collapsed in this incident. Another example of flashover events took place on April 18, 1988, at the Arnaud substation in the Hydro-Québec network [7]. A series of six flashovers, caused by insulators covered with wet snow, resulted in a major power interruption for a large part of the province of Québec.

This problem has motivated researchers to investigate this phenomenon, and numerous studies have been carried out for over 30 years [1-16]. It has been found that one of the most evident phenomena is the frequent existence of air gaps with adjoining icicles near the HV terminal of energized insulator strings [2][7][8], due to the corona discharge activities at the tip of icicles around the electrodes.

Concerning ice distribution along insulators, it should be noted that in general, during icing events, only the windward face of the insulator is covered with ice and icicles [2][3], while the opposite side is free of ice. In addition, the ice accretion along the insulator's surface is not uniform, as several parts are ice free; these areas are referred to as air gaps due to the heating effect of corona discharge activity, increase in air temperature, or ice shedding.

The existence of air gaps will inevitably distort electrical field distribution around the insulators and cause a significant voltage drop across the gaps [17] [18] as shown in

Figure 1-1, and non-uniform electrical field distribution along the ice-covered insulators. Electrical field stress at the icicle tips is even stronger. If the electric field stress in these areas is high enough, the corona discharges will be initiated. This can lead to the formation of local arcs across the air gaps causing a substantial increase in leakage current and a concomitant melting of ice. The discharge activity in these areas is shown in Figure 1-2 as an example, which causes a substantial increase in leakage current and melting of the ice.

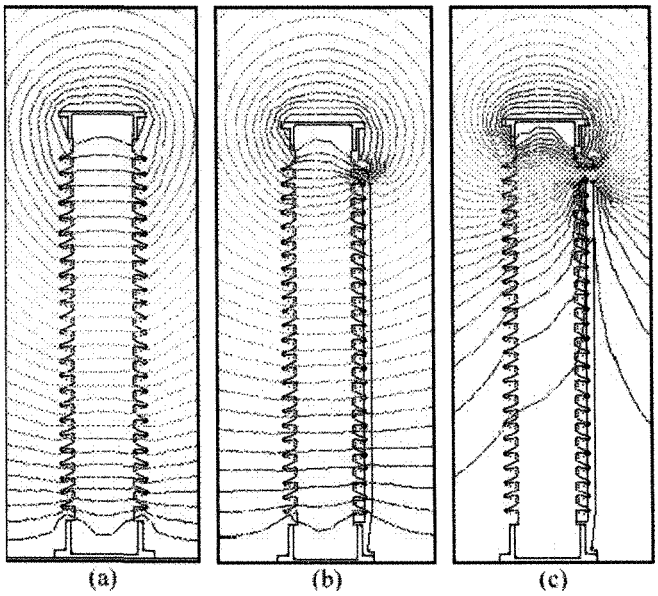

(a) Clean insulator, (b) Insulator with dry ice having an upper air gap,

(c) Insulator with ice having water film and a upper air gap

Figure 1-1 Electric field distribution around ice-covered insulators

The flashover process consists of several stages [3], including the accretion of ice, the formation of air gaps, the inception of corona discharges at icicle tips, the formation of

local arcs across the air gaps, the development of local arcs along the ice surface, and the final flashover. Therefore, the flashover on the ice-covered insulators is a very complex phenomenon [19] which is influenced by many factors, such as the distribution of the electric field, the state of the ice surface, the characteristics of the air gaps, the environmental conditions and the insulator geometry.

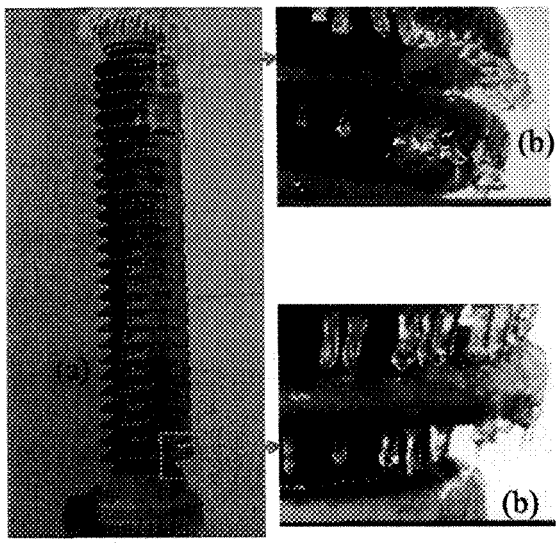

(a). Ice-covered post-station insulator with air gaps;

(b). Inception of corona discharge along the air gaps.

Figure 1-2 Corona discharges along the air gap

Although numerous investigations of the discharge activities on the ice-covered insulators have been carried out, so far very few investigations on the corona occurring from icicles can be found. The spectrum of corona discharge falls mainly within the ultra-violet spectral range, i.e. the light wavelength λ=280-400 nm. Because this type of

discharge is too difficult to be observed with the naked eye, so this discharge is not yet completely understood and its influence on the electric field distribution and consequent flashover process on the ice-covered insulators is ignored too.

The occurrence of corona discharges at icicle tips is the first stage of the flashover process, and will produce a large quantity of space charges around the icicles [8, 9]. In turn, these space charges will affect the electrical field distribution around the icicles, and consequently affect the successive discharge activities as well as their development [20] [84]. Therefore, the corona discharges at icicle tips play an important role in the formation of the initial arcs and even in the flashover process.

A more thorough review of previous studies is presented in Chapter 2 of this thesis.

1.3 RESEARCH OBJECTIVES

In order to advance our understanding of corona discharge at the icicle tip, this research will propose a simplified icicle configuration based on the laboratory investigation, and a method using CoroCAM IV^{+} and sensors to detect corona discharge characteristics occurring from icicles. The relationship between applied voltage and discharge modes will be revealed, and several parameters affecting these discharge properties will be considered, including the influence of air gap distance and freezing water conductivities as well as icicle status on the inception voltage and glow. These investigations will also be analyzed and discussed in detail.

The overall objectives of the present Ph.D project are to systematically study the

corona discharge phenomena using an icicle/iced-plate air gap systems its possible influence on the discharge activities of the ice-covered insulators. This study will be carried out based on the collaboration between NSERC/Hydro-Quebec/Universitė de Quebec à Chicoutimi (UQAC) Industrial Chair on Atmospheric Icing of Power Network Equipment (CIGELE) and the high voltage laboratory of Chongqing University (CQU).

More specifically, the objectives are as follows:

- Design of a physical model to simulate the air gaps of icicles/ice-covered insulator surface occurring on the ice-covered insulators;
- Creation of the detecting and measuring system for observing and recording the characteristics of corona discharge;
- Determination of the corona inception voltage and investigation of the discharge volume at V_{inc}, discharge frequency and discharge current waveform under a variety of conditions;
- Study of the statistic characteristics of discharge magnitude and revelation of the existence of space charge and its influence on the sequential discharge activities;
- Establishment of a mathematical model for calculating the space charge diffusion and drift, and analyzing the effect of space charge on the discharge processes of the ice-covered insulators.

1.4 METHODOLOGY

In order to attain the objectives of this study, a series of laboratory experiments were initially carried out in a climatic room and the results were subjected to a theoretical and statistical analysis. The main methods used in this study are summarized as follows:

1. In order to simulate corona discharge in different temperature and pressure levels, a climate chamber is set up;
2. The air gap on the ice-covered insulators is investigated and the parameters of icicle configuration are determined. An aluminum model is designed to form the icicle and a metallic plane with a thickness of 2 mm is introduced to simulate the ice on the insulator surface;
3. To study the corona discharge, a CoroCAM IV^{+} is used to record the corona discharge and a current pulse sensor is designed and calibrated to detect the discharge pulses and current pulse waveform;
4. The test systems consist of the HVDC generator, the icicle/iced-plate system, the current pulse sensor, CoroCAM IV^{+}, data acquisition system and a computer [20][21][22];
5. In order to eliminate the background noise and the interference from HV electrode and wires, a 10 mm diameter aluminum tube is introduced to avoid the effect of sharp point as source of corona discharge [23];
6. The statistic method is introduced to calculate the discharge magnitude; meanwhile, the relationship between the discharge magnitude and the time

interval is presented in order to reveal the influence of the space charge on sequential discharge activities [20] [24][84];

7. A physical mechanism of space charge is proposed to explain the effect of space charge based on the observed phenomena;
8. A mathematical model is proposed to verify the experimental result on the space charge.

1.5 STATEMENT OF ORIGINALITY

In this work, the electric discharge in the air gaps on the ice-covered insulators and the space charge formation process were firstly systematically studied using an icicle/ice-covered plate system.

The author designed the physical model and an experiment setup to detect and study the initial electric discharges at icicle tips. These investigations included the corona inception voltage, the discharge volume at V_{inc}, the repetition rate of discharge pulses, the waveform of discharge current pulse and the discharge pulse magnitude, and their affecting factors.

In order to reveal the existence of space charge and its influence on the succedent discharge activities, the relationship between the discharge magnitude and the time interval was determined and a mathematical model was established to analyze this discharge phenomenon. The drift and diffusion process of the space charge clouds can be estimated

using this mathematical model. Finally the possible influences of space charge on the flashover processes on the iced-covered insulators were investigated.

1.6 STRUCTURE OF THE THESIS

This thesis is comprised of 9 chapters.

The present chapter is an overall introduction for this PhD thesis. In this chapter, the research objectives, methods used, and main contributions of this study are briefly described.

The literature review in the second chapter summarises some previous investigations related to the present research. The chapter is divided into three parts: first, investigations of ice physics; secondly, investigations of the ice-covered insulators; finally, investigation of corona discharge, including the measurement method and the discharge pulse characteristics etc.

The experimental set-up and the test procedures are described in Chapter 3. The physical model is presented, and the design and the performance of current pulse sensor are illustrated in details, finally all experimental parameters are interpreted.

The experimental results are presented and analyzed in Chapters 4, 5, and 6. Chapter 4 mainly focuses on the corona inception voltage and the discharge volume at V_{inc}. Chapter 5 deals with the discharge pulse series and the discharge pulse waveform. Chapter 6 reveals the statistical results of discharge pulse magnitude.

In Chapter 7, the influence of space charge on the sequential discharge activities is analyzed and the schematic illustrations of space charge are proposed to explain its influence on the discharge activities and development.

Chapter 8 sets up a mathematical model of space charge drift and diffusion, and some calculated results will be presented to validate the experimental results. In addition, the influence of space charge on the flashover processes will be analysed.

In Chapter 9, general conclusions are deduced from the preceding discussions, and some recommendations are proposed for future research.

CHAPTER 2

LITERATURE REVIEW

CHAPTER 2

LITERATURE REVIEW

2.1 INTRODUCTION

A large number of studies have been carried out on the flashover on ice-covered insulators. The current chapter presents a brief overview of these studies, and mainly involves three different fields: ice physics, arc discharge on the ice-covered insulators and corona discharge. Concerning the corona discharge, up to now, there have been very few studies performed using icicles, but most investigations focused on metallic electrodes.

2.2 INVESTIGATION OF ICE CHARACTERISTICS

2.2.1 Electrical Conductivity of Ice

For a perfect single ice crystal (homogenous crystalline structure without any pollution), the number of free electrons is negligible and the only mechanism of electrical conduction under a DC field is "proton jump" [25] [26]. Therefore, the conductivity of pure ice is very low; when some impurities exist in the ice, the conductivity increases

significantly. The impurities play a major role in electrical conduction. In addition, polarization effects at external and internal surfaces (cracks, bubbles in the latter case) contribute to the true conductivity of ice. Furthermore, it has been reported that the dc conductivity of ice samples depends very significantly on the time period between sample preparation and the experiment due to ageing effects [27].

Under an alternating field, additional phenomena can occur [26]. Whereas ice does not have permanent electric dipole moment, it is readily polarized (by shifts in the electron cloud distribution and by proton jumps). Under DC field, the same electric energy is dissipated in the reversing of induced dipole moment. This dissipative effect, called dielectric absorption, gives rise to an effective electrical conductivity, i.e. it is much larger than the dc conductivity of pure ice.

Experimental results showed that the pure ice may be classified as a semiconductor due to its specific conductivity of 10^{-8}~10^{-9} S/cm [26]. It has been revealed that the conductivity of ice made from de-ionized water is roughly independent of temperature between -20 °C and -0.1 °C, whereas the conductivity of tap water ice increases with the temperature by a factor of ten within this range. Most of the increase appears between -5 °C and -0.1 °C [28].

Measurements on ice samples formed from ice with controlled conductivity ($80x10^{-4}$ S/m~$160x10^{-4}$ S/m) showed that the surface conductivity is about $1x10^{-6}$ S when the air temperatures are below 0 °C [29]. As the temperature rises above 0 °C, surface conductivity increases rapidly; this can be explained by the formation of a liquid water film on the ice surface. As the water covers the surface uniformly, conductivity value tends to

saturation. A maximum value of about 5 $x10^{-6}$ S is reached for ordinary frozen ice formed with freezing water of $160x10^{-4}$ S/m.

Regarding the atmospheric ice accretions on actual HV insulators, it has been shown that the conductivity of the melted surface layer of the ice build-up clearly exceeds the value of the freezing water [30]. Specifically, the conductivity value of the undersides of the insulators and the icicles exceeds the freezing water conductivity by 100 times. This is explained by the process of wet ice accretion on the insulators, where impurities diffuse to the surface before the water freezes.

2.2.2 Physical Characteristics of Ice Surface

It has been reported that ice seems to be a member of the small family of solids, which may exhibit anomalous surface properties in the sense that a quasi-liquid transition layer exists on at least some crystal faces at temperatures somewhat below the melting point [33]. A phase change of the ice surface to a quasi-liquid state is observed at a temperature a few degrees below the melting point. The temperature ranges from -6 °C to -3 °C. This estimated temperature appears to agree with the critical temperature in the measurements of the surface conductivity of ice, where a large increase in surface conductivity is observed for temperatures above T=-4 °C [29]. Another study on the surface and volume conductivity of a single ice crystal [32] showed also that the value of surface conductivity increases rapidly as the temperature rises. A threshold value was defined, where the surface conduction becomes more dominant than the volume conduction ranging

between -35 °C < T < -10 °C. An investigation on the surface conductivity of ice samples formed under various freezing conditions revealed that the ice bulk conductivity is very low compared to the surface conductivity in the range of ambient air temperatures between -12 °C and -8 °C [29]. Therefore, two different temperature characteristics are suggested for the regions above and below the threshold temperature [33].

Recent investigations show that a very thin quasi-liquid layer is present on the ice surface even for very low temperatures [34] [35] [36] [37]. This layer is quite small at lower temperatures, extending over just a few molecular layers for a temperature T=-10 °C, and it becomes thicker with increasing temperatures [34]. Detailed molecular-scale pictures of the ice surface at temperatures as low as 90 K, obtained by low-energy electron diffraction, show that water molecules are bound in a lattice, but these are not frozen like those in the layers beneath them [37]. Thus, greater molecular mobility exists in the ice surface than in the crystalline bulk. The ice can be seen as being composed of three parts: a core region of bulk ice surrounded by a surface and a subsurface region, which can all be distinguished by their vibrational spectra [36]. The high degree of vibrational motion by the water molecules in the surface layer is attributed to the absence of other molecules above them, resulting in unsatisfied bond. The existing bonds between the atoms are weakened, which gives rise to liquid-like vibrational motion and frees molecules to interact with other particles [37]. Above a certain temperature, this enhanced motion leads to a state of high energy ("high density phonon bath") and a separation of individual molecules from their original sites. This phonon-bath enables a high rate of accommodation of molecules and an easy energy transfer [35]. The un-relaxed surface bi-layer can be characterized on an

atomic level by both three co-ordinate molecules with either dangling hydrogen or dangling oxygen and four co-ordinate molecules distorted with respect to tetrahedral symmetry [36].

In addition to the fact that a quasi-liquid layer is always present on the surface of the ice, another phenomenon contributes to an increased surface conductivity. Due to the fact that the potential energy of the crystal lattice varies inversely with the number of dislocations, foreign molecules are excluded at the liquid-solid interface during the ice formation [38]. When a water-salt solution is cooled down, pure water freezes first and forms an ice crystal. Then, the salt ions diffuse into the liquid phase, resulting in higher concentration of ions and thus higher electric conductivity of the surface layer [38]. Measurements on actual HV insulators confirm that the conductivity of the melted surface layer significantly exceeds the conductivity of the freezing water that was initially used to form the ice [28] [29] [30] [39].

2.3 FACTORS AFFECTING FLASHOVER CHARACTERISTICS ON THE ICE-COVERED INSULATOR

2.3.1 Air Gaps

2.3.1.1 Formation of Air Gaps

Flashover phenomena have been studied worldwide for over 30 years. At **UQAC**, the Research Group on Atmospheric Environment Engineering (GRIEA) and the more recently created **NSERC/Hydro-Québec/UQAC** Chair on Atmospheric Icing of Power Network Equipment (**CIGELE**) have worked in this field for over 25 years

[1][2][17][18][51][52][53]. One of the most evident phenomena found for ice accretion on energized insulators is the frequent presence of air gaps near the HV terminal [2][3][17][40][41][42][43][47] and other sections of insulators completely covered in ice. These air gaps are formed during the growth period of icicles due to the activity of corona discharge at the icicle tips. The high temperature of partial arcs make icicles melt and then slow or stop the growth of icicles between insulators sheds in these areas. The appearance of partial arcs halts further elongation of the icicles and may even melt them. This process is the basis of air-gap formation and, when the accumulation is terminated, a careful examination of the ice surface shows the presence of air gaps around the electrodes.

If the electric field across the air gaps is high enough, corona discharge is initiated. This leads to the development of local arcs to form arcs along the ice surface and will cause a substantial increase in leakage current, and probably bring the flashover happen when the arc reaches a critical length. Therefore, these air gaps and consequent corona discharges play an important role during the whole flashover development process [14].

2.3.1.2 Geometric Form of Icicle Tip

The geometrical dimensions and typical number of icicles are important parameters for the establishment of numerical models for further studies such as electrical field calculations. A small number of scientific publications are conducting investigations with artificial icicles. The geometrical parameters reported in the literature are summarized and listed in Table 2-1 by **S. Brettschneider et al** [44]. Their length varies between 3 cm [45] and 5 cm [46]. In [47], **Farzaneh et al.** presented photographs of icicles grown on

industrial high-voltage insulators under various electrical field conditions. The curvature radii vary between 1.5 mm in the case of positive DC and 3 mm in the case of AC. An angle to the vertical of 14° to 15° was estimated from these pictures.

Field observations over several winter periods were reported in [41]. An average value of 5 mm was observed for the thickness of ice, whereas the length varied widely depending on the type of insulator and the severity of the freezing rain conditions.

Table 2-1 Parameters of artificial icicles reported in literatures

Literature reference	[46]	[48]			[45]	[49][1]		[50]	[51]	[52][2]		
										AC	DC+	DC-
Diameter of icicle tip (mm)		6.5	7	10						8	8	8
Length (mm)	50	60	40	80	50			30-50		120	150	120
Angle(°)					15	60	0[3]	20		14	14	14
Curvature radius(mm)					2.5			2.5-10	40×10^{-3}			
Conductivity [μS/cm]								95				
Radius of plane (mm)		50			200							

Note: (1) two different geometrical shapes proposed
(2) Icicle formed on energized insulators with various voltage types
(3)Icicle shape is cylindrical with rounded tip

2.3.1.3 Influence of Air Gap on Electric Field Distribution

The flashover of ice-covered insulators is mainly caused by non-uniform voltage distribution along the insulator string. Studies on the electrical field distribution along ice-covered insulators have been carried out at **CIGELE** for several years. **M.Farzaneh et al.** [17][18] found that when the insulator is covered with ice, especially when the water film is present on the ice surface, the original electric field distribution will be dramatically distorted and very high electrical field strength will appear at the air gaps[18], which may cause corona discharges and, frequently, local arc formation.

C. Volat et al [53] found that, for one standard post insulator, the first four sheds withstand about 50% of applied voltage under clean conditions and about 70% with ice accumulation. The Electric field strength at these areas increased observably, and it was observed that the corona discharge and local arcs always start at these air gaps. If the applied voltage is high enough, the arc will propagate along the ice surface and may result in a complete flashover.

2.3.1.4 Influence of Air Gaps on Flashover Voltage and Breakdown Voltage

Farzaneh et al [54] found that the number and position of air gaps have significant effects on the flashover voltage of ice-covered insulators. In 4 different configurations of air gaps, the 50% withstand voltage, V_{50}, has the lowest value when two air gaps appear at the top and the bottom of the insulator string, respectively. It has the highest value with the 3 air gap configuration. The position of the air gap also has an obvious effect on the

flashover performance of ice-covered insulators. When two air gaps are at the bottom of an insulator string, an additional air gap will be created near the ground electrode during flashover, resulting in the occurrence of 3 local arcs along the ice and in a flashover voltage higher than that with two air gaps at the top and bottom of the insulator string respectively.

X. Chen et al [55] investigated the influence of the air gap on the flashover performance of a cylindrical ice sample. The maximum withstand voltage, V_{MF}, increases with the increase in air gap length, which was also influenced by the position of the air gap. These studies prove that the presence of air gaps do indeed influence the flashover voltage of ice-covered insulators.

C. Volat et al [53] revealed the relationship between the breakdown and air gap distance based on point to plate system and under temperatures of -1 °C. Results show the breakdown voltage increased linearly with an increase in air gap distance, which is in agreement with the results of a metallic rod-to-plan configuration [75]. Meanwhile, other investigations found that there are pronounced voltage drops along the first four sheds for the clean insulators, which are responsible for the presence of air gaps close to the HV electrode.

Three additional series of tests were carried out by **T. Changiz** [57] to study the effects of the initial air gap on V_{MF} of a 40 cm length insulator having three different applied water conductivities of 30, 65 and 100 μS/cm. The air gap was artificially created to encompass 15% of the total insulator length. The results show that the only effect of the initial air gap length is to increase the threshold voltage for breaking down the air gap.

Then, after establishing the arc along the air gap, and when melting water is present on the insulator surface, this length has no more effect on discharge phenomena.

2.3.2 Freezing Water Conductivity

This major parameter influences the flashover voltage of insulators considerably. In general, the higher the conductivity, the lower the flashover voltage will be [1][2][17]. These results show that the maximum withstand stress (E_{WS}) decreases as a power curve function of water conductivity. However, in some cases, due to the ice shedding, the increase in conductivity may lead to higher flashover voltage [1].

Fujimura et al [58] and **Matsuda et al** [59] carried out flashover tests on insulators covered with ice formed from water with different conductivities, respectively. They reported that the flashover voltage is dependant on the conductivity of the freezing water. When the conductivity is high, the withstand voltage of an insulator is low.

Kannus et al [60] examined the effect of the resistivity of freezing water on the leakage current of AC flashover tests. When the resistivity of freezing water was decreased from 90 Ωm to 9 Ωm, the leakage current pulses appeared earlier during the icing period and the amplitudes increased rapidly. In conclusion, the flashover voltage of two suspension insulator units was found to be linearly proportional to the square root of the resistivity of freezing water.

The effect of freezing water conductivity on the withstand voltage of ice-covered post insulators was also studied at **CIGELE** [17][62][63]. The gradient of the maximum

withstand voltage decreased with an increase in the freezing water conductivity up to a value of 80 μS/cm. After this level of water conductivity, the gradient of the maximum withstand voltage tended towards a saturation value.

2.3.3 Temperature

The rise in air temperature from values under the freezing point to values around or above 0°C causes the ice surface to melt. The formation of a water film, in general very highly conductive [30] at the ice surface, in turn causes an increase in voltage drop across the air gaps, and the formation of local arcs as a consequence. Under certain conditions, local arcs develop into a flashover arc along the whole insulator length.

The critical flashover of insulators under melting conditions seems to depend on the rate of increase in air temperature [71]. The maximum withstand stress (E_{WS}) of a composite EPDM and the porcelain IEEE standard insulators under slow and fast ice melting conditions, was obtained at UQAC. The investigation shows that while a relatively slow rise in air temperature from -12 °C to +1 °C, at a rate of 2.4 $°Ch^{-1}$, is most severe for porcelain IEEE standard insulators, rapid melting at 24 $°Ch^{-1}$ lowers the E_{WS} of the composite EPDM insulator tested [71].

2.3.4 Air Pressure

At high altitudes, the electric performance of insulators is not only influenced by atmospheric icing, but also enhanced by low air pressure [17]. The influence of air pressure

on the critical flashover voltage of polluted or ice-covered insulators is generally expressed as follows:

$$\frac{V}{V_0} = \left(\frac{P}{P_0}\right)^m$$

Where V is the critical flashover voltage, at pressure, P, and correspondingly, V_0, at standard sea level pressure, P_0.

Exponent m is a constant and indicates the degree of influence of air pressure on the critical flashover. Using a triangular ice sample and also a short insulator [61][101][102], the value for m while using DC and AC high voltage was determined. These results show that air pressure has an obvious influence on the minimum flashover voltage, V_{MF}, of test objects; in some cases, the results indicate that the reduction in the minimum flashover voltage could reach 40%, as ambient pressure decreases from 103.3 to 30 kPa.

2.3.5 Ice Type

Sugawara et al [151] investigated how the AC withstands voltage varied with ice density for two standard suspension insulator units covered with artificial ice. The withstand voltage decreased slowly with an increase in the ice density from 0.6 to 0.8 g/cm^3. For an ice density of 0.9 g/cm^3, the withstand voltage was markedly smaller than that observed for an ice density of 0.6 or 0.8 g/cm^3.

Fujimura et al [58] measured the withstand voltage of an ice-covered suspension insulator string formed in a cold room and a snow-covered insulator where the snow

originated from a mountain. The AC withstand voltage of an ice-covered insulator was approximately 40% lower than the withstand voltage of an insulator covered with snow. The DC withstand voltage of ice-covered an insulator was practically the same as that measured for a snow-covered insulator.

M. Farzaneh et al [17] [63] studied the effects of dry and wet grown ice on the maximum withstand voltage gradient of different types of insulators. The maximum withstand voltage gradient of insulators under wet-grown ice conditions was substantially lower than that under dry-grown ice conditions. The results suggested that glaze and hard rime were more dangerous to power systems than soft rime.

2.4 CORONA DISCHARGE

Corona discharge is an electric breakdown phenomenon that is confined to localized region of the insulating medium between two conductors at different potentials [75]. The localization of the discharge may be the consequence of an electric-field enhancement restricted to a region that is relatively small compared with the dimensions of space or gap between the conductors.

This characteristic arises either because the electric field strength beyond a certain point is too low to support continued growth of the discharge or because accumulation of space charges produced during the discharge activities acts to reduce the local Electric field strength to levels insufficient to sustain the discharge.

Corona discharges occurred in the H.V. equipment and on power transmission lines have been widely studied, mostly in air [68] [72] [77] [110], SF_6 [20] [99] and mixture gases [20].

2.4.1 Study of Corona Discharge Related to Ice and Water

A relatively large number of publications and reports focused on the flashover performance of ice-covered insulators. Only a few concentrated on the fundamental aspects of discharge in the air gap between two formed electrodes.

On a smooth conductor located along the axis of a cylindrical cage, **J.Luan Phan-cong et al** [64] observed that pulsative corona currents developing in the air surrounding the water drop and corona discharge are greatly affected by the changes in the physical properties of the water drop. Corona activities are very intensive at temperatures above freezing but are considerably attenuated at temperatures below the freezing of the water drop. The amplitude of current pulses was observed on icicle points and mainly at positive polarity.

H. W.Bandel 1951[45] compared the difference of corona discharge in ice and water using a 0.13cm outer diameter water electrode, and later **Loeb L.B** [100] concluded all the experimental results. The result showed that the character of the oscilloscope manifestations with ice points was profoundly affected by the low conductivity of ice. Decreasing the resistance of the icicle tip by shortening its distance increased the discharge pulse amplitude. Under DC+ voltage, for pure ice, no discharge pulses could be detected up

to 19kV, and the pulses from the ice point were smaller than those from the metal point and the water point. With the smaller electrode tip, the corona discharge phenomenon could not be seen with the naked eye, and could only be photographed using long exposure. Under DC- voltage, investigation showed that it was particularly hard to fix the threshold accurately for the rise, because of the small triggering volume for a negative point and erratic shape.

In order to quantify the difference in the behavior of the corona discharge on the ice surface with different temperature levels, **Brettschneider S.** [65] investigated some discharge characteristic parameters, such as the corona inception voltage and the arc development velocity. It was found that the corona inception voltage on ice surface and the corona propagation velocity on the wet ice surface are lower and faster than those on the dry ice surface.

2.4.2 Measurement Methods for Corona Discharge Pulses

Corona discharge displays pulsating characteristics. Investigations in [66] [91] revealed that these steep-front and short duration pulses have high-frequency harmonic components, reaching to tens of MHz. Generally, in air, the central frequency spectrum of the corona varies from 150 k to 5 MHz.

The recent upsurge of research on corona phenomena, one kind of partial discharge (PD), has been driven in part by development of fast new digital and computer-based techniques that can be applied to process and analyze signals derived from PD

measurement [67]. There seems to be an expectation that, with sufficiently sophisticated digital processing techniques, it should be possible to gain new insight into the physical and chemical basis of PD phenomena.

As the improvement of digital techniques continues, many methods and equipment have been developed for PD measurements. Some of them have been proposed by researchers as follows:

- Precise pulse shape and pulse-burst characterizations using broad-band detection [68][69];
- Recording of phase-resolved PD pulse height distribution using various types of digitizers or multi-channel analyzers[70][72];
- Quantification of PD pulse-to-pulse or phase-to-phase memory propagation effects using stochastic analysis [20][73];
- Removal or reduction of noise using digital filtering techniques [74].

2.4.3 Characteristics of Corona Discharges

2.4.3.1 Corona Inception Voltage

The corona inception voltage (V_{inc}) is defined as a voltage level at which the corona occurs. It increases with an increase of gap length and then tends to be saturated [75], and V_{inc} under negative polarity is slight lower than that under positive polarity. When the applied voltage is increased further, the discharge is transited into glow discharge under positive DC. V_{inc} under AC voltage is slightly lower than that under DC.

At room temperature, V_{inc} declines almost in proportion to the decrease in ambient gas pressure. This led to a study on the starting potential of positive and negative point discharge as a function of pressure. Additionally, with an increase in temperature, V_{inc} decreases, but the influence of temperature on V_{inc} is more minor than that of pressure [76].

Many parameters influence V_{inc} and they have been subjected to extensive investigations such as: electrode protrusions[77], water droplets[78], gap spacing[79], atmospheric weather conditions as well as actual conductor surface conditions [80] and air turbulence. All these parameters affect the corona starting conditions and no theory has been put forth to explain the observed phenomena and relationships. However, scattered explanations do exist for some observations.

2.4.3.2 Statistical Properties of Corona Pulse

The PD current pulses exhibit significantly statistical variation, such as pulse amplitude, pulse shape, and time to occur. The factors affecting the stochastic behaviour of corona pulses were summarized and they [20] include : (1) probability of initiatory electron injection as a function of Electric field strength and location; (2) the dynamics of dielectric surface charging; (3) the rates of discharge-generated ion space charge and/or metastable species dissipation; (4) fluctuations in gas density or composition; (5) presence of ionizing radiation; (6) memory propagation association with influence of residuals from previous PD pulses on the initiation and development of subsequent pulse. Statistical variations in PD behavior are often largely determined by the effects of pulse-to-pulse memory

propagation whereby the residual space charge, etc. left behind by a PD pulse will influence the probabilities for initiation and development of subsequent pulses.

Although the Trichel-pulse phenomenon appears to have a very regular and well ordered behavior, its stochastic properties have been found in relatively recent experimental work to be rather complex. **Mason and Young** [81] first showed that there was a significant correlation between the successive pulse time separations, which was later verified by **R.J.Van Brunt et al** [20]. Using the conditional time interval distributions $P(\Delta t_n/\Delta t_{n-1})$ and $P(\Delta t/q)$, it was found that the time to the next pulses is significantly dependent on the amplitude of the previous pulse as well as the previous pulse time separation. **Malik and Al-Arainy** [82] measured the statistical distributions of Trichel-pulse amplitudes and reported difficulty in obtaining reproducible results for 'identical' discharge gap conditions.

A large number of investigations have been carried out on a metal electrode in various gases [54]. The results revealed that the corona discharge is a stochastic process due to the influence of space charge occurrence [54]. To date, the statistical distributions of corona pulse amplitudes have been reported for DC coronas in air gaps of point-plane electrodes. The influences of gap length, applied voltage level and polarity on the corona pulse height distribution were examined in detail. It was shown that for DC coronas, in general, pulse amplitude follows a Gaussian type of probability distribution. However, exceptions to these behaviours were found near the corona inception level, near the pulse-to-glow transit level, or in more uniform field gaps. The corona pulse amplitudes were

reasonably reproducible for positive coronas, while for negative coronas, the pulse amplitudes were sensitive to the applied voltage level and less reproducible.

Some authors measured the sequential generation of PD pulses in order to investigate the space charge behavior and the corona stabilization effect in SF_6 gas under AC and DC conditions [83]. Consequently, the following results have been obtained:

- The sequential generation of PD shows the larger magnitude of the first PD and the smaller magnitude of the sequential PD;
- The charge of the first PD under AC conditions depends on the instantaneous voltage;
- Subsequent PD has small charges, independent of the instantaneous voltage;

The charge magnitude of the first PD was proportional to the instantaneous voltage, and was independent of the applied AC voltage. This is related to the size of the critical volume and the statistical time lag. The critical volume means the volume where the Electric field strength is higher than the critical Electric field strength of discharge inception in SF_6 gas.

Al-Arainy et al [84] found that in the point-to-plane air gaps, under both positive and negative half cycles of AC voltage, the pulse amplitudes follow a Gaussian type of probability distribution when the applied voltage is near the corona inception level. As the applied voltage is progressively increased, the deviations from a Gaussian type of probability distribution also increases for the positive and negative half-cycles of AC voltage. However, in the positive half-cycle, the applied voltage magnitude does not affect the AC corona average pulse amplitude as it does the DC corona, and is slightly lower than

that for positive DC. For the same applied voltage level, as the gap length is increased, the average pulse amplitude decreases for both DC and AC. In the negative half-cycle of the AC corona, for a given gap, when the applied voltage increases, the average amplitude decreases while the standard deviation increases. For a given voltage, as the gap length is increased, the pulse deviation decreases. It should be noted that, for the DC corona, the variation in pulse amplitudes are due to the statistical nature of the corona phenomena only. However, for the AC corona, the sinusoidal variation of applied stress introduces further spread in the corona pulse amplitudes. Therefore, the AC corona pulse parameters exhibit higher statistical variation as compared to the DC corona. It has been observed for positive corona in SF_6 that discharge-induced changes in the electrode surface material can also have significant effects on the discharge behavior under some conditions. Some electrode materials such as nickel are found to be more resistant to reaction with corona-generated SF_6 decomposition products than other materials like aluminum or stainless steel.

Florkowska et al [85] investigated that the mean amplitude of discharge pulses at voltage range between inception voltage V_{inc} and 1.05 times of V_{inc} increases with an increase in electrode tip radius. The discharge frequency N increases with applied voltage to a critical voltage, V_{cr}, above which the discharge frequency decreases to a few pulse. This reduction of discharge frequency is accompanied by the change from pulse discharge to pulseless discharge.

2.4.4 Memory Effect of Space Charge

The importance of memory effects of space charge was first realized from the measurement of pulse-amplitude and time separation distributions of the negative point-plane Trichel-pulse corona [20] [112]. In the case of Trichel pulses, the memory effect on the initiation and growth of subsequent discharge events results from the influence of space charge and metastable excited species generated during a discharge pulse.

Steiner [86] and **Van Brunt** [20] and **Kulkarni** [87] independently reported the evidence of strong correlations among successive negative-corona pulses, which were expected from the work of **Mason et al.** [88] and were implied by earlier physical descriptions of the phenomenon proposed by **Lama and Gallo** [89]. It was suggested by **Lama et al.** [89] that, after a discharge pulse occurs, the gap contains moving negative-ion space-charge clouds that perturb the electric field enough to influence the development of subsequent pulses. When the mean time interval between pulses becomes sufficiently long that all residual ions from the previous pulse have cleared, the dependence of the discharge pulse amplitude and the time interval ceases and a loss of memory ensues. The influence of a moving space charge could, in fact, be similar to that which is known to affect the recovery of Geiger counter tubes following the occurrence of a discharge pulse [90].

The significant influence of space charge clouds on the growth of Trichel pulses was demonstrated by **R. J. Van Brunt et al.** [20] from the measurement of conditional pulse amplitude distribution $p_1(q_n/\Delta t_{n-1})$. The n^{th} discharge pulses will have amplitude between q_n and q_n+dq_n if its time separation Δt_{n-1} from the previous event is restricted to lie within a narrow window between Δt_{n-1} and $\Delta t_{n-1}+\delta$ (Δt_{n-1}). Investigation results verified that

it is correct to express the relationship between the time interval and pulse amplitude distributions using conditional distributions $p_1(q_n/\Delta t_{n-1})$[75] [91].

The statistical variability of coronas, including the pulse-to-pulse memory propagation has been carefully studied in [20] [92]. Memory effects are closely related to the probabilities of corona initiation and growth. However, the behaviors of pulse-to-pulse memory propagation are more complicated under AC than those under DC voltage, due to the change of electrical field. Therefore, the characteristics of memory effects cannot be measured for entire consecutive corona except for those with the time separation and the time interval shorter than the critical time interval.

2.4.5 Model of Space Charge

A time-lag recovery model was developed by **U.Tormm et al** [93] to describe the discharge behavior of defects with a single discharge site. It can be used to study physical discharge properties based on statistical measurements. It is applicable for corona discharge in the air as well as internal partial discharge.

Barbara Florkowska et al [86] proposed a model to explain the influence time of space charge ions on sequential discharge activities. The gap transit time for negative ions can be estimated using the expression

$$t = \int_0^t dt = \int_0^{\xi=a} \frac{d\xi}{\mu E(\xi)}$$

where a is the point-to-plane gap distance; E is the unperturbed axial Electric field strength, and μ is the ion mobility which is assumed to be independent of E. Thus, there should be a loss of memory due to space charge from previous corona pulses if $\Delta t_n > \Delta t$. Successive pulses satisfying this condition are essentially equivalent to the first pulse treated in Morrow's model.

Previous works on the effects of positive space charge produced by corona streamer growth in non-uniform field systems has been concerned with the experimental determination of their electrical properties and the formulation of a quantitative model. In 1965, **Dawson et al.** [94] proposed a model to simulate the effect of positive space charge in the streamer tip. This model has successfully elucidated the possibility of propagating even in zero-ambient fields. **Gallimberti** [95] developed the model more rigorously in 1972. Through an equivalent electron avalanche and energy balance condition, **Perlps** [96] has indicated that positive space charges deposit the streamer channel, except when the streamer rackets the cathode. In 1974, **Khaled** [97] introduced a new approach to simulate the effect of the space charge by use of ring charges. In 1976, **Arima** et al. [98] introduced a model in which the space charges produced by corona streamer distribute within a part of sphere of radius being the corona streamer length.

Hinterholzer et al [99] investigated the influence of space charge on the breakdown behaviors of gas under impulse voltage: AC voltage and very fast transient over-voltage (VFTO). A model of space charge stabilization was also set up. The space charge occurrence depends on many parameters such as voltage steepness, gas pressure and tip geometry. When the velocity v_1 of the positive SF_6-ions at the boundary of the critical

volume exceeds the maximum growth velocity of the critical volume $V_{cr/m,}$ the formation of positive space charge in the front of the streamer region will occur, which may reduce the electrical field in front of the protrusion beneath the critical field strength. Therefore, further ionization processes may be stopped and a high voltage level may be required to initiate the finial breakdown. The model of space charge and some results were shown in **Figure 2-1** and **Figure 2-2**, respectively.

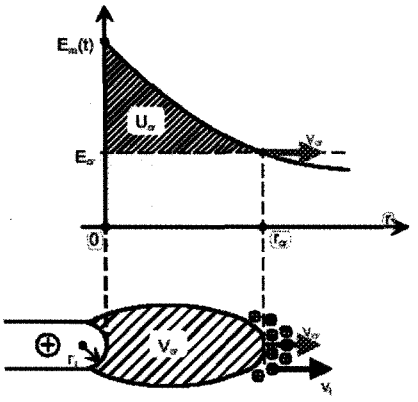

Figure 2-1 Extension of the streamer region and field distribution at the tip of a protrusion

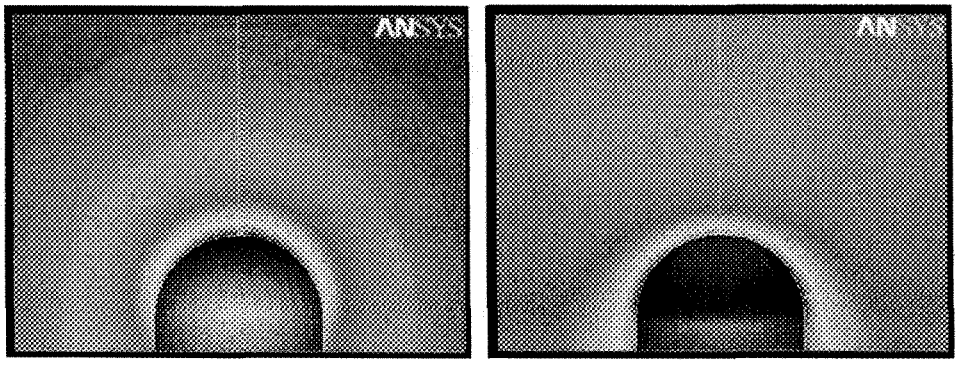

(a). (b).

a. space charge density: 0 pC, gas pressure: 0.2 MPa, voltage steepness: 1 kV/μs

b. space charge density: 80 pC, gas pressure: 0.2 MPa, voltage steepness: 1 kV/μs

Figure 2-2 Spatial field distribution in the front of a needle

2.5 CONCLUSIONS

In spite of the numerous investigations on the ice-covered insulators and the corona discharge, little information is applicable to the present study. This research is summarized in **Figure 2-3**. The whole study field of ice-covered insulators is highlighted in yellow.

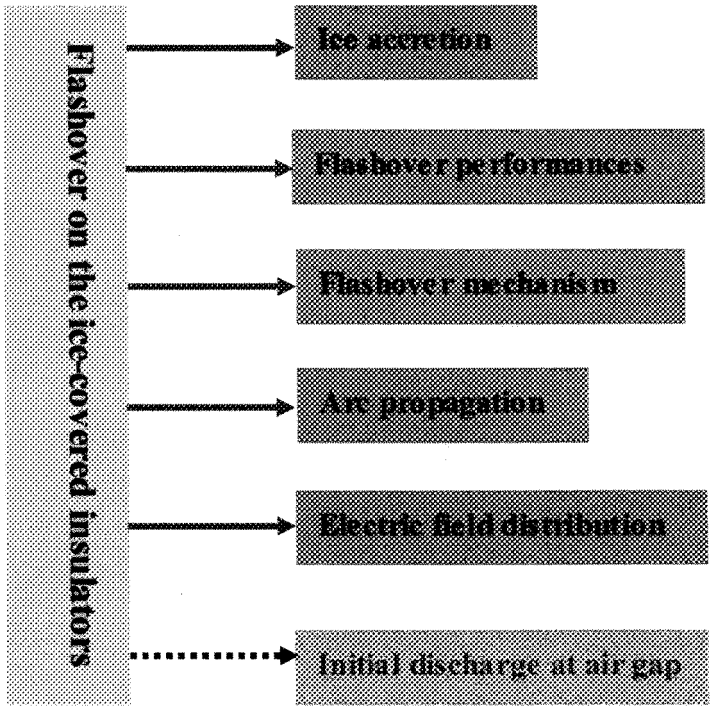

Figure 2-3 Researched fields and remaining gap on the ice-covered insulators

Generally, fundamental ice physics has been widely investigated, and the results show that ice properties are different from the normal conductor. Specifically, when the ice is solid, the air gap has been frequently observed on ice-covered insulators and its influence

on insulator flashover has been highly focused. The results also showed that the discharge activities (corona discharge) initiates from these air gaps. The methods of detecting corona pulsative pulses were driven in part by development of new, fast digital and computer technology. It has been given significant attention in many fields, including on ice surfaces and point-plane systems. Most studies demonstrate that the space charge behavior has an evident influence on the sequential process.

From the literature review, two principal questions have yet to be clearly answered:

- Discharge characteristics, such as corona inception voltage, discharge pulse magnitude and pulse waveform of coronas occurring at the icicle tip under various conditions;
- The role of corona discharge in the whole discharge process and the potential effects of space charge on the sequential discharge activities.

These two questions motivated this Ph.D thesis, which systematically investigates the corona discharge and reveal the existence and influence of space charge using an icicle/iced-plate system.

CHAPTER 3

EXPERIMENT SET-UP AND PROCEDURES

CHAPTER 3

EXPERIMENT SET-UP AND PROCEDURES

3.1 INTRODUCTION

This chapter provides technical and practical information on the experimental set-up (Figure 3-1), the physical model, the measuring methods and the test procedure.

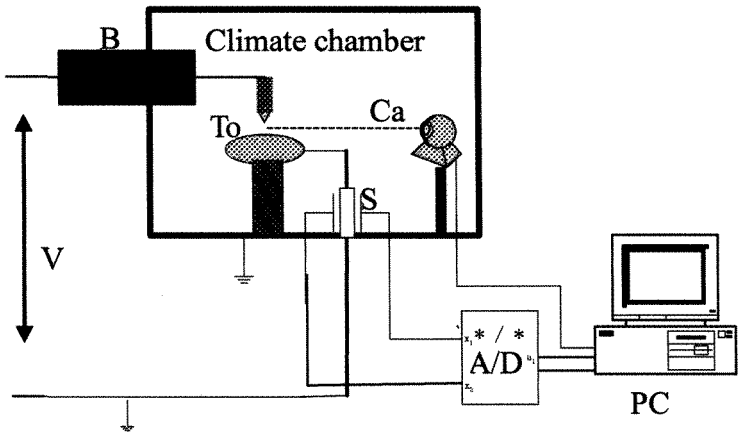

A/D: PCI-9820; B: Bushing; Ca: CoroCAM IV+; PC: Personal computer;

S: Current sensor; To: Test object;

Figure 3-1 Experiment set-up

The detailed arrangements of a current pulse sensor, an icicle and an ice-covered plate electrode system inside the chamber are shown in Figure 3-2.

First, the components of set-up are described. Next, the design and preparation of the physical model consisting of an icicle and an ice-covered plate are explained. Then, a corona detecting system (CoroCAM IV^{+}) and a current pulse sensor are illustrated. Finally, the test procedure and all experimental parameters are listed and some chosen values are given, and ultimately the data process program and method are introduced.

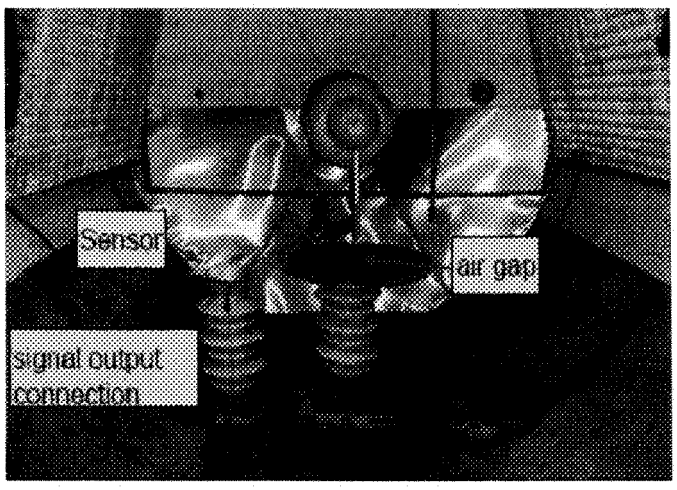

Figure 3-2 Arrangement of air gap system inside the climate chamber

3.2 TEST FACILITIES

3.2.1 Climate Chamber

To simulate low pressure at high altitude and cold temperature in cold region, all tests were carried out in the climate chamber, as shown in **Figure 3-3** at the HV Lab in **CQU**. The climate chamber is 2 m in diameter and 3.8 m in length. It is equipped with a refrigerating system, a vacuuming system, a spraying system, a wind-producing system and a HV source. The related control plate is shown in **Figure 3-4**.

The temperature inside the climate chamber can be controlled to between 20 °C and -36±1 °C. The air pressure can be adjusted to between 101 kPa and 34.6k Pa to simulate the conditions at high altitude. The HV source satisfies the requirement of the international standard (IEC 60507).

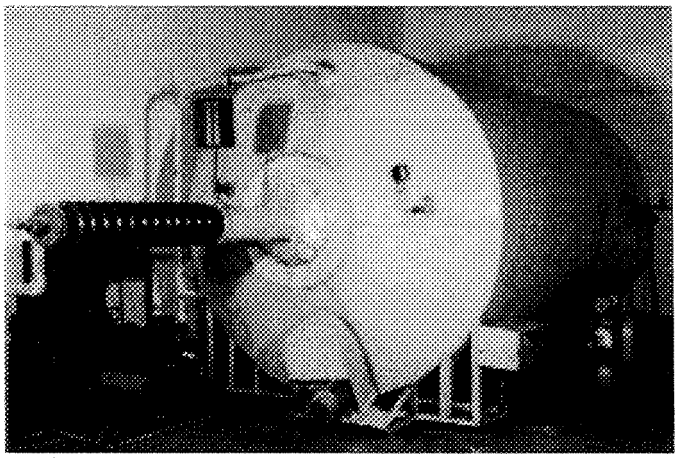

Figure 3-3 Climate chamber (3.8m×Φ2.0m)

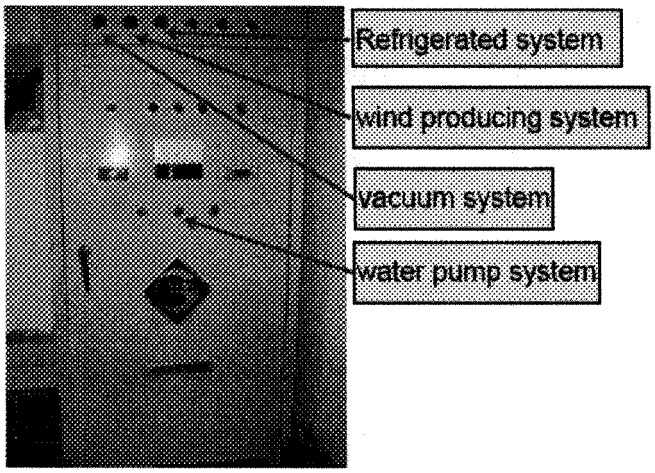

Figure 3-4 Control plate of climate chamber

3.2.2 Corona Detecting Systems

It is well known that some icicle tips exist [2][3][17][40][41][42][47] on the ice-covered insulators. Under high voltage, the electric field strength around these icicle tips is strong enough to produce the corona discharge before the breakdown of air gaps and visible arc formation. However, visible observation of corona with the naked eye is very difficult, because coronas emit weak radiation, mostly in the ultra-violet spectral range, i.e. λ = 280-400 nm, as presented in **Figure 3-5**.

One of the main tools to detect the corona discharge is the ultra-violet camera, CoroCAM IV^{+}, as shown in **Figure 3-6**(a). It can provide a quick way to depict areas of high electrical stress as well as allowing monitoring of discharge activities. It has two different recording modes, live mode and integrated mode, and has been widely used for studying corona discharge on electrical equipment [129].

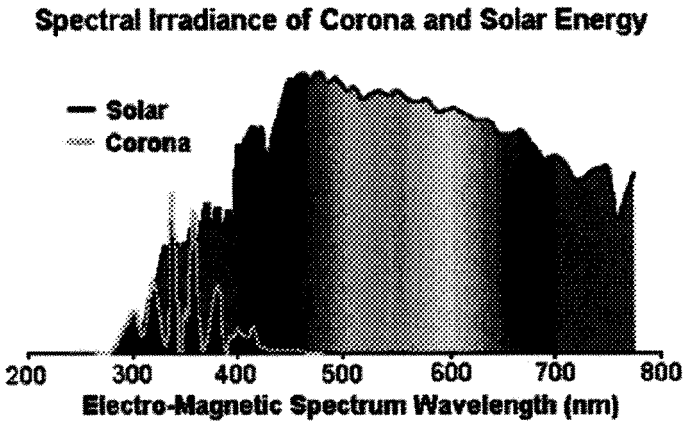

Figure 3-5 Electro-magnetic spectrum wavelengths

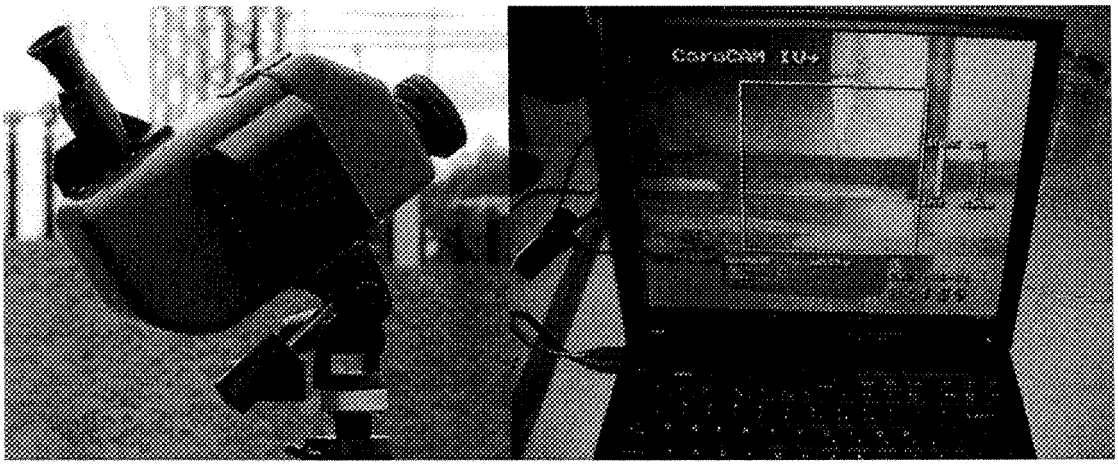

(a). CoroCAM IV^{+} (b). Computer connecting with CoroCAM IV^{+}

Figure 3-6 CoroCAM IV^{+} and connected computer

Because the UV can be blocked by normal glass, in order to accurately detect the corona discharge activities, CoroCAM IV^{+} with the gain of 99% and the integrated mode is installed inside the climate chamber, 2m away from the test sample. It is adjusted to focus on

the icicle tip. Meanwhile, the chamber is kept dark to avoid external interference. Additionally, a computer to record the corona activities inside the climate chamber is connected to CoroCAM IV^{+} with a cable, as shown in **Figure 3-6**(b).

3.2.3 Corona Discharge Measuring Systems

The corona is a local electrical discharge that only partially bridges the insulation between conductors.

The detection and measurement of corona discharge is based on the exchange of energy taking place during the discharge activities [39]. The corona discharge displays pulsating characteristics, which are very important to reveal the discharge fundament and the occurrence of space charge as well as its influence on the sequential discharge activities.

So far, the most frequently used and successful detection methods are the electrical ones to which the new IEC Standard 60270 [103] is related. These methods aim to separate the impulse current linked with discharge from any other phenomena. The adequate application of different discharge detectors has become quite well defined and standardized in [103].

Generally, the hardware used in the discharge measuring systems includes a current pulse sensor, a sampling resistor, an A/D converter, and a personal computer (PC).

3.2.3.1 Measuring Circuit

Electric discharge detection methods are based on the appearance of a discharge pulse at the terminals of test object. The most fundamental quality of the corona discharge pulse measurements is to detect the apparent charge of a discharge pulse [39][103]. Most discharge measuring systems are integrated into the test circuit in accordance with schemes as shown in **Figure 3-7**. In order to measure this weak current pulse signal, some requirements are necessary to the components in this circuit:

- The coupling capacitor C_k should be of low inductance;
- The high-voltage supply should have a sufficiently low level of background noise;
- The high voltage connection should have a sufficiently low level of background noise;
- Impedance or a filter may be introduced at high voltage to reduce background noise.

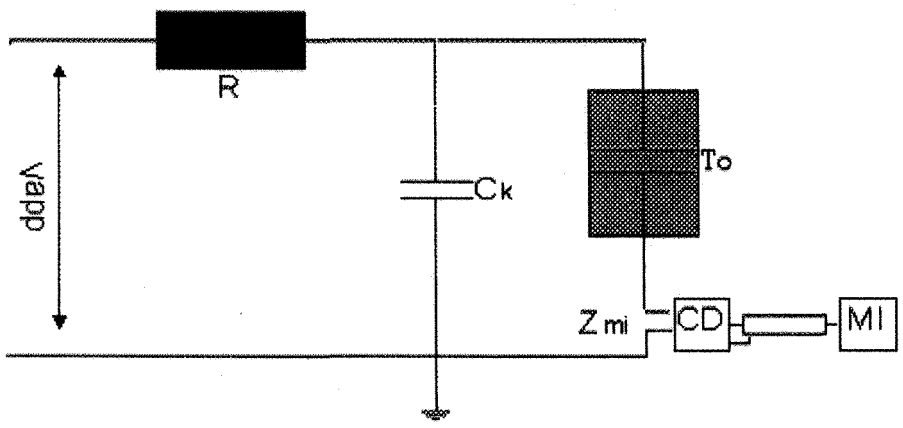

V_{app}: voltage supplier; Z_{mi}: input impedance of measurement system; To: test object; C_k: coupling capacitor; CD: coupling device; MI: measuring instrument;

Figure 3-7 Coupling device CD in series with the test object

3.2.3.2 Current Pulse Sensor and its properties

The principle of a current pulse sensor as shown in **Figure 3-8** [102] is basic accessories measurement of current and power in AC current. Its secondary winding provides a current i_2 proportional and in phase with the primary education current i_1.

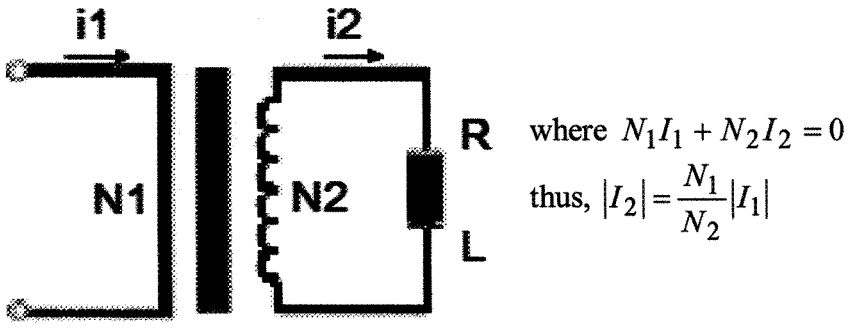

Figure 3-8 Principle of transformer of current pulse sensor

Based on the above principle, a current pulse sensor is designed and its detailed construction is shown in Figure 3-9. Coiling wire that is in series with a sampling resistor of 50Ω is installed in a shielding aluminum box, and there is a narrow air gap in the inner radius to induce the magnetic field of the current pulse. The ground wire crosses the center hole of the aluminum box.

Before testing, the optimization characteristics between the sensitivity and the current frequency band must be determined in advance as shown in Figure 3-10. The lower limit

frequency and upper limit frequency of current sensor are 100 kHz and 10 MHz, respectively. The lower and upper limit frequencies f_1 and f_2 are the frequencies at which the transfer impedance has fallen by 6 dB from the peak pass-band value. The mid-band frequency, f_m, and bandwidth, Δf, are defined by:

$$f_m = \frac{f_1 + f_2}{2} = 5.05MHz$$

and

$$\Delta f = f_2 - f_1 = 9.9MHz$$

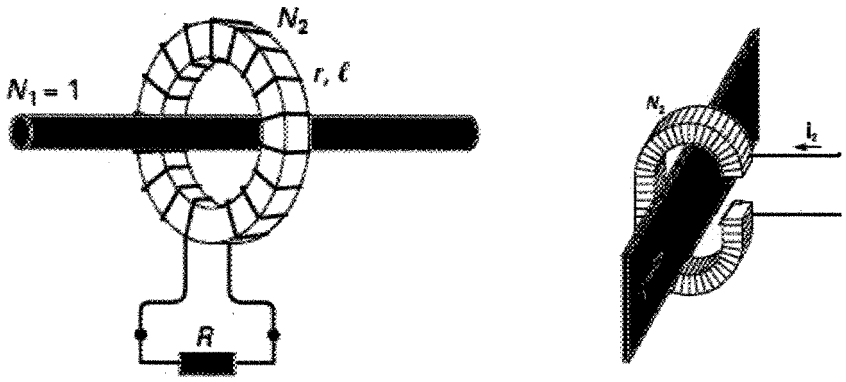

(a). Connection circuit of current pulse sensor;

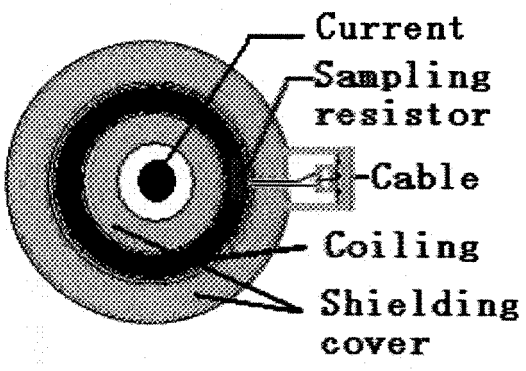

(b). Profile of current pulse sensor;

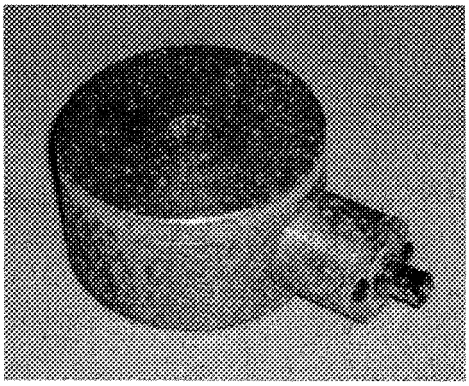

(c). Current pulse sensor;

Figure 3-9 Illustrative diagram of current pulse sensor

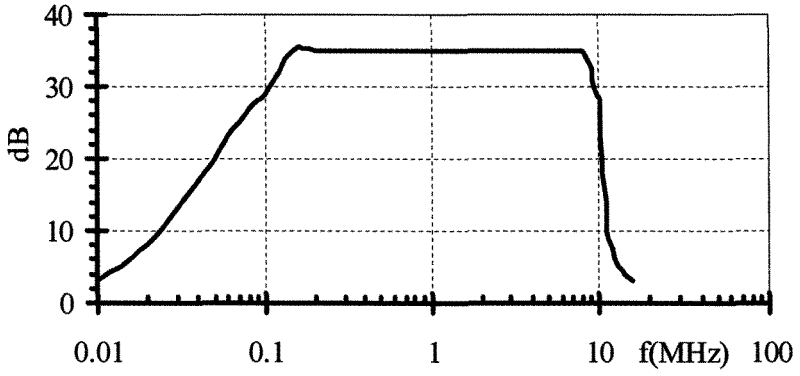

Figure 3-10 Relationship between amplitude and frequency of current pulse sensor

3.2.3.3 Calibration of Discharge Detection

In order to avoid the integration errors in the measurement results, calibration of measuring systems [39] intended for the measurement of the fundamental discharge quantity q is made by injecting short-repetition duration-current pulses with the well-known charge quantity q_0 across the test object, whatever the test circuit is used. The calibration circuit is illustrated in Figure 3-11. These current pulses are generally derived from a calibrator which comprises a generator producing step voltage pulses of amplitude V_0 in series with a precision capacitor C_0.

In calibration, a short rising time of 50 ns is now specified for the voltage generator to produce current pulse. If the voltage V_0 also remains stable and is exactly known, repetitive calibration pulses with charge magnitudes q_0 can be calculated as: $q_0 = V_0 C_0$.

This investigation shows that the waveform of discharge current pulse is different between a dry icicle and a wet icicle, and that the relationship between the magnitude of discharge current pulse and the output voltage amplitude of sensor is also different. The corresponding relationship is illustrated in Figure 3-12.

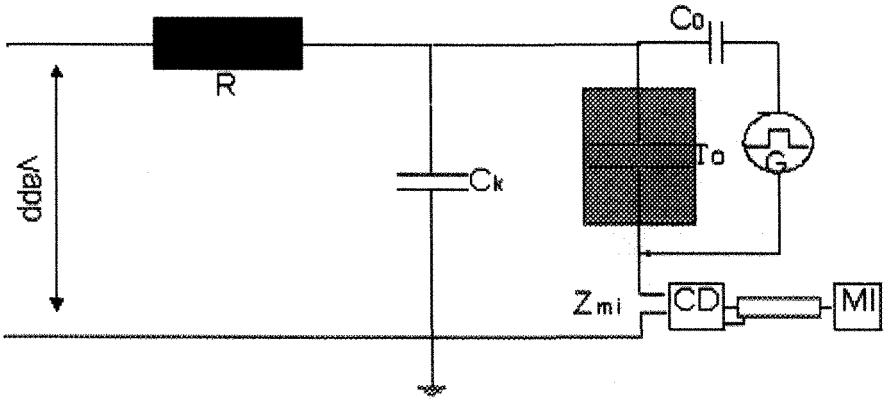

C_k: Coupling capacitor; G: Step pulse generator;

To: Test object; C_0: Calibration capacitor;

Figure 3-11 Usual circuit for the calibration of discharge pulse measuring

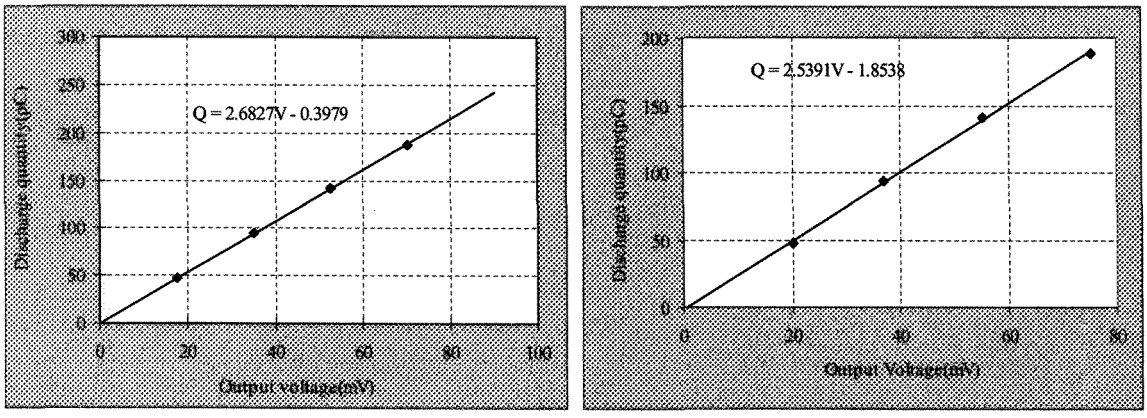

(a). icicle at T=0 °C (b). icicle at T=-5 °C

Figure 3-12 Relationship between the output voltage and the quantity of discharge pulse

3.2.3.4 Data Acquisition Board

Because the signal from the current pulse sensor is analog, a multi-channel acquisition board is used to transform the analog signal into digital signal.

The ADLINK PCI-9820 card shown in Figure 3-13 is a 65 MS/s, high-resolution PCI digitizer with deep SODIMM SDRAM memory that features flexible input configurations, including programmable input ranges and user-selectable input impedance. With the deep on-board acquisition memory, the PCI-9820 is not limited by the PCI's 132 MB/s bandwidth, and can record the waveform for extended periods.

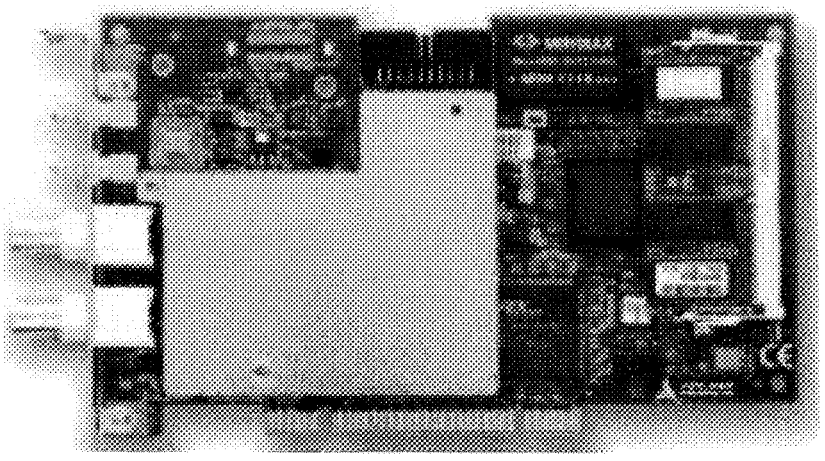

Figure 3-13 Data acquisition card of PCI-9820

The PCI-9820 device features two analog input channels triggered by analog or digital signals. The small signal bandwidth of each channel exceeds 30 MHz, which satisfies the inquest sampling theory. The input ranges are programmable as either ±5 V or ±1 V. The 14 bit A/D resolution makes the PCI-9820 ideal both for time-domain and frequency-domain applications.

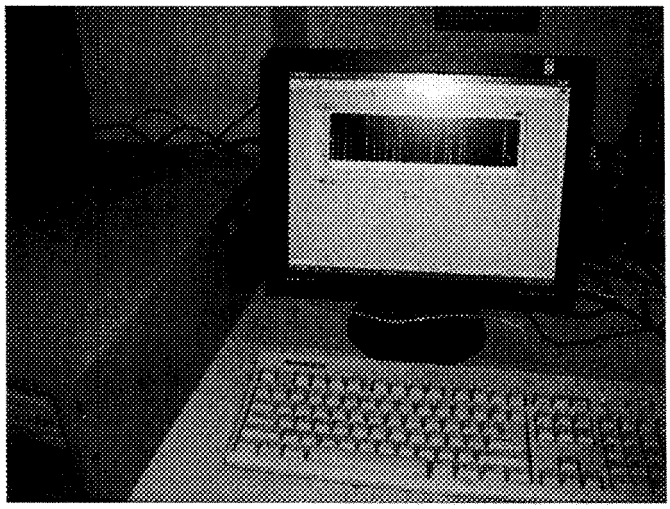

Figure 3-14 Computer to record the discharge current pulses

Once the corona occurs, simultaneously, the discharge current pulses series is detected and stored temporarily in the buffer until the completion of the data acquisition process. It is able to replay, manage, transform, draw live and store data on the PC's hard disk quickly and conveniently. The stored data are then transferred to a PC with a 2.5 GMHz Pentium processor, 1 GM-byte memory, and a 160 G-byte hard disk, presented in Figure

3-14. A sampling program based on Labview 7.0 was installed in this computer to measure and record the discharge current pulse, as shown in Figure 3-14.

3.2.4 Data Process System

In order to further analyze the discharge magnitude and the effect of space charge, it is necessary to extract the time and the magnitude of discharge pulses from each trace with an analysis algorithm illustrated by the flowchart, as shown in Figure 3-15.

The method of extracting the discharge magnitude and corresponding discharge time from the discharge pulse series is illustrated as follows: while reading the input data array, the two empty arrays were initiated to store the voltage amplitude of the discharge pulse and the discharge pulse time, respectively. Before extracting the data, an absolute value of the chosen threshold according to the visual discharge pulse [39][126], was determined, which is slightly higher than the amplitude of the background noise. Then, all vertical values of inputted array were compared with the absolute value of chosen threshold. Until the end of the array, if the voltage amplitude of discharge pulse is higher than the absolute value of a chosen threshold (a discharge pulse occurrence), the completed information including the voltage amplitude of the pulse and the discharge time for every detected point was extracted and stored in two temporary arrays, respectively. In one discharge pulse waveform, the maximum amplitude voltage value of discharge pulse was extracted further and the time according to that point was proposed as the time of discharge activity. Both of them were stored in two arrays: one for the maximum pulse voltage and another for the time point. Afterwards, according to the knowledge of the measurement of the fundamental discharge

quantity [39], and the relationship as shown in Figure 3-12, all discharge pulses were transferred into the discharge magnitudes for the following analysis.

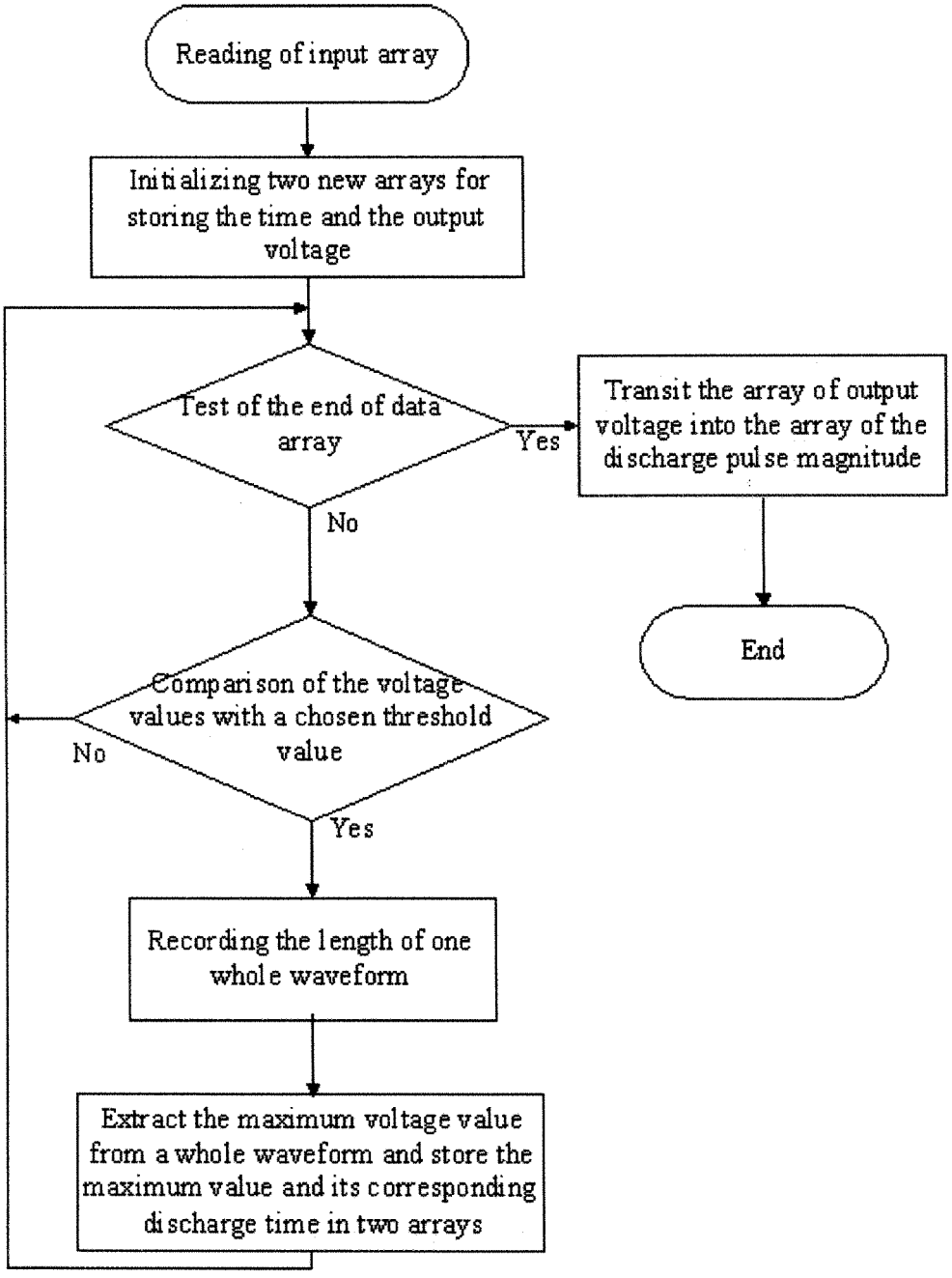

Figure 3-15 Flowchart to extract the discharge time and the discharge pulse magnitude

Due to the stochastic characteristics of corona discharge pulses [20], a data-processing system based on Mathlab 6.5 was designed to analyze the test data. The interface of the data processing system is illustrated in Figure 3-16. This program can handle most statistical analyses such as calculating the mean magnitude, the standard deviation and the relationship between the discharge magnitude and the time interval etc.

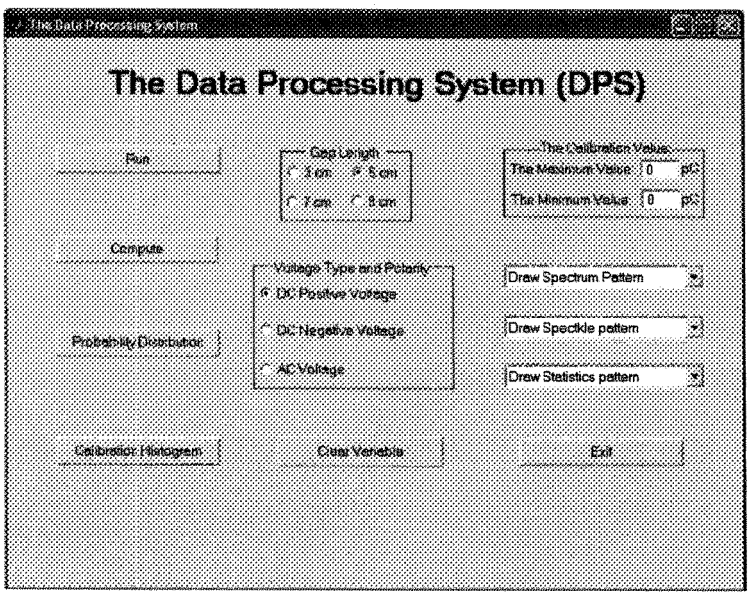

Figure 3-16 Menu of data process system program

3.3 PHYSICAL MODEL: ICICLE AND ICE-COVERED PLATE SYSTEM

3.3.1 Geometric Configurations

Previous investigations have shown that the icicles on real insulators have very complex shapes [41] [44] [47] and that these shapes have been impossible to reproduce. Meanwhile, the insulator surface was also covered by ice accumulation. Corona discharge activities occurring at a sharp point were very sensitive to the electrode dimension and configuration [20] [105]. Thus, a simplified geometric model was necessary to reproduce the natural discharge initiation and early stages along the ice-covered insulators.

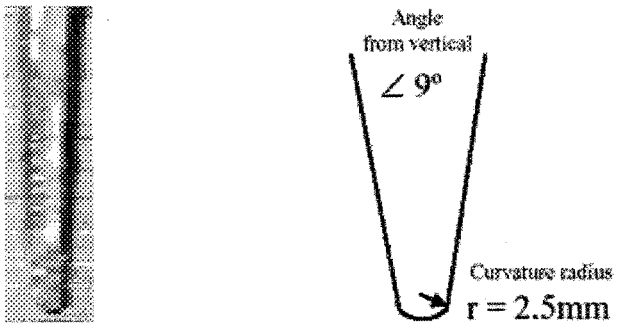

(a): Icicle grown on an energized insulator; (b): Typical parameters

Figure 3-17 Typical icicle shape

The advantage of a simplified geometry is that the investigation can be concentrated on each single experimental parameter without any effects of unexpected conditions. Based on numerous investigations carried out in the CIGELE of UQAC [44] [53], a typical icicle grown on an energized insulator in the laboratory and the corresponding physical parameters

are shown in Figure 3-17. In addition, a plate with radius of 20 cm is included in order to simulate the surface of ice-covered insulators. This icicle to ice-covered plate system was previously used to research the breakdown voltage of air gaps [44] [53] as well. Employing this model with the same geometry configurations is one extension and in accordance with previous investigations of CIGELE.

3.3.2 Procedure of Icicle and Iced Plate Formation

In order to reproduce icicles in a re-occurring manner, they must always have the same geometry configurations to avoid possible influence on the experimental outcome. Several aluminums moulds shown in Figure 3-18 were produced using the representative icicle shape. Water of a given conductivity was frozen in this mould at a constant temperature of –12°C [2][3][19]. A small stainless steel rod was incorporated into the base of the icicle to serve as an electrical contact. After a period of at least 12 hours, the mould was held under tepid water in order to free the icicle. The icicle tip was artificially produced as shown in Figure 3-18 (b).

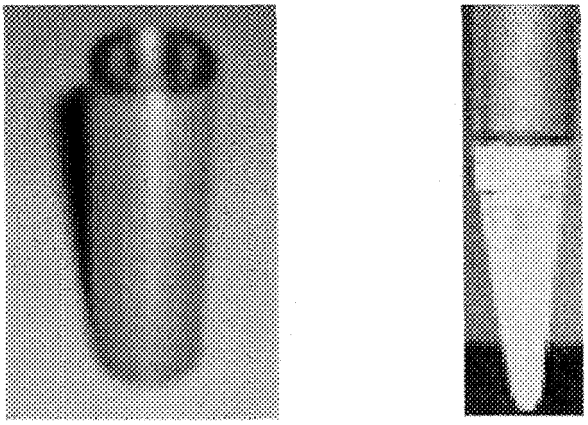

(a): Aluminum mould to form icicle; (b): Artificial icicle

Figure 3-18 Icicle module and artificial icicle

In order to simulate the ice layer on the insulator surface, a round plate with a depth of 2.5mm was filled with water which has been given conductivity and placed horizontally in a small chamber with temperature of -12 °C for 12 hours to form the ice. The parameters of an icicle to ice-covered plate are listed in Table 3-1 and the whole arrangement of the physical model is shown in Figure 3-19.

Table 3-1 Parameters of icicle and ice covered plate gap system

Length of icicle (mm)	Angle of icicle tip(°)	Curvature radius of Icicle(mm)	Radius of plate (mm)	Thickness of ice (mm)
35	18	2.5	200	2

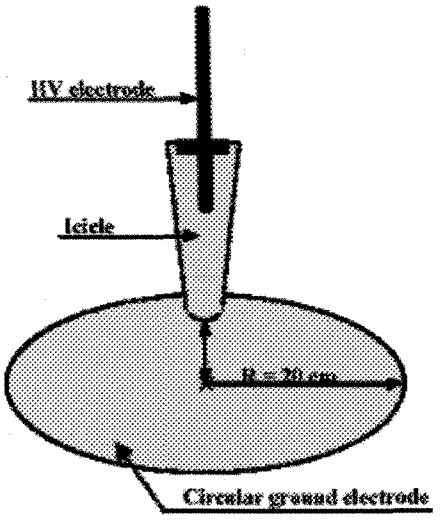

Figure 3-19 Icicle and ice-covered plate electrode system

At least 1 hour prior to the test, the icicle to ice-covered plate system was moved into the climate chamber, in which the temperature and the atmospheric pressure were adjusted to the expected values, and installed.

3.4 EXPERIMENT PARAMETERS

Table 3-2 summarizes the complete range of various experimental parameters in this study. The methods of adjusting the different experimental parameters and the method of measuring the parameters are described in following sections.

Table 3-2 Various experimental parameters in the test

Parameters	Value

Ice type	Glaze
Icing Temperature(°C)	-12±0.2
Environmental temperature during test (°C)	0 °C for "wet" ice
	-5 °C for "dry" ice
Freezing water conductivities (μS/cm)	80 or 320
Atmospheric pressures (kPa)	100,90,80 or 70
Distance of air gap (cm)	3,5,7,or 9
Voltage types	AC or DC

3.4.1 Freezing Water Conductivity

The range of conductivity was chosen in accordance with values observed on natural icing sites [106][107]. In addition, the researches revealed that the influence of freezing water conductivity on flashover voltage of iced insulators is significant [17]. As the present investigation deals with the influence of the total electric conductivity of the ice samples, sodium chloride (NaCl) was used to adjust the conductivity of freezing water. In this study, two different water conductivities, 80 μS/cm and 320 μS/cm, were chosen.

The method of determining the conductivity refers to requirements of a common procedure in the laboratories of **CIGELE of UQAC** [61] and other institutes [52][104][108] are to measure the freezing water conductivity before forming ice and icicles. To obtain water with certain conductivity, NaCl is added to de-ionized water while its conductivity is constantly measured with a conductivity-meter of the type 'YOKOGAWA SC82', until the

desired value of conductivity is reached. By this method, it is ensured that the chosen value is obtained exactly, even if the conductivity of the de-ionized water changes or the salt used is of inconsistent quality. Since the electrical conductivity of water changes with temperature, all the measured conductivity is corrected to a value at the temperature of 20 °C.

3.4.2 Environmental Temperature

It is well known that the flashover voltage depends on the status of ice surface on insulators [31], and it is generally higher on a dry ice surface than that on a wet ice surface. Therefore, two different temperatures were introduced to simulate the characteristics of corona discharge on the two opposite conditions: dry and wet icicle surfaces. Generally, ice at a temperature of -12 °C is considered "dry ice" [29] [34] [36]. However, the researches of ice physics reveals that ice surface status begins to change its solid condition even at the temperature of -39 °C, which is clearly below the melting point. Generally, the thickness of the liquid-like layer increases with an increase in temperature, which ranges between -6 °C<T<-3 °C in different literature [30][32][33].

In this study, due to the limitation in the operation temperatures of CoroCAM IV^{+}, there is very thin liquid-like layer that exists on the ice surface at T=-5 °C, it has still been chosen for simulating relative "dry ice" situations.

The temperature was measured by a digital thermal meter with a resolution of ± 0.1 °C, which is integrated in the control panel of the climate chamber. It may measure the ambient air temperature in the centre of climate chamber. As the air is continuously

circulated inside the climate chamber, the air temperature is considered to be constant through the whole climate chamber.

The icicle and iced plate were installed in the climate chamber about one hour before the test. In order to allow the air temperature of climate chamber to be kept at a stable value, a fan was started to create the air flow, making the temperature inside the chamber uniform and stable, and the heat exchange between the ice and the environment sufficient. Based on these considerations, all environmental temperature values marked in this study may be supposed to be the "icicle surface temperature".

3.4.3 Gap Distance

The existence of air gaps significantly influenced the flashover voltage, and the distance of air gap on the ice-covered insulators varied from 3 to 12 cm [2] [17]. In addition, previous experimental results revealed that the characteristics of corona discharge are influenced by the gap distance. Therefore, the effect of gap distance on the corona discharge was also investigated in this study.

When the icicle and iced plate system is installed, the height of icicle may be adjusted vertically. The gap between them may be determined accurately by using several gauges with constant heights of 1 cm, 2 cm and 5 cm.

3.4.4 Atmospheric Pressure

Air pressure is another important factor influencing the flashover voltage of ice-covered insulators [52][61][101][102]. Some related investigations on flashover voltage at low air pressure have been carried out [61]. In order to simulate the corona discharge at the low air pressure of high altitudes using a vacuum system, the air pressure inside the climate chamber as shown in Figure 3-3 could be adjusted to any value between 101.3 kPa and 30 kPa corresponding to an altitude of 9000 m. According to what is known about discharge, the corona discharge tends to appear as a glow discharge with non-pulse discharge at low air pressure. Hence, in this study, the minimum atmospheric pressures were only controlled down to 70 kPa, corresponding with 3000 m in altitude.

3.4.5 Applied Voltage

In order to investigate the corona characteristics under different voltage polarities and voltage types, all experiments in this study were carried out under AC or DC voltage, respectively.

The AC high voltage systems consisted of a 25 kVA/100kV transformer and a 25 kVA regulator, and the DC voltage is supplied by half-wave rectifier system. The power source is shown in **Figure 3-20**(a).

The DC high voltage system as shown in **Figure 3-20**(b) has a ripple factor, δV. According to the International Standard IEC 60-1 or IEEE Standard.4-1995, δV is defined as follows:

$$\delta V = 0.5(V_{\max} - V_{\min})$$

and it is less than 3%. Therefore, it follows the test requirements.

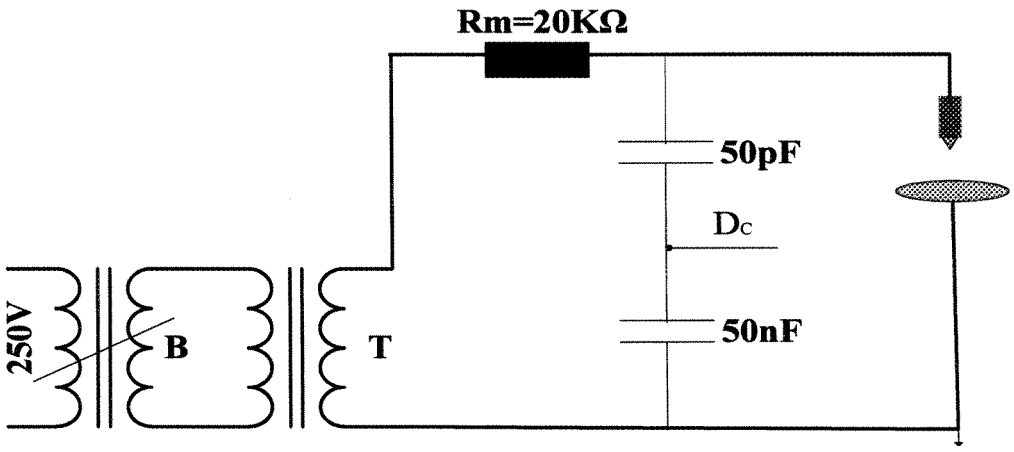

(a) AC

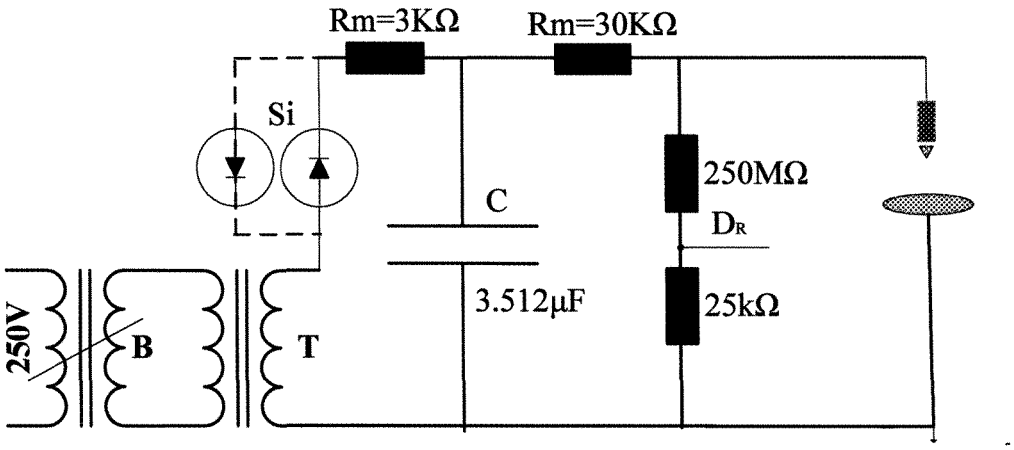

(b) DC

B: Regulator 25k VA/250V; T: Transformer, 100 kV; R_m: Protecting resistor;

Dc: Capacitive voltage divider; D_R: Resistive voltage divider; C: Capacitor;

Figure 3-20 High voltage power supplier system

3.5 TEST PROCEDURE

In order to prevent the corona interference or background noise from testing circuit, an aluminium tube with a diameter of 10 mm was used to connect all devices from transformer to test sample as shown in Figure 3-21. Additionally, some semi-balls were used to eliminate sharp points in connection points. The whole test procedure is expressed in Figure 3-22.

Before the test, the applied voltage was increased gradually without a test sample until the signals of pulse discharge were detected by the detecting system. The voltage level

at this point was normally referred to as the maximum operational voltage (MOV). During the test, all test voltage levels were carried out below the MOV.

The icicle and ice-covered plate electrode were prepared as described previously, and then were installed inside the climate chamber vertically, as shown in Figure 3-1. The temperature inside the climate chamber was adjusted to expected value: -5 °C for simulating "dry" ice and 0 °C for simulating "wet" ice, respectively. The gap distance between the icicle and the iced plate was adjusted in advance as the test requirement.

After installing the electrode, the icicle position in CoroCAM IV$^+$ was adjusted precisely in the middle of CoroCAM IV$^+$ screen as shown in Figure 3-6. If low pressure was needed, the vacuum system was turned on to evacuate the atmospheric pressure down to required value.

The inside of the climate chamber was kept dark. The applied voltage was raised gradually at the rate of 1 kV/s until a certain voltage level was reached, at which point the occurrence of corona or glow was observed by CoroCAM IV+, and the discharge current pulses were recorded. This voltage level was recorded as the corona inception voltage or glow inception voltage (V_{inc}); the test was repeated, the average value of 6 times V_{inc} was determined as V_{inc}. Then, the applied voltage was further increased by a step of 0.5 kV to observe the discharge characteristics at high voltage levels. At every level, the applied voltage was sustained for ten seconds. Meanwhile, the video or picture of the corona or glow discharge was recorded by the computer connecting to CoroCAM IV$^+$ and the corona pulse signals were measured by the computer connecting to the current pulse sensor, simultaneously.

Due to the easy melting property of an icicle tip, the icicle was changed after completing one test, and then all procedures were repeated again.

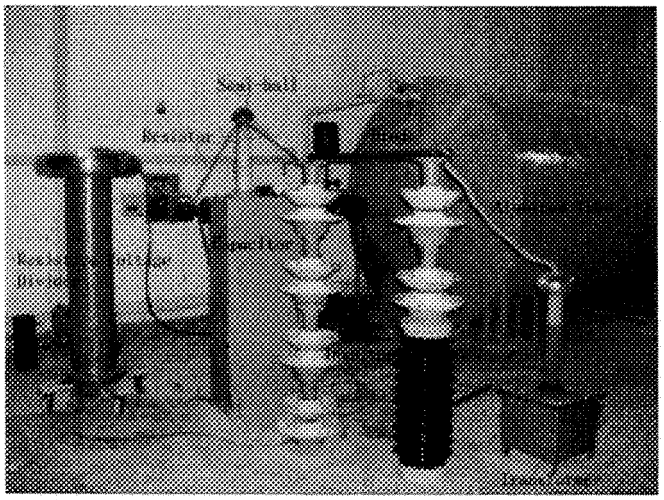

Figure 3-21 Connection circuit under DC voltage

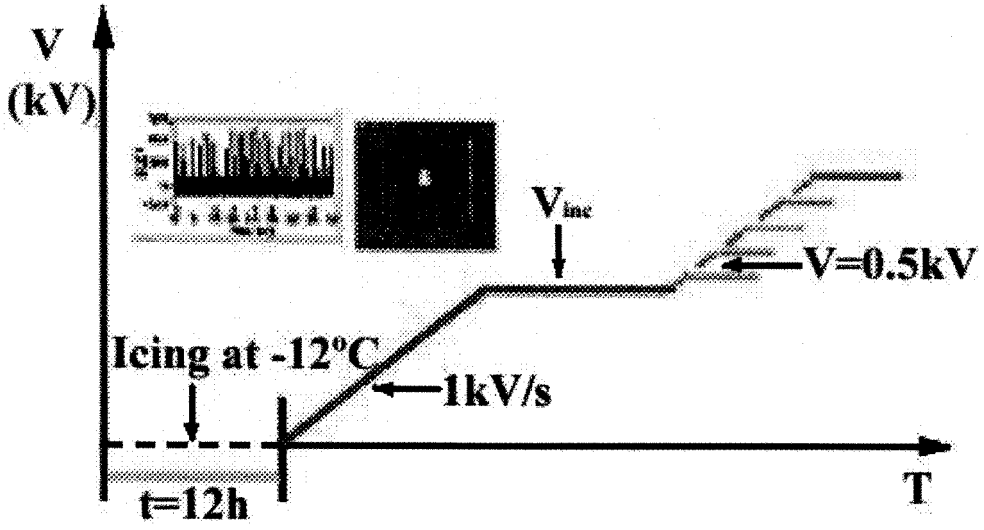

Figure 3-22 Test methodology and procedure

3.6 CONCLUSION

A physical module of an icicle to iced-plate electrode system was proposed to simulate a natural icicle on a real ice-covered insulator surface. A system to detect the corona and corona current pulse was set up. This measurement system had a minimum inter-pulse time resolution of 33 ns and a vertical amplitude resolution of 14 bits. The methods for producing corona, recording the current pulse, and transforming and analyzing the test data were determined.

CHAPTER 4

INCEPTION VOLTAGE AND INCEPTION VOLUME OF CORONA DISCHARGE

CHAPTER 4

CORONA INCEPTION VOLTAGE AND DISCHARGE VOLUME

4.1 INTRODUCTION

The corona discharge is an initial phase of flashover on the ice-covered insulators. Its occurrence is potentially dangerous and may cause some damage to the power systems. However, this discharge is invisible. Hence, its occurrence is often ignored in the investigation of the whole flashover process on the ice-covered insulators. To date, there have been very few investigations on the corona inception, the first step in flashover process, this chapter focuses mainly on this discharge activities.

In this study, V_{inc} is determined by means of CoroCAM IV^{+}. When the applied voltage increases gradually and reaches a certain value, a small discharge volume can be observed with CoroCAM IV^{+}. This voltage level is defined as the corona inception voltage, V_{inc}.

In this chapter, some experiment results on V_{inc} under different conditions are

obtained and discussed. These conditions include the gap distance, the environment temperature, the freezing water conductivity, the voltage type, and the voltage polarity as well as the atmospheric pressure. Then, the discharge volume at V_{inc} under different conditions is presented.

4.2 THE CORONA INCEPTION VOLTAGE (V_{INC})

4.2.1 Effects of Gap Distance

In a given condition of σ=80 μS/cm and T=0 °C, the different gap distances of 3 cm, 5 cm, 7 cm and 9 cm were selected to study on its effect on V_{inc}, and the relationship between them was shown in Figure 4-1,4-2 and 4-3 for DC+, DC- and AC voltage, respectively.

It is observed that V_{inc} increases with an increase in the gap distance and tends to become saturated at long gap distance. When the air gap distance is raised from 3 cm to 9 cm, under DC+ voltage, V_{inc} increases from 19.1 kV to 24 kV. The difference between them is 4.9 kV and the percentage is 20%. Under DC- voltage, V_{inc} increases from 18.6 kV to 23.7 kV. The difference is 5.1 kV, and the percentage of V_{inc} is 27.4%. Under AC voltage, V_{inc} increases from 16.2 kV to 22.7 kV, and V_{inc} increases by 40.1%. It is noticeable that the gap distance has a more obvious influence on V_{inc} under AC voltage than that under DC voltage.

The relationship between V_{inc} and the gap distance is a logarithmic function and can be generally expressed as the following Equation:

$$V = k\ln(d) + b \text{ ---------- (4-1)}$$

Where, V is V_{inc}, in kV, d the air gap distance, in cm, and k, b are constants listed in Table 4-1. The above function is applicable for an icicle to ice-covered plate gap system with a distance ranging from 3 cm to 9 cm at T=0 °C.

The above investigation shows that the influence of gap distance on V_{inc} is consistent between metallic electrodes [110] and icicle electrodes. The different investigations show that the breakdown voltage of an icicle to plane system [53] and the flashover voltage of ice-covered insulators [54] [55] both increase with an increase in the gap distance.

The phenomena above-mentioned can be explained as follows: at long distances, a high voltage is expected to produce the critical electrical field strength at the vicinity of electrode tip, allowing electrons to form avalanches.

Table 4-1 Value of parameters **k** and **b** in V_{inc}

	DC+	DC-	AC
k	4.23	4.49	5.90
b	14.07	13.76	9.49

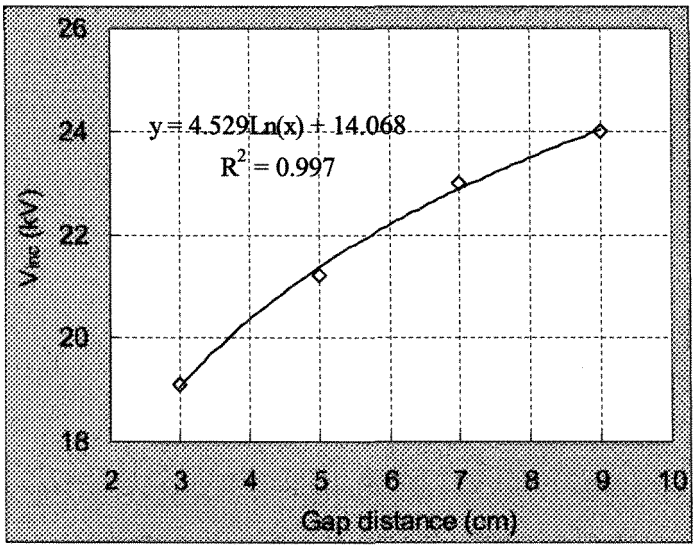

Figure 4-1 Relationship between V_{inc} and the gap distance under DC+ voltage

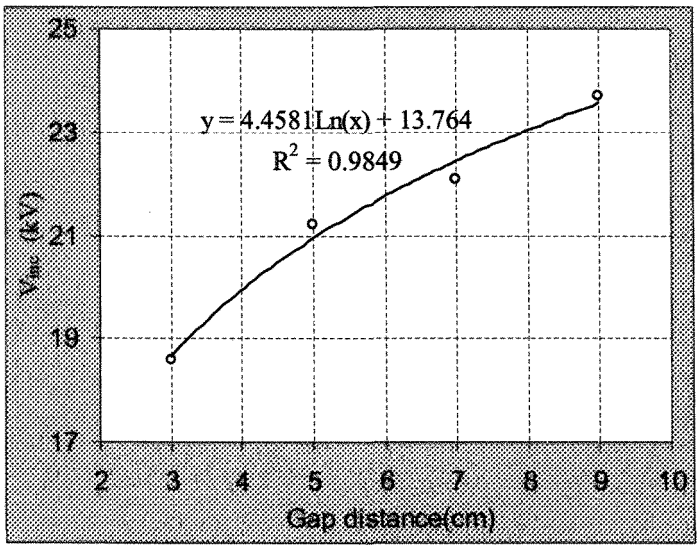

Figure 4-2 Relationship between V_{inc} and the gap distance under DC- voltage

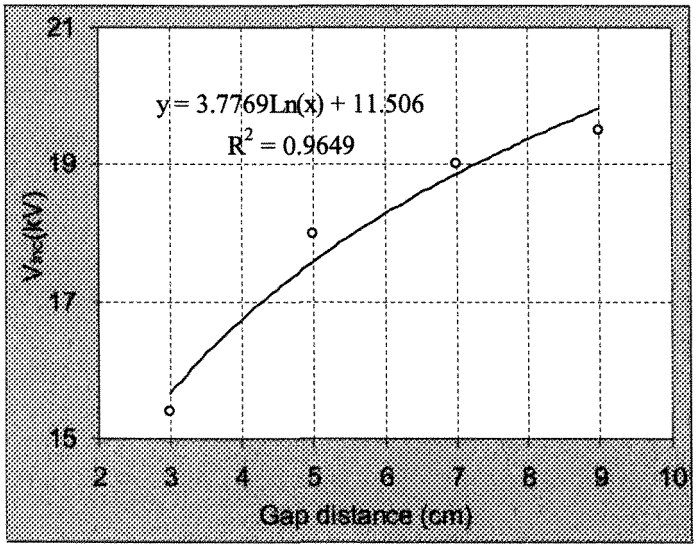

Figure 4-3 Relationship between V_{inc} and the gap distance under AC voltage

The electric field at the vicinity of the electrode was calculated based on the experimental results of V_{inc} using the following equation (4-2) [85]:

$$E_{inc} = \frac{2V}{\ln(\frac{4d}{r})} \cdot \frac{1}{2x + r - (\frac{x^2}{d})} \qquad (4\text{-}2)$$

where, V is the applied voltage, in kV; d the distance between the icicle tip and the ice-covered plate, in cm; r, the icicle radii, in cm and x is the distance between the point calculated and the icicle tip in radial direction, in cm.

When T=0 °C, the calculated results of electric field strength corresponding to V_{inc} under DC+ voltage and DC- voltage are listed in the Table 4-2. Observed that the critical electric field strength of corona discharge is approximately 27 kV/cm, and this is in agreement with the value proposed by **R.Morrow** [111] and slightly lower than that proposed value in [6]. In conclusion, the experimental results are approximately in

agreement with the theoretical values.

Table 4-2 Calculated electric field strength corresponding to V_{inc} at T=0 °C

Gap Distance		3cm	5 cm	7 cm	9 cm	Morrow [111]	Gallagher[112]
Electric field strength (kV/cm)	DC+	27.4	26.8	27	27.3	27	30
	DC-	27.1	26.8	26.2	27.1		

4.2.2 Effects of Environmental Temperature

In given freezing water conductivity of 80 μS/cm, the two temperatures of 0 °C and -5 °C are chosen to compare its effect on V_{inc}. The relationships between them are presented in Figure 4-4, 4-5 and 4-6 under DC+, DC- and AC voltage, respectively.

It may be observed that V_{inc} is obviously affected by the change of temperature, and V_{inc} at T=0°C is noticeably lower than those at T=-5 °C. The difference between V_{inc} at two temperatures increases slightly with an increase in the gap distance.

Under DC+ voltage, Figure 4-4 shows that when the temperature increases from -5 °C to 0 °C, the minimum difference between V_{inc} at two temperatures is 1.7 kV according to d=5 cm, and V_{inc} decreases around 7.9%. However, the maximum difference on V_{inc} between them is 3.2 kV occurring at d= 9 cm, and V_{inc} decreases almost 11.8%.

Under DC- voltage, Figure 4-5 shows that when the temperature increases from -5 °C to 0 °C, the minimum difference between V_{inc} at two temperatures is 2.6 kV

originating at d=3 cm, and V_{inc} decreases 12.3%. The maximum difference is 4.1 kV corresponding to d=9 cm, and V_{inc} decreases 14.6%.

Under AC voltage, Figure 4-6 shows that when the temperature varies from -5 °C to 0 °C, the minimum difference between V_{inc} at two temperatures is 0.8 kV according to d=3 cm, and V_{inc} decreases only 4.9%; however, the maximum difference of V_{inc} between two temperature is 3.2 kV for d= 9 cm, and V_{inc} reduces by 14.1%.

The above result on the influence of temperature on V_{inc} is also in agreement with its influence on the flashover voltage of ice-covered insulators [31], where the flashover voltage on the ice-melting conditions is significantly lower than those for insulators covered by the dry ice.

The influence of temperature on V_{inc} can be explained as follows: although the conductivity of ice made of de-ionized water is roughly independent from the temperature in a range of -20 °C and -0.1 °C, the conductivity of ice surface will change with temperature [32]. Most of the increase in surface conductivity appears between -5 °C and -0.1 °C, which is in accordance with the increase in the thickness of the water film on the ice surface [28]. The conductivity of the water film can reach values as high as ten times that of freezing water conductivity [30]. Thus, an increase in temperature from -5 °C to 0 °C greatly changes the properties of the icicle surface. In addition, the melting process tends to reduce the interfacial free energy, which is more likely to cause discharge occurrence because of increase in electron emission.

In this study, because of the operating limitations of CoroCam IV^{+}, the temperature in the climate chamber could only be set at -5 °C to simulate the dry ice surface. Actually,

the status of the ice surface is not exactly solid and the conductivity increases. Compared to the temperature of 0 °C, the thickness of water film on the icicle surface at -5 °C is still negligible. The ice surface may be considered to approximate "dry" ice.

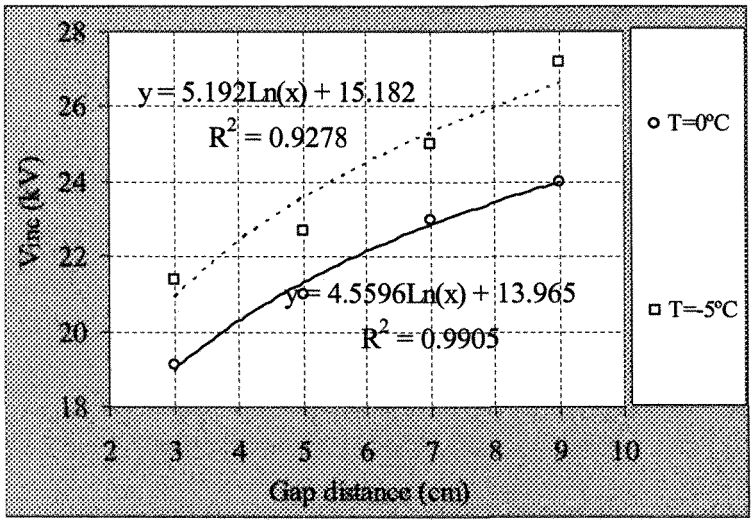

Figure 4-4 V_{inc} at different temperature levels under DC+ voltage

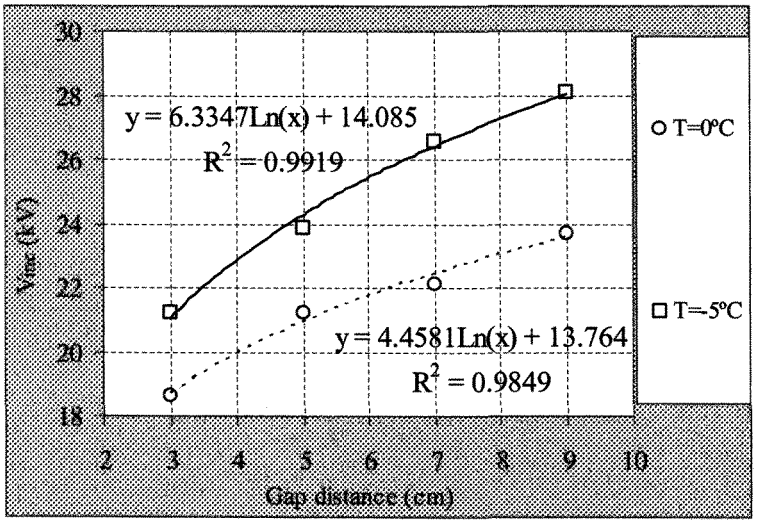

Figure 4-5 V_{inc} at different temperature levels under DC- voltage

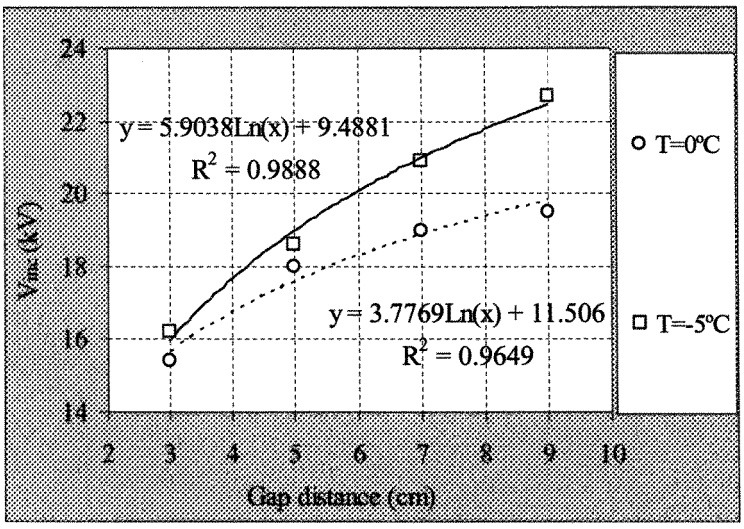

Figure 4-6 V_{inc} at different temperature levels under AC voltage

The electric field strength distribution around the icicle was simulated using the Femlab software at different temperatures. In the calculation, the ice surface at T=0 °C was assumed to have a water film of high conductivity, however, the ice surface at T=-5 °C was considered to be dry, with a very low conductivity. Moreover, the surface charge accumulated on the ice surface is assumed to be negligible as well. The simulation results of the electric field strength for d=5 cm are presented in Figure 4-7. It has been found that the electrical field stress in the vicinity of an icicle tip increases linearly with an increase in gap voltage. At the same applied voltage level, the electric field strength at T=0 °C is evidently higher than that at T=-5 °C. For example, at the applied voltage of 20 kV, the electrical field stress is approximately 23 kV/cm at T=-5 °C and 30 kV/cm at T=0 °C, respectively. This suggests that the voltage drop along the icicle at T=-5 °C is greater than that at T=0 °C for the same applied voltage.

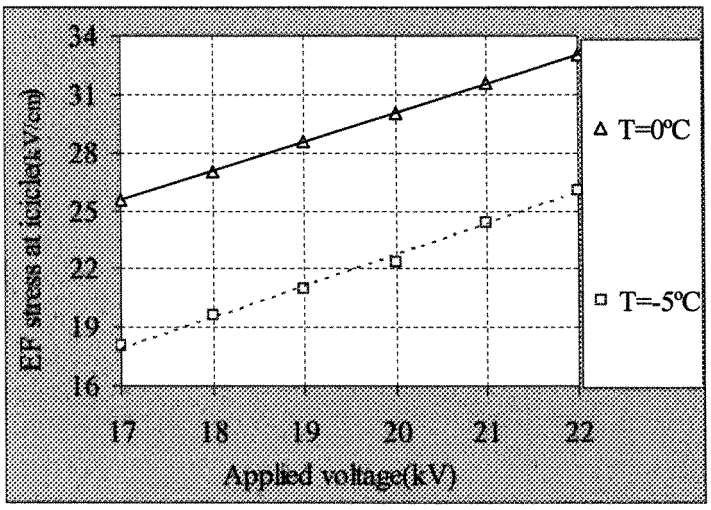

Figure 4-7 Electric field strength under different voltage levels (d=5 cm)

Table 4-3 Simulation parameters during calculation of electric field strength

	Air	Ice at T=-5 °C	Ice at T=0 °C
Relative permittivity ε_r	1	73	81
Water conductivity (μS/cm)	0	0	810
Thickness of water film (mm)	-	1	1

4.2.3 Effects of Freezing Water Conductivity

At the temperatures of 0 °C and -5 °C, two different conductivities of 80 μS/cm and 320 μS/cm were chosen to reveal the relationship between V_{inc} and the water conductivity. All results are presented in Figure 4-8, 4-9 and 4-10, under DC+ voltage, DC- voltage and AC voltage respectively.

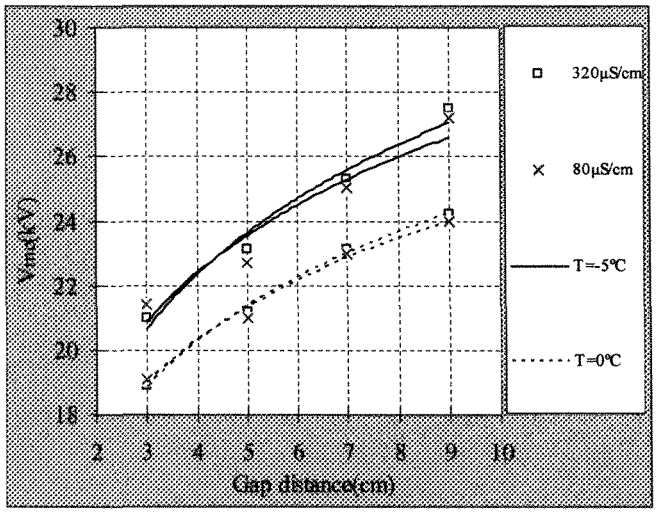

Figure 4-8 Influence of conductivity on V_{inc} under DC+ voltage

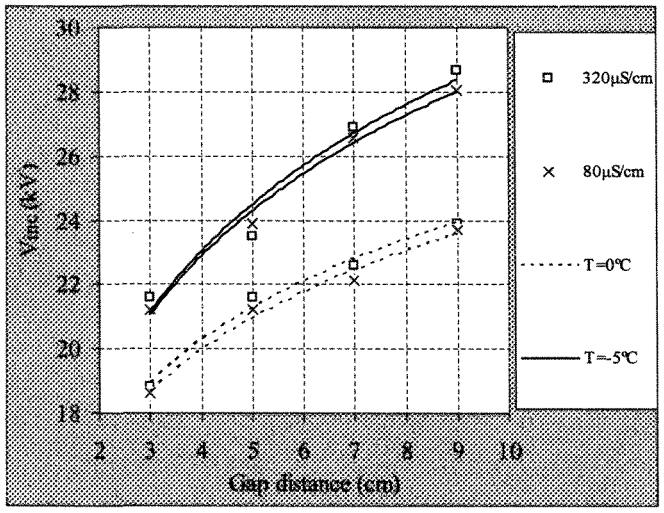

Figure 4-9 Influence of conductivity on V_{inc} under DC- voltage

It has been found that the influence of water conductivity on V_{inc} is not evident. All values of V_{inc} for various gap distances and temperatures under two different conductivities

are incredibly close, and the fitting curve is approximately overlapped.

Under DC+ voltage (Figure 4-8), V_{inc} is slightly higher at σ=320 μS/cm than that at σ=80 μS/cm. The maximum difference between them is only 0.6 kV occurring at d=5 cm and T=-5 °C. When the conductivity decreases from 320 μS/cm to 80 μS/cm, V_{inc} decreases 2.6%. Under DC- voltage (Figure 4-9), it is observed that the maximum difference of V_{inc} is 0.6 kV occurring at a condition of d=9 cm and T=-5 °C. V_{inc} reduces by 2.1% when the conductivity decreases from 320 μS/cm to 80 μS/cm. Under AC voltage (Figure 4-10), the maximum difference of V_{inc} happens at d=9 cm and T=-5°C. It is 0.6 kV, and reduces by 2.6%.

The above results show that the freezing water conductivity has a slight effect on V_{inc}, which does not accord with its influence on the flashover voltage of ice-covered insulators [58] [59] [17] [62]. During the flashover process, arcs will propagate along the ice surface; therefore, the water conductivity of the ice surface will determine the arc properties and influences arc propagation. During the corona discharge, the discharge activities are decided by the electric field strength at the vicinity of icicle for DC+ voltage on the ice surface for DC- voltage. The change of water conductivity does not essentially modify the interfacial free energy, and therefore its influence on V_{inc} is ignored. However, during the temperature change processes, the surface potential energy of the ice surface undertakes a physical change. This is why the surface conductivity does not influence the corona discharge characteristics as the temperature does.

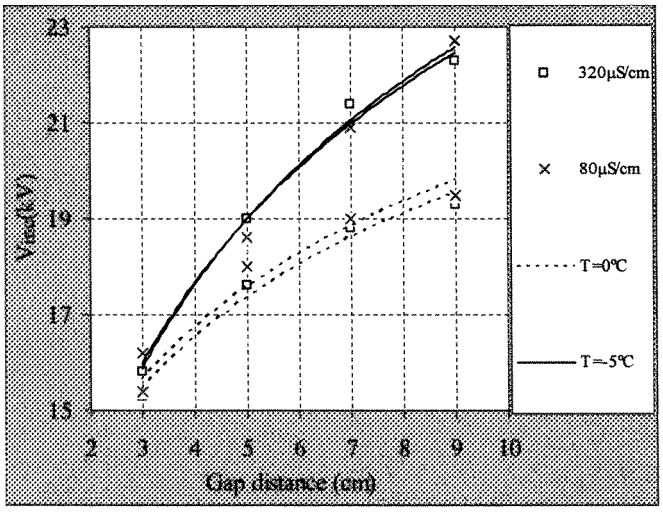

Figure 4-10 Influence of conductivity on V_{inc} under AC voltage

4.2.4 Effect of Voltage Type and Polarity

For a given conductivity of 80 μS/cm, the influence of voltage type and voltage polarity on V_{inc} was investigated; the results are shown in Figure 4-11. Obviously, V_{inc} is affected by both the voltage type and the voltage polarity. In addition, the influence of voltage polarity on V_{inc} is complex under DC voltage, because this influence is different at the different temperatures.

Figure 4-11 shows when the conductivity and temperature are the same, the values of V_{inc} under DC voltage are apparently higher than that under AC voltage. For example, at d=5 cm and T=0 °C, the values of V_{inc} under DC+ and DC- voltages are 3.7 kV and 3.2 kV, i.e. 24% and 20.8% higher than that under AC voltage, respectively.

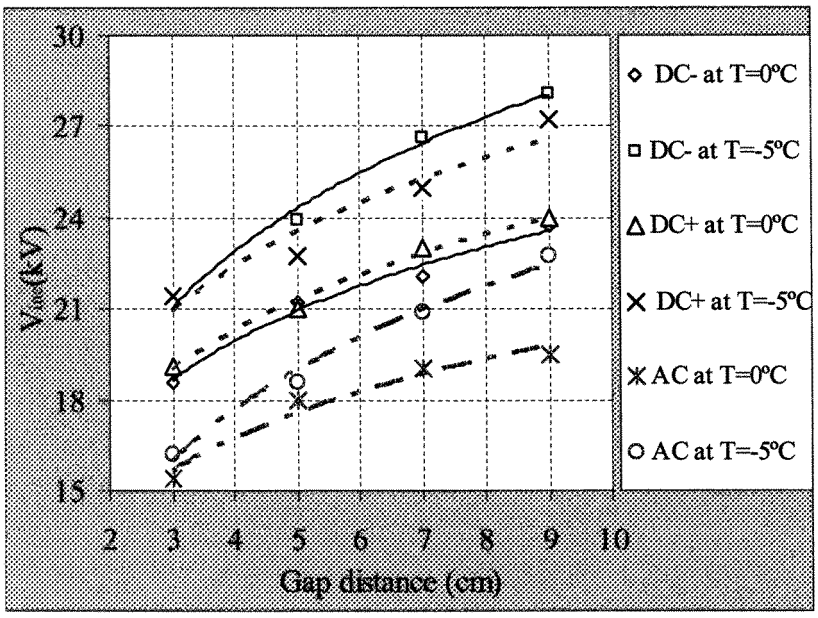

Figure 4-11 V_{inc} under various voltage types and polarities (σ=80 μS/cm)

When T=0 °C, V_{inc} under DC+ voltage is slightly higher than those values under DC- voltage. For example, at a given condition of d=5 cm and σ=80 μS/cm, V_{inc} is 21.2 kV and 21 kV under DC+ and DC- voltage respectively. However, when T=-5 °C, V_{inc} under DC+ voltage is somewhat lower than those under DC- voltage. For example, at a given condition of d=5 cm and σ=80 μS/cm, V_{inc} is 22.7 kV and 23.9 kV respectively under DC+ and DC- voltage. Hence, under DC conditions, the characteristic of V_{inc} is changed by the environment temperature of the icicles.

The investigations on V_{inc} on a metallic electrode have been carried out by different authors [14]. The results show that V_{inc} under DC- voltage is always lower than those under DC+ voltage. It can be observed from Figure 4-11 that V_{inc} is also affected by voltage polarity, but this influence varies with temperature. At T=0 °C, V_{inc} is lower under DC-

than that under DC+ voltage, which is in agreement with the findings using the metallic point-plate system [14]. However, at T=-5 °C, V_{inc} is lower under DC+ than that under DC-, which is not consistent with the results obtained with the metallic electrode. The reason is not yet understood, and more tests would be needed to clarify that.

The above results show a noticeable difference between effect of voltage type on the flashover voltage and V_{inc}. The flashover voltage of ice-covered insulators under AC voltage is always higher than that under DC voltage [2] [19] due to the extinguishing and re-ignition of arcs. However, V_{inc} under AC voltage is lower than that under DC voltage. This can be explained as follows: under AC voltage, the applied voltage is a sinusous function and can be presented as the following equation (4-3):

$$V = V_0 \sin(\varpi \cdot t) \text{ ---------- (4-3)}$$

Under AC voltage, once the instantaneous voltage is higher than V_{inc}, the corona discharge may occur, or else the discharge activities will be suppressed. Generally, under AC voltage, V_{inc} is expressed as $1/\sqrt{2}$ of the peak voltage, which causes a lower V_{inc} This discharge activity does not like the flashover phenomena, which exist extinguish and re-ignition processes of arcs under AC flashover processes, thus, a higher voltage and more energy are needed in the flashover process, which results in a higher flashover voltage.

4.2.5 Effects of Atmospheric Pressures

In order to reveal the influence of atmospheric pressure, P, on V_{inc}, for a given condition of T=0 °C and σ=80 μS/cm, four pressures of 100 kPa, 90 kPa, 80 kPa and 70

kPa are selected to determine the relationship between V_{inc} and P in this study. The pressure of 70 kPa corresponds to the altitude level of 3 km, and the pressure of 100 kPa corresponds to the altitude level of the lab site in CQU.

Under AC and DC+ voltage, the corona discharge generally occurs directly as the glow discharge at low pressure, hence the first discharge voltage observed by CoroCAM IV$^+$ is supposed as V_{inc}. The relationships between the atmospheric pressure and V_{inc} under DC+, DC- and AC voltages are illustrated in Figure 4-12, 4-13 and 4-14 respectively. It has been found that V_{inc} decreases line with a reduction of the atmospheric pressure under DC+ voltage, DC- voltage and AC voltage.

Figure 4-12 shows that under DC+ voltage, V_{inc} is 21.0 kV for 100 kPa and 15.7 kV for 70 kPa respectively when d=5 cm. V_{inc} decreases almost 5.3 kV and 25.3% when the atmospheric pressure decreases from 100 kPa down to 70 kPa.

Figure 4-13 presents that under DC- voltage, when d=5 cm, V_{inc} is 21.2 kV at 100 kPa and 15.7 kV at 70 kPa, and V_{inc} decreases around 5.5 kV in voltage and 24.0% in percentage when the pressure decreases from 100 kPa to 70 kPa.

Figure 4-14 illustrates that under AC voltage, when d=5 cm, V_{inc} is 18.0 kV at 100 kPa and 14.3 kV at 70 kPa, respectively. V_{inc} decreases 3.7 kV in voltage and 20.1% in percentage, when the pressure decreases from 100 kPa down to 70 kPa.

Similar investigations were also carried out using a metallic needle to plate system [112] and a water point electrode to plate electrode system [100]. The result revealed that under AC and DC voltage, V_{inc} declines almost linearly with a reduction of the atmospheric pressure. In addition, the influence of the atmospheric pressure on V_{inc} is also similar to that

on the flashover voltage of ice-covered insulators and polluted insulators [61] [101] [102], in which the flashover voltage decreases with a decrease in the atmospheric pressure. That is, the influence of pressure on V_{inc} and on the flashover voltage is consistent.

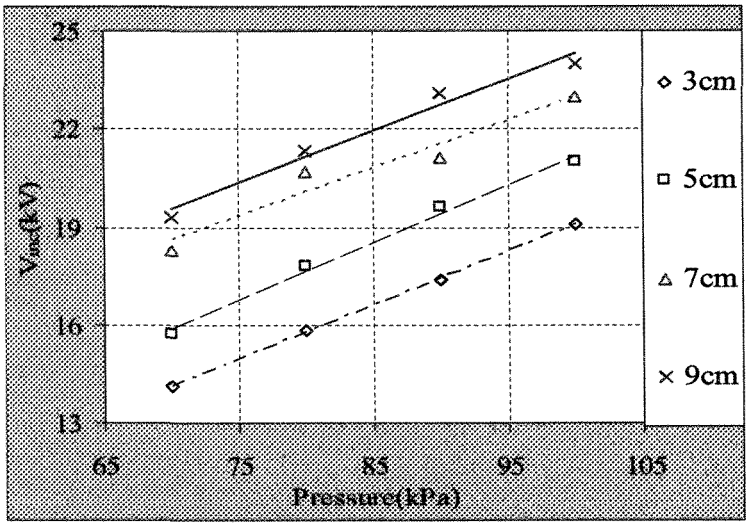

Figure 4-12 V_{inc} vs. the atmospheric pressure under DC+ voltage

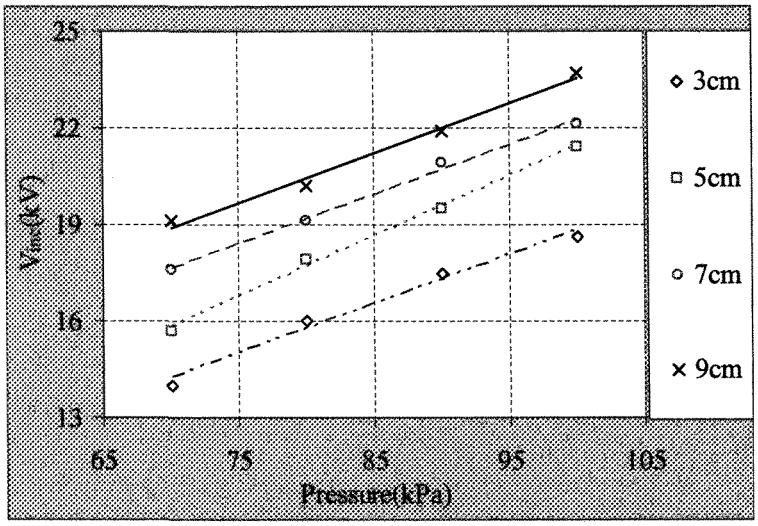

Figure 4-13 V_{inc} vs. the atmospheric pressure under DC- voltage

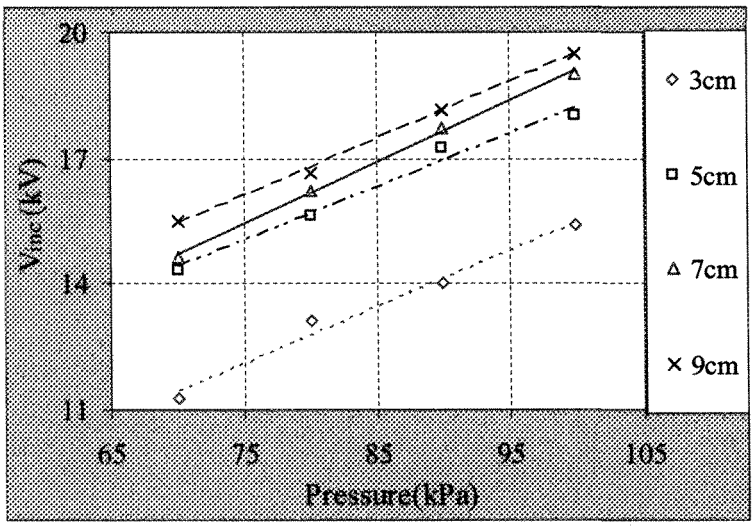

Figure 4-14 V_{inc} vs. the atmospheric pressure under AC voltage

The influence of the atmospheric pressure on V_{inc} can be explained as follows: because the corona discharge is restricted to a critical volume, where $(E/N) > (E/N)_c$. However, under low atmospheric pressure, the density of air, ***N***, decreases, the ionization efficiency can notionally be maintained at a constant level at constant value of ***E/N*** so that the electrical field stress, ***E***, can be reduced in proportion to ***N*** and the atmospheric pressure. Therefore, V_{inc} may be expected to be reasonably low under low pressure.

The relationship between V_{inc} and pressure shown as Figure 4-12, 4-13 and 4-14 can be expressed as following:

$$\frac{V}{V_0} = \left(\frac{P}{P_0}\right)^m \text{ ---------- (4-4)}$$

where, V and V_0 in Equation (4-4) represent V_{inc} at low air pressure P (high altitude) and at

the standard air pressure P_0 (101.3kPa), respectively. m is an exponent, which characterizes the influence of atmospheric pressure on V_{inc}.

In order to determine the relationship between pressure and V_{inc}, all results in Figure 4-12, 4-13 and 4-14 are redrawn by using $Ln(V/V_0)$ and Ln (P/ P_0) and the results are shown in Figure 4-15. Applying the regression analysis to the above results, the value of Exponent m in all conditions are presented in Table 4-4 and the relationship between value of Exponent m and gap distances are determined and presented in Figure 4-16.

Table 4-4 Values of Exponent m under different conditions

	3 cm	5 cm	7 cm	9 cm
DC+	0.851	0.775	0.699	0.622
DC-	0.798	0.764	0.655	0.612
AC	0.851	0.785	0.738	0.656

From Figure 4-16, under both DC and AC voltages, all values of Exponent m decrease with an increase in gap distance, which suggests that the influence of air pressure on V_{inc} is not constant and becomes weak at long air gap. This is different from the influence of the atmospheric pressure on the flashover voltage of polluted or ice-covered insulators, in which, the influence of atmospheric pressure on the flashover voltage of polluted or ice-covered insulators is a constant.

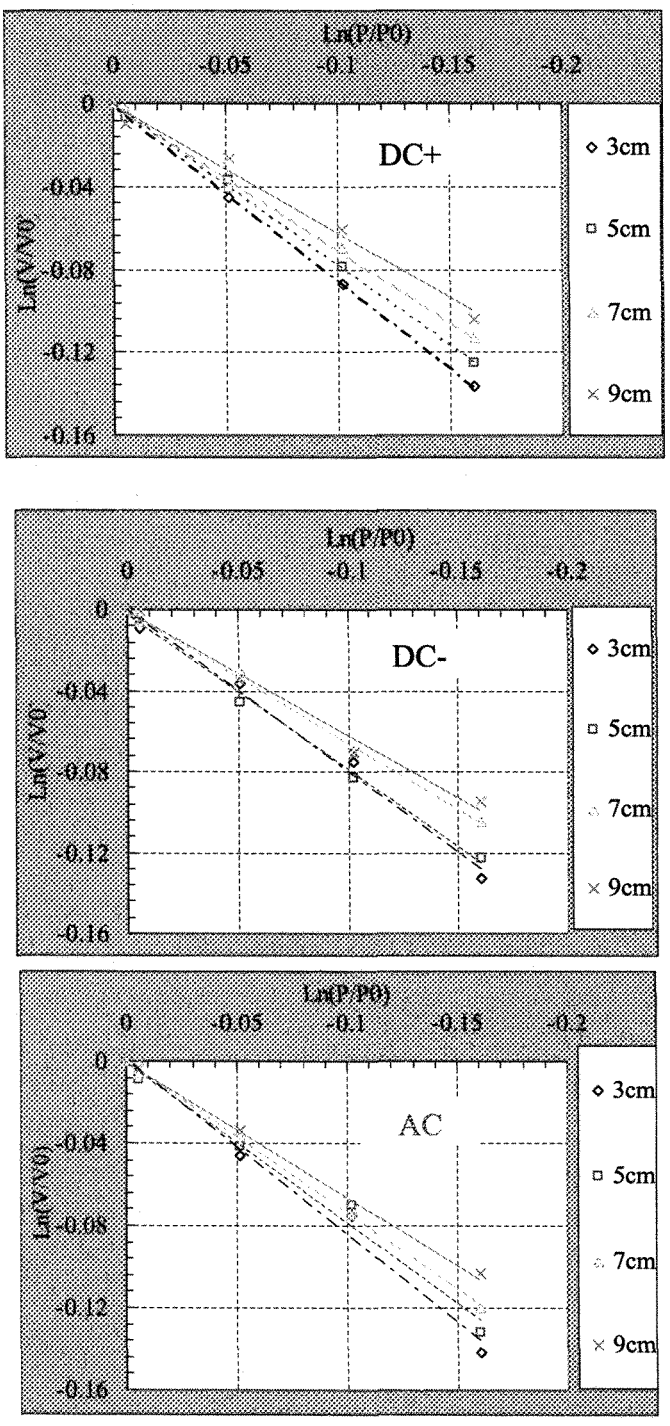

Figure 4-15 Relation between the ratio of V/V_0 and the ratio of P/P_0

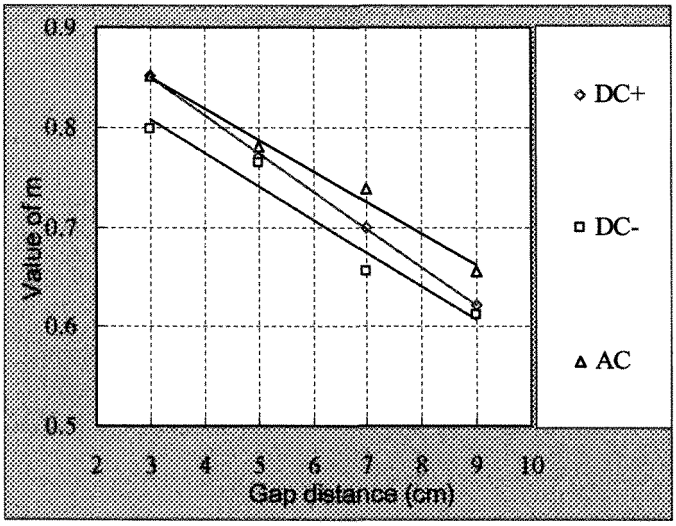

Figure 4-16 Relation between the value of Exponent m and the gap distance

Applying regression analysis to the results in the Figure 4-16, Exponent m may be expressed as a function of gap distance d, shown as in Equation 4-5:

$$m = -a \times d + b \text{ ---------- (4-5)}$$

Where a and b are constants, respectively and listed in Table 4-5

The values of a and b are not obviously affected by voltage type and polarity; therefore, the average value can be suggested in Table 4-5. This relationship is applicable for DC and AC voltage, when the gap distance varies from 3 cm to 9 cm and the atmospheric pressure ranges between 70 kPa and 100 kPa.

Table 4-5 Values of a and b in Exponent m

	DC+	DC-	AC	Mean value
a	-0.038	-0.055	-0.041	-0.045
b	0.963	0.907	0.943	0.938

4.3 THE DISCHARGE VOLUME AT V_{INC}

In order to reveal the corona discharge characteristics, it is necessary to determine the discharge volume at V_{inc} under various conditions. In this study, the discharge volume at V_{inc} is captured at the level of V_{in}. Because the distance between the test sample and CoroCAM IV$^+$ is fixed to be a constant, the scale of corona discharge volume is kept the same. Meanwhile, because of the response limitation of CoroCAM IV$^+$, there is some error while capturing the discharge volume at V_{inc}. Therein, these errors causing certain precise results should be concerned in the following studies.

4.3.1 Effects of Environmental Temperature

For a given condition of d=5 cm, the discharge volume at V_{inc} at the icicle tip at two temperatures of -5 °C and 0 °C as well as that at a metallic electrode are determined and the results are presented in Figure 4-17.

Figure 4-17 shows that the discharge volume at V_{inc} is different at different electrodes. Under DC+ and DC- voltage, the discharge volumes at V_{inc} at icicle are both small points at T=-5 °C, and it increases observably at T=0 °C. The discharge volume at

V_{inc} at the metal electrode is the biggest compared to those at the icicle electrode at different temperatures under DC+ voltage. although, under DC- voltage, a similar phenomenon to that under DC+ voltage can be observed, the influence of change of the temperature on the discharge volume at V_{inc} is not as obvious as that under DC+ voltage.; furthermore, the change is not significant while comparing the discharge volume at V_{inc} at the metal electrode and at the icicle at T=0 °C.

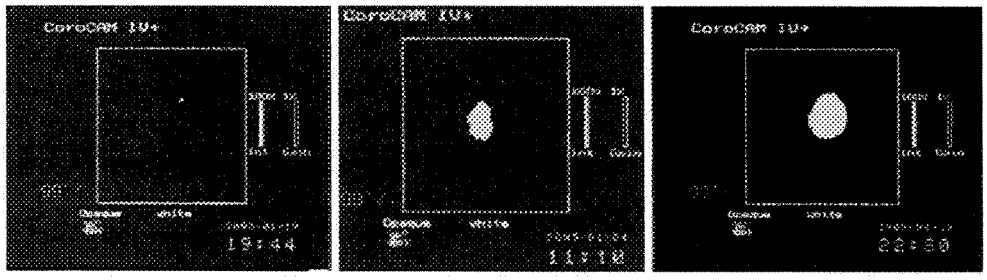

I. T=-5 °C II. T=0 °C III. Metal electrode

(a) DC+ voltage

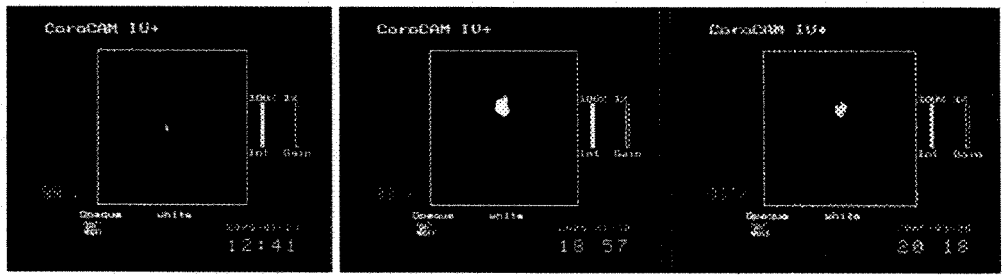

I. T=-5 °C II. T=0 °C III. Metal electrode

(b) DC- voltage

Figure 4-17 the discharge volume at V_{inc} under icicle electrode at different temperatures or metal electrode (d=5 cm)

To date, to the best of my knowledge, no similar investigations have been carried out except that H.W.Bandel [45] mentioned that the discharge at icicle tip could not be seen visually; therefore more tests on the discharge volume at V_{inc} are needed for investigating the influence of icicle tip at different temperature on the discharge volume at V_{inc} in the next studies.

4.3.2 Effects of Gap Distance

In a given condition of T=0 °C and σ=80 μS/cm, the discharge volume at V_{inc} for various gap distances are presented in Figure 4-18.

It may be observed that the discharge volume at V_{inc} reduces constantly with an increase in the gap distance. When the gap distance is 3 cm, the discharge volume at V_{inc} is large. However, when the gap distance increases to 9 cm, it becomes very small. The decrease in the discharge volume at V_{inc} with the gap distance is because the electric field distribution becomes non-uniform in long gap distance, which therefore causes the critical electric field volume to reduce.

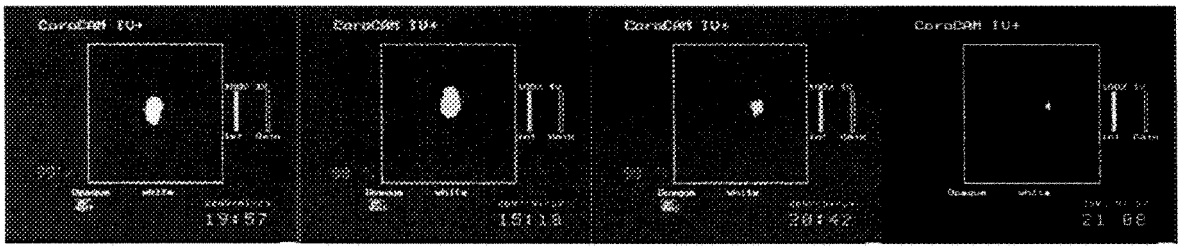

I. 3 cm II. 5 cm III. 7 cm IV. 9 cm

(a) DC+ voltage

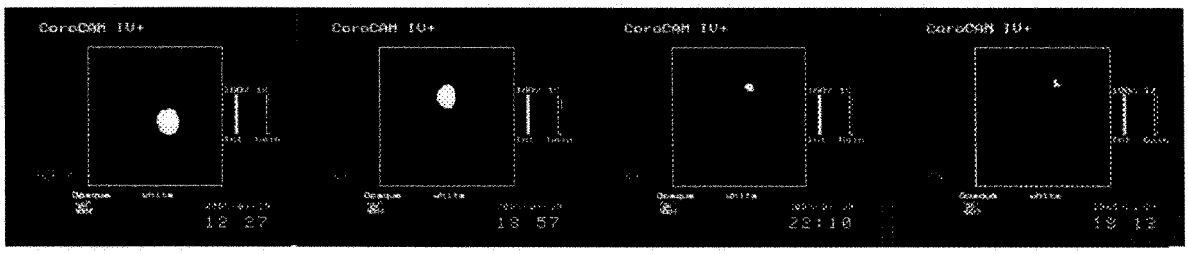

I. 3 cm II. 5 cm III. 7 cm IV. 9 cm

(b) DC- voltage

Figure 4-18 Discharge volume at V_{inc} at different air gap distances

(T=0 °C and σ=80 μS/cm)

4.3.3 Effects of Atmospheric Pressure

For given conditions of d=7 cm and T=0 °C, the discharge volume at V_{inc} at different pressures are shown in Figure 4-19. Noticeably, under low pressure the period of corona discharge is very short and it directly transits into the glow discharge no matter under DC or AC voltage, which causes a relative small discharge volume. Therefore, the glow discharge volume was recorded and concerned as the discharge volume at V_{inc} in this study.

Noted that the discharge volume at V_{inc} is affected significantly by the air pressures and it reduces with a decrease in pressure. The discharge volume at V_{inc} is very evident at P=100 kPa, and diminishes into a very small area at P=70 kPa. Because the discharge volume at low pressure of 70 kPa is so small, sometimes it is very difficult to observe.

The occurrence of glow discharge at low pressure can be explained as follows: the occurrence of glow depends on the formation of the adequately highly concentrated negative ions around the electrode. Under low pressure and low temperature, the lifetime of negative ions is significantly longer than those at the standard environmental conditions due to fewer collisions. Therefore, the density of negative ions in the air is high. This is the reason why the glow discharge occurs more easily at low pressure than at standard pressure. Under DC- voltage or negative half cycle of AC voltage, the work function of the cathode surface depends on its material and is independent from the Electric field strength as well. At the initial discharge stage, fewer initiatory electrons are emitted from the electrode surface; thus, the icicle tip can exist and is not deformed yet, which is a guarantee of glow occurrence under DC- voltage [20] [105].

In addition, the glow discharge at icicle electrodes was observed more frequently compared to the metallic electrode system due to the water molecule existence. The existence of water molecule was also another factor, which increases the probability of negative ion formation, as in the following behavior: $H_2O + e \Leftrightarrow O_2^-(H_2O) + h\nu$

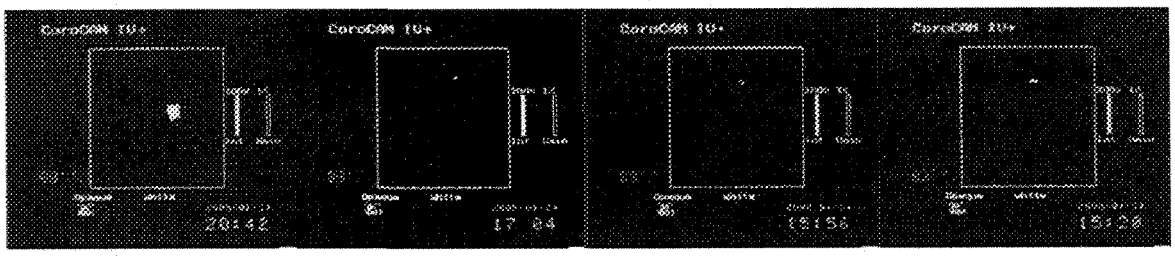

I. 100 kPa II. 90 kPa III. 80 kPa IV. 70 kPa

(a) DC+ voltage

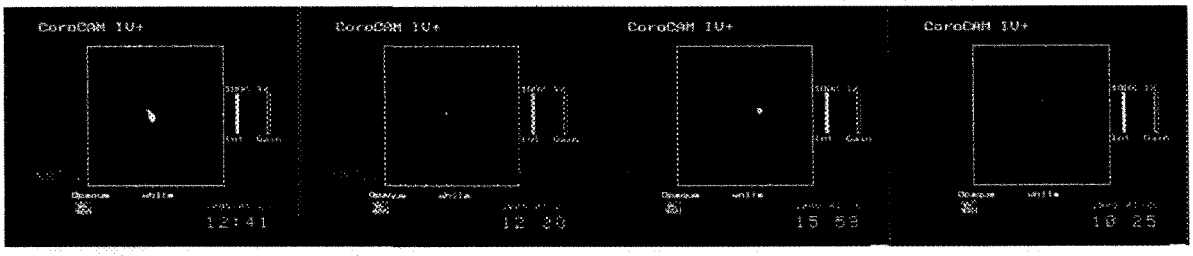

I. 100 kPa II. 90 kPa III. 80 kPa IV. 70 kPa

(b) DC- voltage

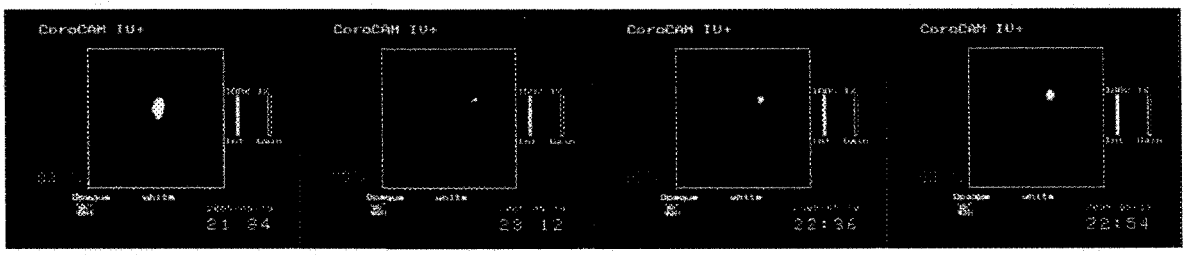

I. 100 kPa II. 90 kPa III. 80 kPa IV. 70 kPa

(c) AC voltage

Figure 4-19 Discharge volume at V_{inc} at the different pressure levels (T=0 °C and d=7 cm)

4.4 CONCLUSIONS

1) V_{inc} increases with an increase in air gap distance in a logarithmic function. The

influence of gap distance on V_{inc} is more evident under AC than that under DC. At T=0°C, the function of V_{inc} with the gap distance can be expressed as follows:

$$\begin{cases} V_{inc}=4.5\ln(d)+14.07 & \text{for DC+ voltage} \\ V_{inc}=4.49\ln(d)+13.76 & \text{for DC- voltage} \\ V_{inc}=5.90\ln(d)+9.49 & \text{for AC voltage} \end{cases}$$

2) The influence of temperature on V_{inc} is significant. V_{inc} at T=0 °C is lower than that at T=-5 °C. However, the freezing water conductivity has a slight effect on V_{inc}.
3) V_{inc} under AC voltage is lower than that under DC voltage. Under DC voltage, the influence of voltage polarity on V_{inc} is different at different temperatures. When T=0 °C, V_{inc} under DC+ voltage is higher than that under DC- voltage; when T=-5 °C, V_{inc} under DC+ voltage is lower than that under DC- voltage.
4) The atmospheric pressure has an evident influence on V_{inc}. V_{inc} decreases with a decrease in the atmospheric pressure, and the influence of pressure on exponent m decreases with an increase in the gap distance. The relationship between them can be expressed as: $m = -0.033 \times d + 0.938$.
5) The discharge volume at V_{inc} increases with an increase in the temperature and decreases with an increase in the gap distance. In addition, it decreases with a decrease in pressure. At low pressure, the corona discharge occurs directly as glow discharge, which causes a small discharge volume.

CHAPTER 5

CHARACTERISTICS OF CORONA CURRENT PULSE

CHAPTER 5

CHARACTERISTICS OF CORONA CURRENT PULSE

5.1 INTRODUCTION

Generally, the corona discharge appears as discharge pulse sequence, and this discharge is called as high frequency discharge. These discharge pulses may be detected by current pulse sensor with perfect frequency-amplitude characteristics. The related introduction on the current pulse sensor has been described in Section 3.2.3.

This chapter mainly discusses the corona discharge processes and the corresponding current pulse series under various voltage levels. Furthermore, the repetition rate of discharge current pulse and the waveforms of current pulse are revealed and analyzed in detail under some selected parameters. These parameters include:

- Environment temperature;
- Gap distance;
- Voltage type;
- Voltage polarity;

- Atmospheric pressure.

5.2 CORONA DISCHARGE PROCESS

5.2.1 Corona Discharge Process under DC+ Voltage

For a given condition of d=5 cm, σ=80 μS/cm and T=0 °C, the corona discharge process and its current pulse sequence are presented in Figure 5-1 under DC+ voltage.

Figure 5-1 shows that at first, the corona discharge volume increases with an increase in the applied voltage; meanwhile, the frequency of the discharge current pulse increases significantly as well. When the applied voltage is higher than 22 kV, the discharge volume does not increase with an increase in applied voltage any more, and in fact decreases inversely with an increase in the applied voltage. Meanwhile, the discharge pulse frequency decreases too. When the applied voltage increases up to 25 kV, the discharge mode is transited into a relatively stable discharge phenomenon, generally called as the glow discharge [75][105]. In this discharge mode, the discharge volume is not sensitive to the change of applied voltage any more and keeps stable. In addition, there are no discharge current pulses can be detected for glow discharge.

The glow discharge phenomena have been verified in many studies [20][105]. They concluded that the glow discharge only occurs when the concentration of negative ions is high enough [105][116]. It is well known that the shape of icicle electrodes does not change during the discharge process under DC+ voltage. At higher applied voltage, the repetition rate of discharge pulse increases radically. Therefore, more electrons are

produced and attached to molecules to form negative ions, which will cause the glow discharge.

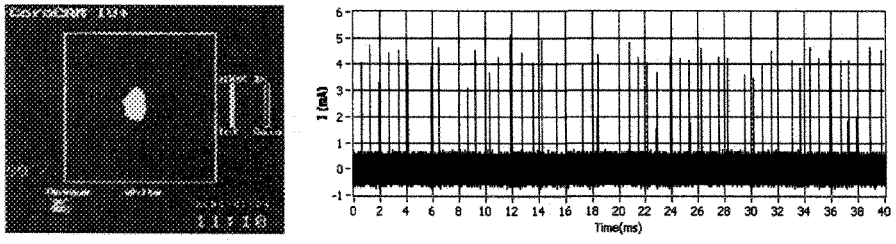

a. V=21 kV

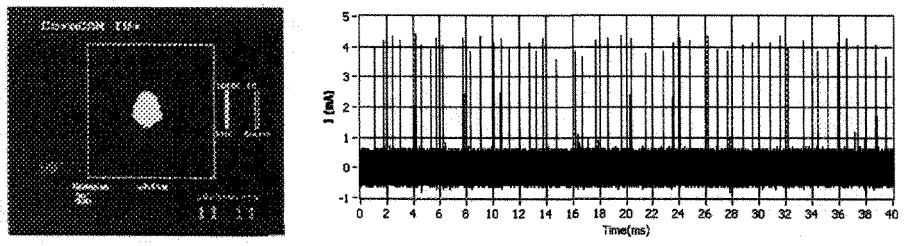

b. V=22 kV

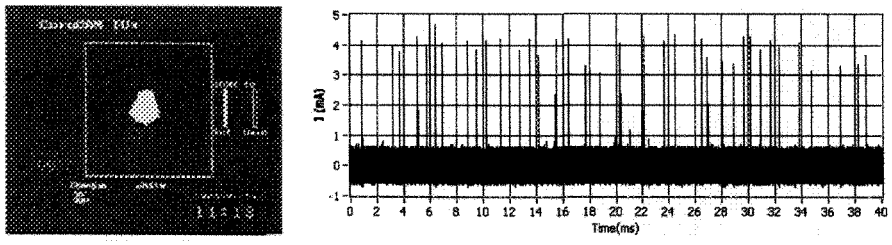

c. V=23 kV

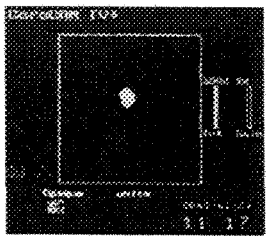

d. V=25 kV

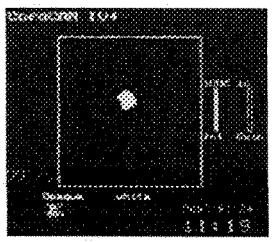

e. V=26 kV

Figure 5-1 Discharge volume and corresponding current pulse sequence under DC+ voltage (d=5 cm, σ=80 μS/cm and T=0 °C)

5.2.2 Corona Discharge Process under DC- Voltage

In a given condition of d=5 cm, σ=80 μS/cm and T=0 °C, the corona discharge processes and their corresponding current pulse sequence are shown in Figure 5-2 under DC- voltage.

Figure 5-2 shows that under DC- voltage, the corona discharge volume increases strictly and becomes more and more irregular with an increase in applied voltage. As the applied voltage increases from 22 kV to 23 kV, the amplitude and the repetition rate of discharge pulses both increases significantly. When the applied voltage is higher than 24 kV, the repetition rate of the discharge pulse decreases, but the amplitude of the discharge current pulse increases. If the applied voltage is high up to 42 kV, another small discharge volume can be observed close to the anode (iced plate). The amplitude of the discharge current pulse is 10 times higher than those at low voltage levels. During the whole discharge process, no glow discharge phenomenon can be observed; therefore, it is different from that under DC+ voltage. Comparisons between DC+ and DC- voltage show that there is no glow discharge observed under DC- voltage, and the discharge current pulse is less uniform under DC- than that under DC+ voltage.

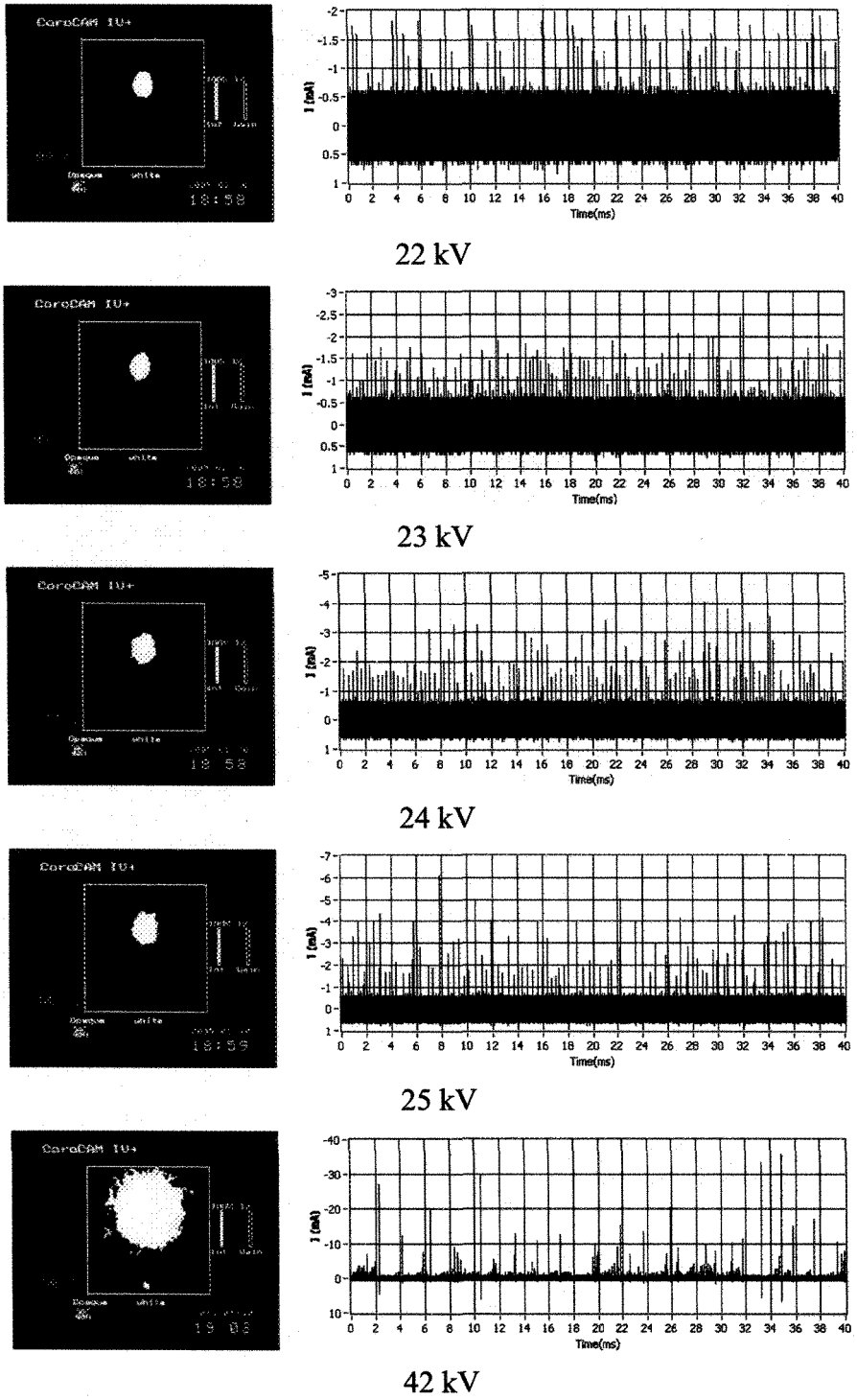

Figure 5-2 Discharge volume and corresponding current pulse series under DC- voltage

(d=5 cm, σ=80 μS/cm and T=0 °C)

5.2.3 Corona Discharge Process under AC Voltage

For a given condition of d=5 cm, σ=80 μS/cm and T=0 °C, the corona discharge phenomena and their corresponding discharge pulse series are shown in Figure 5-3 under AC voltage.

Figure 5-3 shows that the corona discharge volume increases with an increase in the applied voltage up to 19 kV. When the applied voltage is above 19 kV, the discharge volume begins to decrease and transits into the glow discharge at 20 kV. If the applied voltage increases further up to 35 kV, another discharge volume close to the ice-covered plate can be observed. In addition, the discharge pulses occur cyclically and periodically. In some parts, there is no discharge pulse detected. Consequently, the repetition rate of discharge pulse is much less compared to that under DC voltage. For glow discharge, the repetition rate of the discharge pulse decreases in the positive half-cycle. At 20 kV and 22 kV, there is only one discharge pulse detected in each positive half-cycle. However, it increases slightly in the negative half-cycle. The amplitude of the discharge current pulse in the positive half cycle is significantly higher than that in the negative half cycle.

The discharge phenomena are significantly more complex under AC voltage than that under DC voltage, and this complication presents comprehensive characteristics of two polarities of DC voltage. For example, the glow mode may be observed as it is under DC+ voltage and another discharge volume occurs close to the plane as it does under DC- voltage.

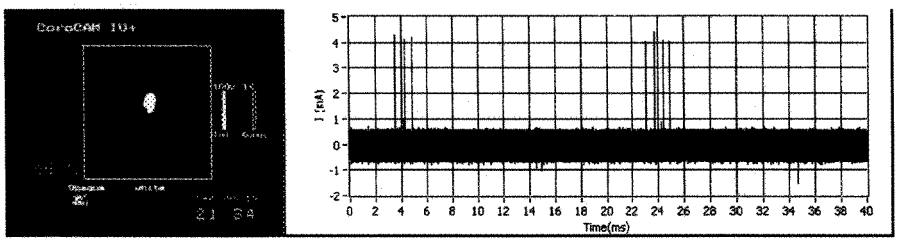

18.4 kV

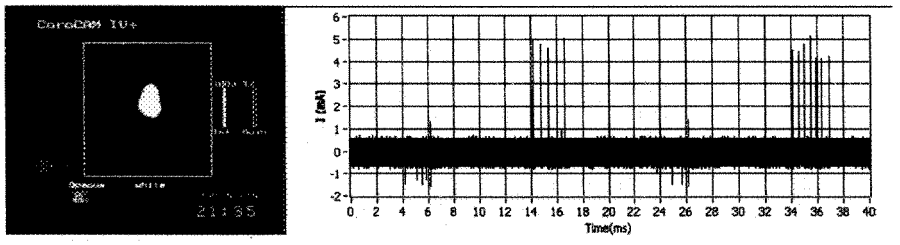

19 kV

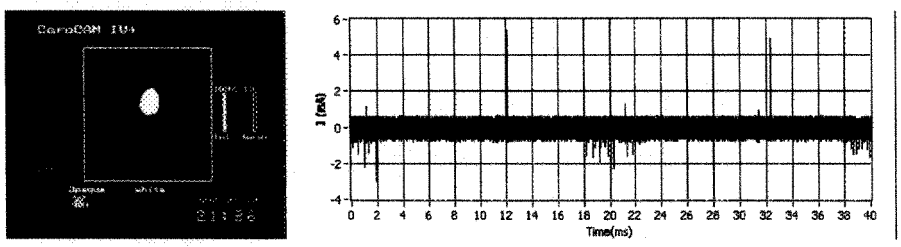

20 kV

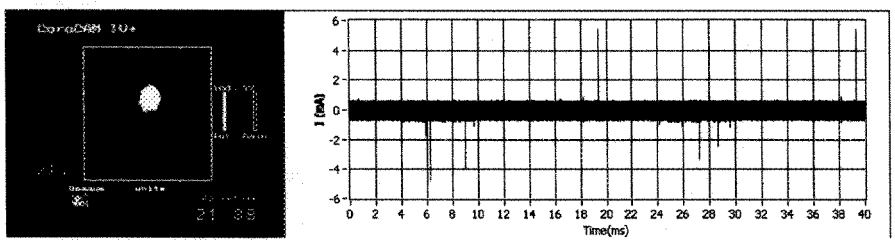

22 kV

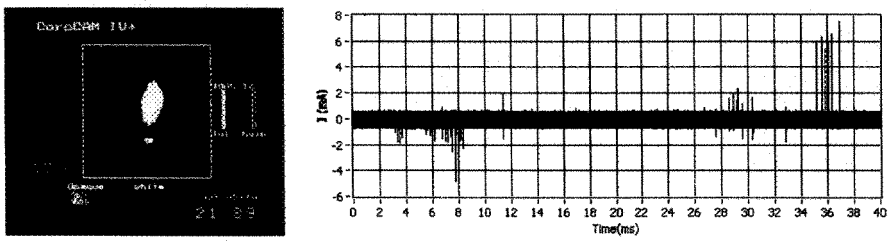

35 kV

Figure 5-3 Discharge volume and corresponding current pulses under AC voltage

(d=5 cm, σ=80 μS/cm and T=0 °C)

The comprehensive phenomena under AC voltage can be interpreted as follows: under AC voltage, the periods of ionization are much shorter than those under DC- and DC+ conditions due to the variation of instantaneous voltage and the reversal of its polarity. The initial electron emission also depends on the applied voltage. As long as the instantaneous voltage is higher than V_{inc}, the influence of AC voltage on the corona discharge can be discussed in the same way as DC voltage by the different polarities. Hence, the discharge characteristics under the positive half cycle of AC is the same as that under DC+ voltage, and that under the negative half-cycle is similar to that under DC- voltage.

5.3 Effects of Corona Discharge on the Icicle Tip Shape

In the tests, although each icicle electrode was only used once, it was found that the corona discharge activities have some influence on the icicle tip depending on the voltage type or the voltage polarity. The shape of the icicle electrode are captured and compared before and after every test by CoroCAM IV^+ and the results are presented in Figure 5-4.

The results in Figure 5-4 show that the shape of icicle tip does not change under DC+ voltage, but the icicle shapes are flattened significantly by the corona discharge activities under DC- and AC voltage. Hence, the influence of corona discharge activities on the icicle shape depends on the voltage type, and the corona discharge under DC- voltage or

AC voltage has more evident influence on the shape of icicle electrode than that under DC+ voltage.

The phenomenon of icicle erosion occurs mainly at DC- voltage or the negative half-cycle of AC conditions, and the reason can be interpreted as follows: Under DC+ voltage conditions, the initiatory electrons may originate in any part of the whole critical volume, which means that the initiation process is much less localized [20][105]. However, under DC- voltage, the first electrons are supplied solely from a small region of the cathode's surface due to the collisions between the positive ions, the photoelectrons and the cathode or electron emission [105]. The mass of positive ions is much bigger than that of the electrons, despite the surface of the ice being bombarded by positive ions under DC- and by electrons under DC+, whereas the energy due to the bombardment of ice is about 3 times higher under DC- than that under DC+ voltage [50]. Both of them are localized and cause temperature increase or icicle-tip melting. Because the energy is different, more superficial melting processes may be expected under DC- voltage than that under DC+ voltage. Consequently, the discharge mechanism under the negative half-cycle of AC conditions is consistent with that under DC- conditions, and therefore, it can be expected that the damage of icicle tip mainly occurs under DC- voltage or the negative half-cycle of AC voltage.

This influence of corona discharge on the icicle's shape was also mentioned by **Y. Teisseyre et al.** [113]. They found that the erosion of an icicle is evident due to the corona discharge and the ionic wind velocity. Furthermore, **M. Farzaneh et al** [114] confirmed

that the loss in ice volume was more severe under DC- voltage than that under DC+ voltage. Therefore, the experiment test is in agreement with existed studies [114].

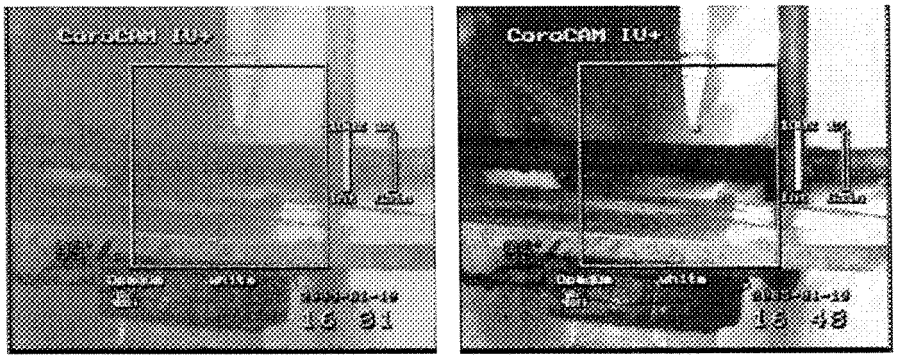

Before testing (a) DC+ after testing

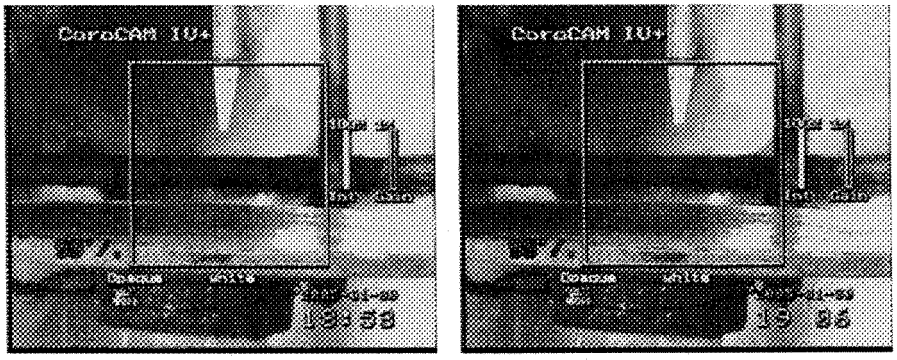

Before testing (b) DC- after testing

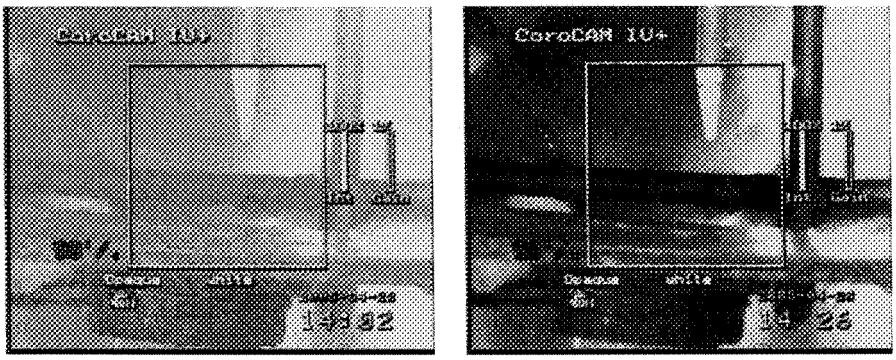

Before testing (c) AC after testing

Figure 5-4 Influence of corona discharge on the icicle tip shape

5.4 REPETITION RATE OF DISCHARGE CURRENT PULSE

5.4.1 Environmental Temperature

To compare the repetition rate of discharge pulses, icicles with gap distances of 5cm, at different temperatures of -5 °C and 0 °C, are chosen. In addition, a metal electrode is used to compare its effect as well. All results are presented in **Figure 5-5**.

Under DC+ (**Figure 5-5**(a)), the repetition rate of discharge pulses is affected by the change of the applied voltage, i.e., it increases first and then decreases. The maximum value of repetition rate is approximately 2460 per second at T=0 °C, and 700 per second at T=-5 °C. Obviously, it is much higher at T=0 °C than that at T=-5 °C. Under metal electrode the maximum value is around 2265 per second, and that is almost the same as that at T=0 °C and significantly higher than that at T=-5 °C.

Under DC- voltage (**Figure 5-5**(b)), the relationship between the repetition rate of discharge pulses and the applied voltage is different from that under DC+ voltage. When T=0 °C, the repetition rate of the discharge pulse first increases and then decreases with an increase in the applied voltage. However, for the icicle electrode at T=-5 °C and for the metal electrode, the repetition rate of discharge current pulse always increases with an increase in the applied voltage, which is in agreement with [105], thus the repetition rate of the discharge current pulse increases with all discharge. Hence, the phenomenon is not similar between the stainless steel and the icicle electrode with T=0 °C.

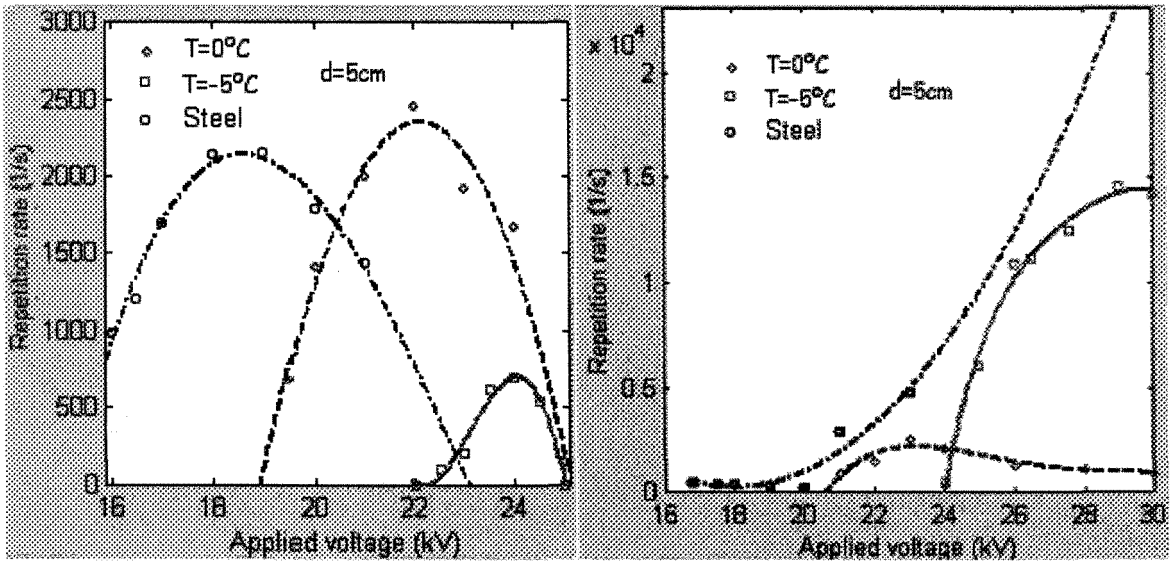

(a).DC+ (b).DC-

Figure 5-5: Repetition rate of discharge current pulse at icicle with different temperatures and metal electrode (σ= 80 μS/cm and d=5 cm)

5.4.2 Gap Distance

It is known that the ice at T=0 °C is potentially more dangerous to the power systems. Hence, in this study, the focus is mainly on the icicle at T=0 °C. In a given condition of T=0 °C and σ=80 μS/cm, the relationship between the repetition rate of the discharge pulses and the gap distance is investigated, and the results are presented in Figure 5-6.

Although all the repetition rates of the discharge current pulse vary with the applied voltage, the maximum value of the repetition rate is affected by the change in the gap

distance. It increases with an increase in gap distance. For example, under DC+ voltage, the maximum value is 1645, 2460 and 2980 per-second for 3 cm, 5 cm and 7 cm, respectively. Under DC- voltage, it is 2376, 2540 and 3060 per second for 3 cm, 5 cm and 7 cm, respectively.

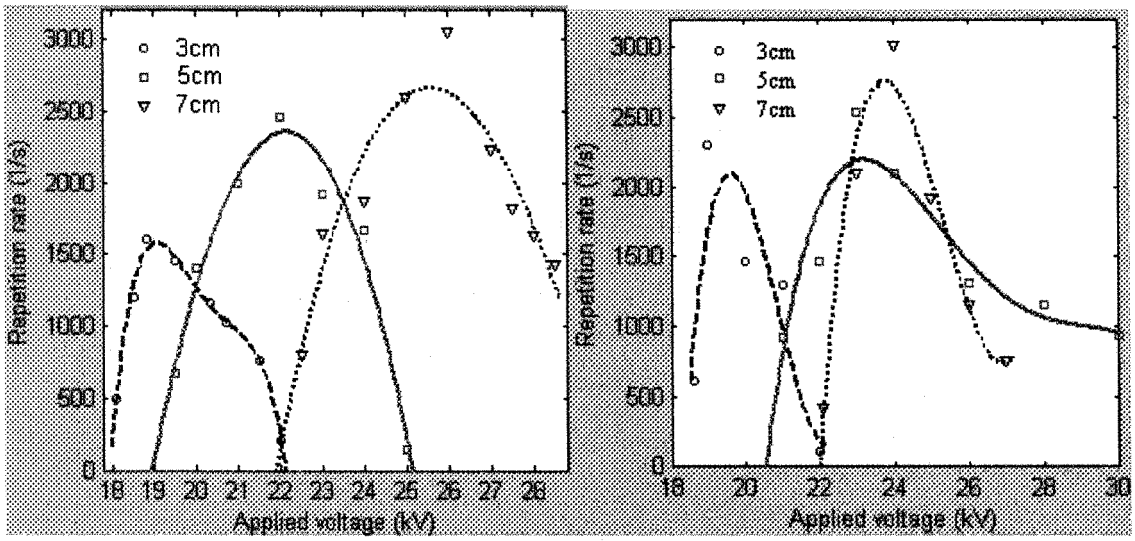

(a).DC+ (b).DC-

Figure 5-6 Discharge repetition rate for various gap distances

(σ=80 μS/cm and T=0 °C)

5.4.3 Voltage Type

In a given condition of σ=80 μS/cm, T=0 °C and d=5 cm, the influence of voltage type on the repetition rate of the discharge current pulses are investigated and the results are presented in **Figure 5-7**. The maximum value of the repetition rate of discharge pulses is much higher under DC voltage than that under AC voltage.

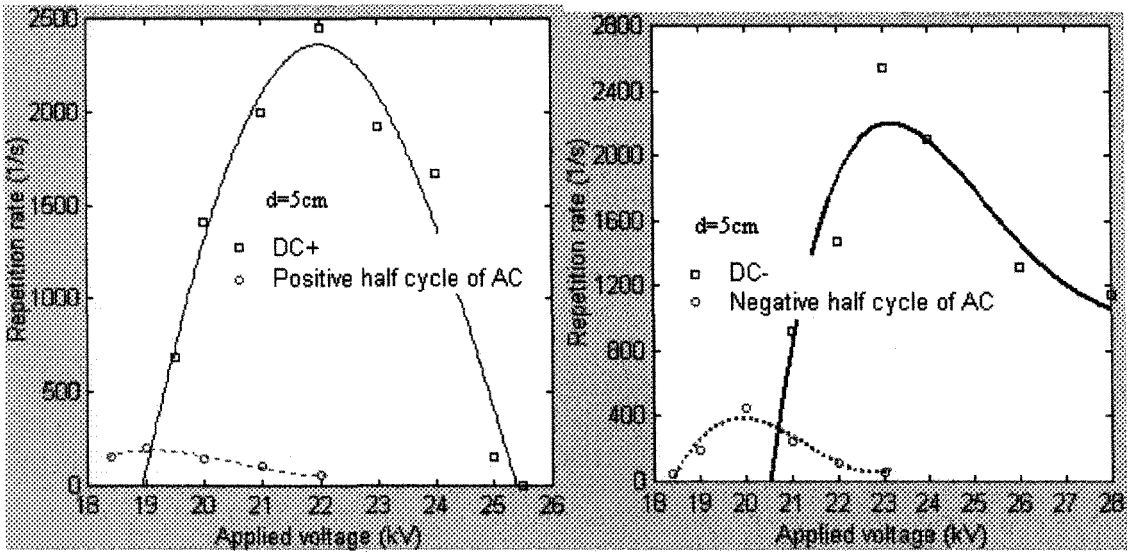

(a) (b)

(a). the repetition rate of discharge pulse under DC+ and the positive half-cycle of AC,

(b). the repetition rate of discharge pulse under DC- and the negative half-cycle of AC.

Figure 5-7 Discharge repetition rate under different voltage types (σ=80 μS/cm, T=0 °C)

The maximum value of the repetition rate under DC+ voltage is around 2460 per second at 22 kV. However, it is less than 200 per second under the positive half-cycle of AC voltage at 19 kV. The maximum value of discharge frequency is 2540 per second under DC- voltage, but it decreases to 460 per second under the negative half cycle of AC voltage. The reason that the maximum value of the repetition rate of the discharge pulses under AC voltage is less than that under DC voltage is that AC voltage has a shorter period of ionization compared to DC voltage and the amplitude value of AC voltage is varied as well, which affects the repetition rate of the discharge pulse.

5.5 WAVEFORM OF CORONA DISCHARGE CURRENT PULSE

5.5.1 Voltage Polarity

In the case of DC voltage and d=5 cm, the typical waveforms of the discharge current pulse obtained on the metallic electrode and the icicle electrode at T=0 °C are presented in **Figure 5-8**. The time interval between two consecutive points is a constant of 33 ns. Hence, the duration of current waveform is proportional to the point number.

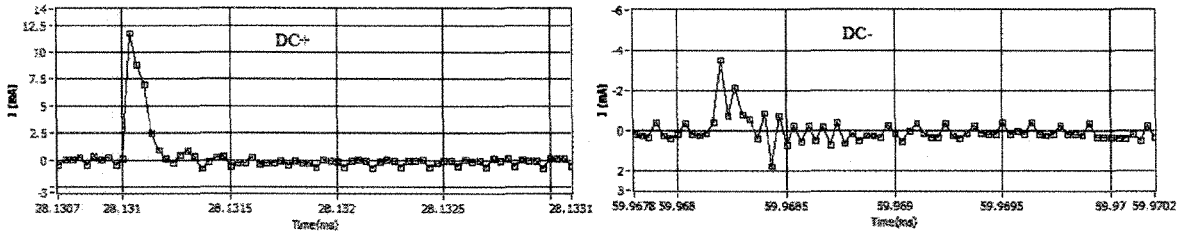

(a). Metal electrode

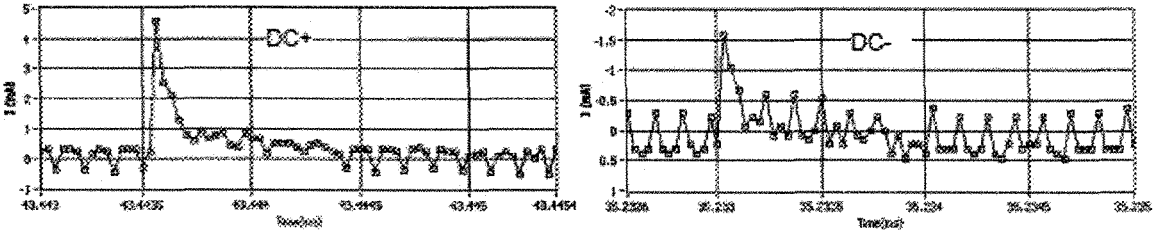

(b). Icicle electrode

Figure 5-8 Typical waveforms of current pulse under different polarities

(σ=80 μS/cm and T=0 °C)

Figure 5-8 shows that the waveform of the discharge current pulse is evidently different under different polarities. First, the waveform of the current pulse is very smooth at the falling part of the current pulse under DC+ voltage. However, there are some fluctuations under DC- voltage. Secondly, some over-pulses exist below the zero under DC- voltage. Finally, the duration of the current pulse is somewhat longer under DC+ voltage than that under DC- voltage. The differences between the waveforms of the current pulse under two different polarities had been investigated in air [117] [118] and in oil [117], respectively, and these results are in agreement with this study.

5.5.2 Voltage Type

For a given condition of T=0 °C and σ=80 μS/cm, the waveforms of the current pulse under AC voltage and DC voltage are presented in Figure 5-9

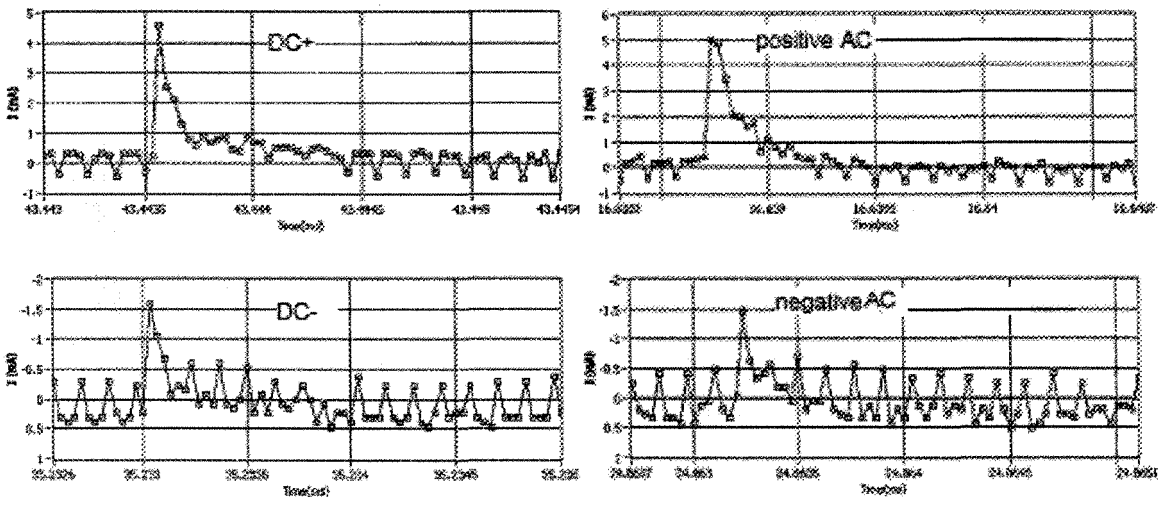

Figure 5-9 Typical waveforms of current pulse under different voltage types

(T=0 °C and d=5 cm)

Figure 5-9 shows that the waveforms of the current pulse are consistent between DC and AC voltage. The waveforms of the current pulse are very smooth and the duration of the current pulse is almost the same under DC+ and the positive half-cycle of AC voltage. However, under DC- voltage and the negative half-cycle of AC voltage, there are also some fluctuations and over-pulses in the falling part of the waveform of the current pulse. Hence, the voltage type does not influence the waveform of the discharge current pulse as the voltage polarity does. This is because the discharge mechanism is in complete agreement between DC voltage and the half-cycle of AC voltage.

5.5.3 Environmental Temperature

For a given condition of σ=80 μS/cm and d=5 cm, the typical waveform of the current pulse for the icicle electrode at T=-5 °C and 0 °C and for a metal electrode are extracted, respectively. The results are presented in **Figure 5-10**.

Figure 5-10 shows that the waveforms of the current pulse at 0 °C and -5 °C are different. The duration of the current pulse is significantly longer at 0°C than that at -5 °C. The main difference occurs at the falling part of the current pulse. The principal parameters on the waveform of current pulse at icicle at two temperature levels and at metal electrode are compared under DC voltage and result is shown in Table 5-1. The rising time of the current pulse for three different electrodes is the same, but the falling time is evidently

different. The falling time is less than 300 ns for the icicle at -5 °C, 500 ns for the icicle at 0 °C, and 500 ns for the metal electrode, respectively (more detail please see **Table 5-1**). Therefore, at the icicle electrode, the falling time and the duration of the current pulse at 0 °C is significantly longer than that at -5 °C. Comparing the waveforms of current pulse under different electrodes, the waveform is very irregular at -5 °C and becomes regular at 0 °C, and the waveform under metal electrode is the most regular.

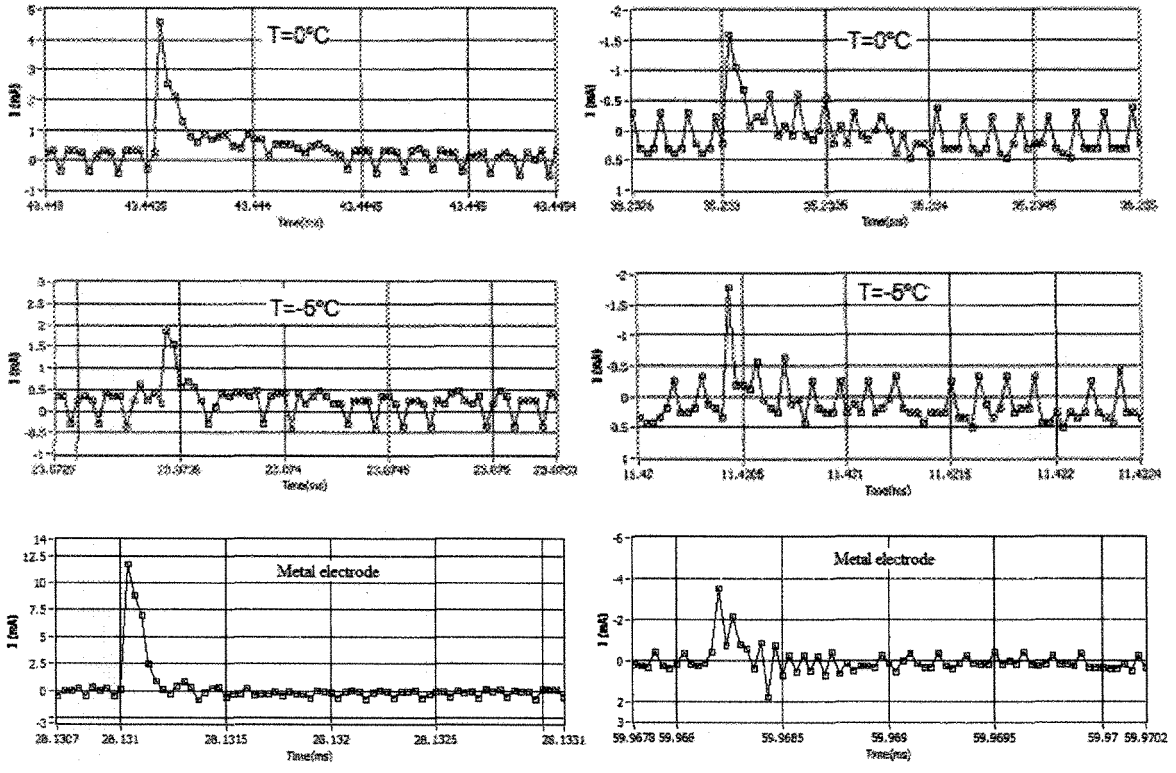

(a). DC+ voltage (b).DC- voltage

Figure 5-10 Typical waveforms of current pulse at two different temperature levels or electrode material (σ=80 μS/cm and d=5 cm)

The influence of electrode conductivity on the characteristics of the discharge pulse has been investigated for the water electrode and the pure ice electrode by **Herman W. Bandel** [45]. The results showed that the amplitude and the duration of discharge pulses from the ice point were obviously smaller and shorter than those from the platinum and water points, and decreasing resistance by shortening the ice point also increased the pulse amplitude. **J.Luan phan-cong** et al. [64] found that the amplitude of the corona current is profoundly affected by the external temperatures, and the amplitude of the pulse on dry ice is smaller compared to that on wet ice. Therein, this study is in agreement with those studies.

Table 5-1 Parameters of discharge current pulse for different electrodes

		Rising time (ns)	Falling time (ns)	Waveform of pulse
Icicle electrode	T=-5 °C	33	200	Irregular
	T=0 °C	33	500	Regular
Metal electrode		33	500	Very regular

5.5.4 Atmospheric Pressure

For a given condition of T=0 °C and d=7 cm, the influence of atmospheric pressure on the waveform of the current pulse is presented in **Figure 5-11**, 5-12, 5-13 and 5-14 for DC+, DC-, the positive half-cycle of AC and the negative half-cycle of AC, respectively. The results show that the waveform of the current pulse varies with atmospheric pressure.

As mentioned previously, the voltage type has no evident influence on the waveform of the current pulse. Therefore, in the following discussion, the main comparisons are focused on the results under DC voltage. The principal parameters of the waveform at different pressure levels are listed in **Table 5-2**.

Figure 5-11 and **Figure 5-13** show that the rising time of the discharge current pulse increases in approximate proportion with a decrease in atmospheric pressure under DC+ and the positive half-cycle of AC. For instance, under DC voltage, the rising time of the current pulse is 33 ns at 100 kPa, and increases up to 99 ns at 70 kPa, whereas the whole duration of the current pulse does not obviously change.

Figure 5-12 and **Figure 5-14** show that under DC- and the negative half-cycle of AC, the rising time of the current pulse does not change noticeably, whereas the falling time of the discharge current pulse increases significantly with a decrease in atmospheric pressure. For example, under DC- voltage, the falling time of the discharge current pulse is 200 ns at 100 kPa and it increases up to 660 ns at 70 kPa. Conversely, the rising time of the discharge current pulse does not change significantly.

Table 5-2 Parameters of discharge current pulse at different pressures

		100 kPa	90 kPa	80 kPa	70 kPa
DC+	Rising time (ns)	33	66	66	99
	Falling time (ns)	600	600	600	600
DC-	Rising time (ns)	33	33	33	33

	Falling time (ns)	200	450	600	660

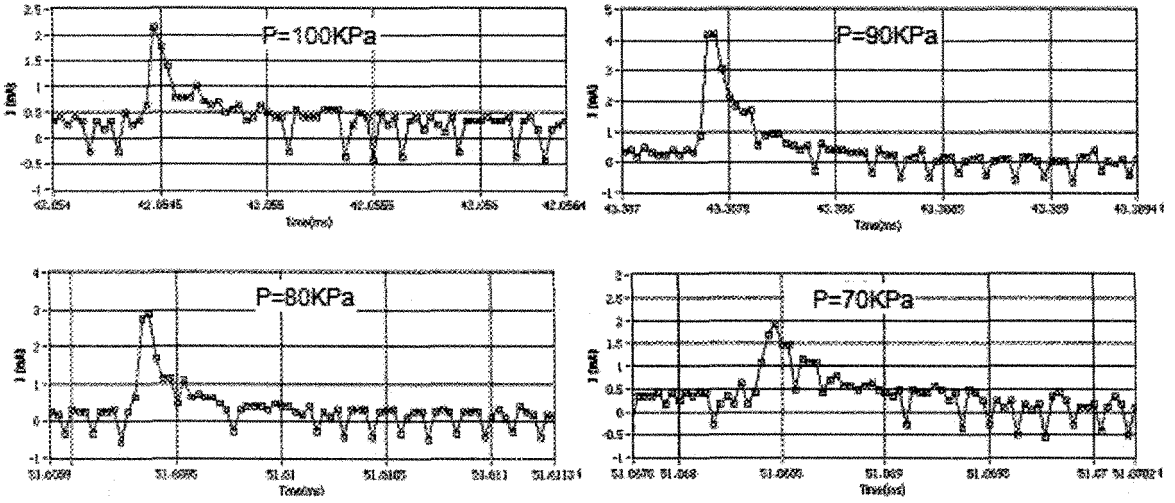

Figure 5-11 Typical waveform of current pulse at various pressures under DC+ voltage (T=0 ºC, σ=80 μS/cm and d=7 cm)

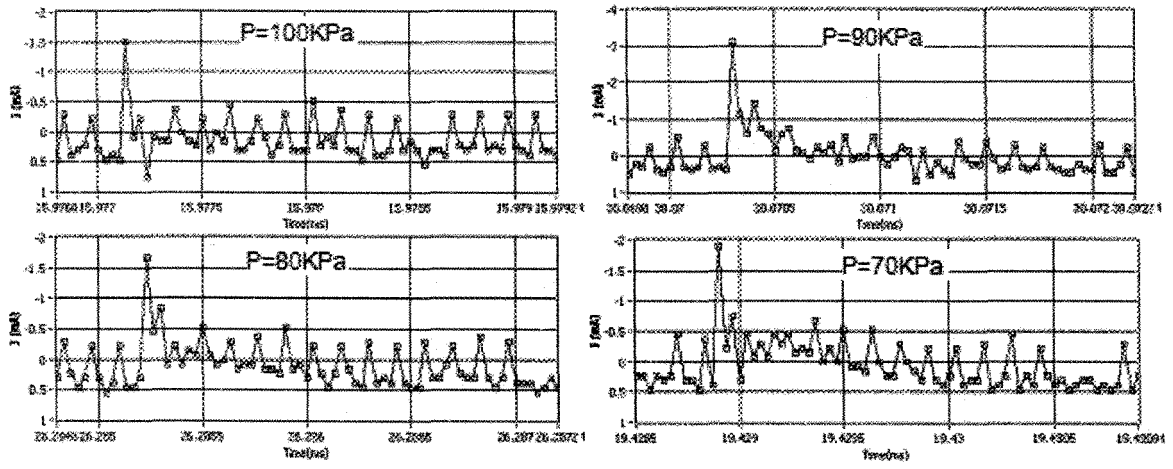

Figure 5-12 Typical waveform of current pulse at various pressures under DC- voltage (T=0 ºC, σ=80 μS/cm and d=7 cm)

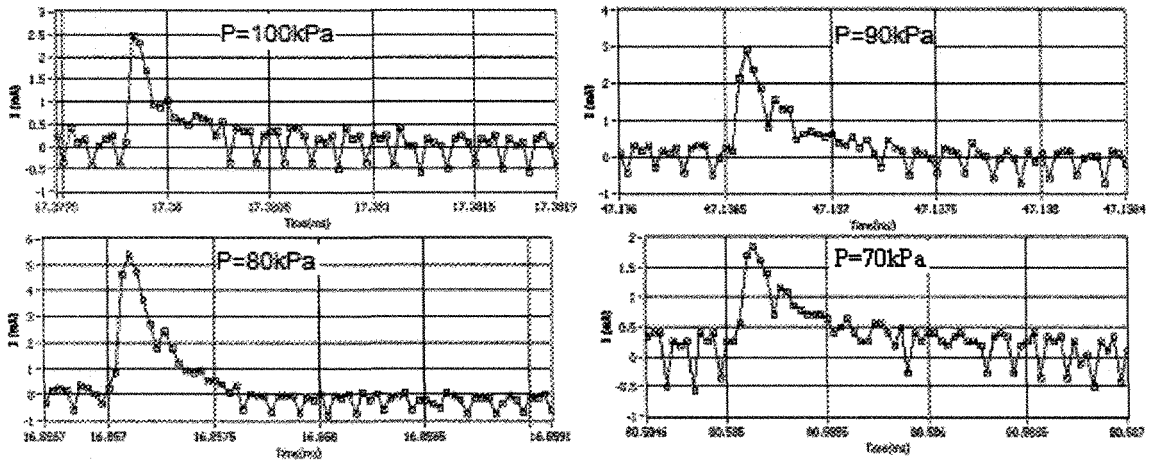

Figure 5-13 Typical waveform of current pulse at various pressures under positive half cycle of AC voltage (T=0 ºC, σ=80 μS/cm and d=7 cm)

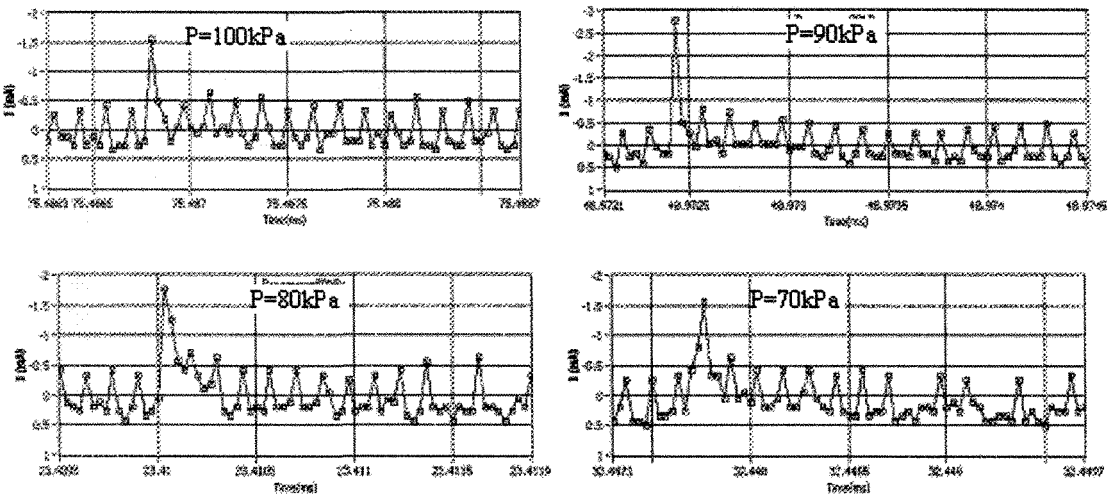

Figure 5-14 Typical waveform of current pulse at various pressures under negative half cycle of AC voltage (T=0 ºC, σ=80 μS/cm and d=7 cm)

M. Cernak et al. [119] and **D. A. Scott** [120] both found that the waveform of the discharge current pulse depended not only on the field configuration at the discharge site,

but also on the pressure of gas. The duration of the current pulse is approximately constant with different radii, but decreases with increasing pressure. Therefore, those results are consistent with this investigation.

5.6 CONCLUSIONS

1). The development of the corona discharge is different under DC+ voltage and DC- voltage. Under DC+ conditions, when the voltage reaches a certain value, the corona discharge transits into the glow. However, under DC- voltage, when the voltage is high enough, another discharge volume occurs close to the iced plate.

2). Corona discharge activities have different influence on icicle shape. Under DC- voltage and AC voltage, the icicle shape is damaged and flattened, but this change is not evident under DC+ voltage.

3). The corona discharge under AC voltage is more complex than that under DC voltage due to the switch in voltage polarity. It has some comprehensive characteristics like DC+ and DC- voltages. One of the major differences between them is that the discharge current pulse occurs cyclically.

4). The repetition rate of the discharge current pulses is affected by the applied voltage, temperature, gap distance, and voltage type. It increases first and then decreases with an increase in applied voltage under DC+ voltage. However, it increases with an increase in voltage at -5 °C and it increases first and then decreases with an increase in voltage at 0 °C. The maximum value of the repetition rate increases with an increase in

the gap distance, and it is evidently higher under DC voltage than that under AC voltage.

5). The waveform of the current pulse is influenced by the environmental temperature, the voltage polarity and the atmospheric pressure, but not by the voltage type. The duration of the current pulse at 0 °C is longer than that at -5 °C. The waveform of the current pulse is smoother under DC+ voltage than that under DC- voltage. Under the DC+ voltage and the positive half-cycle of AC voltage, the rising time of the current pulse increases proportionally with a decrease in the atmospheric pressure. Under DC- voltage and the negative half-cycle of AC voltage, the falling time of the current pulse increases with a decrease in atmospheric pressure.

CHAPTER 6

STATISTICAL ANALYSIS OF DISCHARGE PULSE MAGNITUDE

CHAPTER 6

STATISTICAL ANALYSIS OF DISCHARGE PULSE MAGNITUDE

6.1 INTRODUCTION

The corona discharge has been extensively studied [20][84][124]. All investigations show that corona discharge pulses are stochastic, as discussed in Chapter 5. The discharge pulse magnitude is influenced by many factors. Therefore, a statistical method was proposed to analyze and precisely describe the discharge pulse magnitude. In order to analyze these discharge pulse magnitudes, the relationship between the amplitude of the discharge current pulse and the discharge pulse magnitude was determined and presented in **Section 3.2.3.3**. Based on this relationship, all corona discharge pulses were transited into the discharge magnitudes, and then analyzed in the designed program as shown in **Figure 3-16**.

First, this chapter focuses on the frequency distribution of the discharge pulse magnitude corresponding to the voltage level varying in 1-1.1 times of V_{inc}. Then, principal statistical parameters such as the mean discharge magnitude and the standard deviation are

determined under different conditions. These results are analyzed and discussed in details.

6.2 FREQUENCY DISTRIBUTION OF DISCHARGE MAGNITUDE

6.2.1 Under DC+ Voltage

For a given condition of T=0 °C, σ=80 μS/cm and d=5 cm, the frequency distributions of discharge magnitudes under DC+ voltage are investigated and presented in **Figure 6-1**.

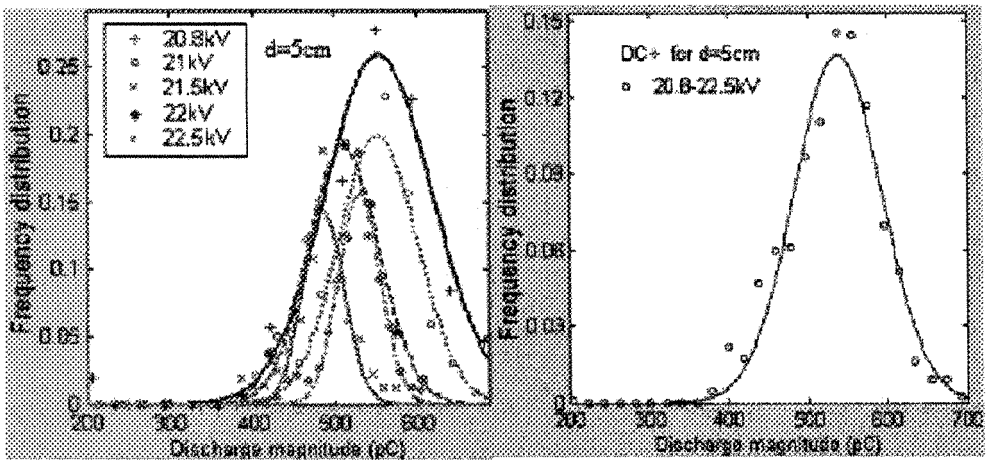

(a). Under various voltage levels (b). Voltage ranging from 20.8 to 22.5kV

Figure 6-1 Frequency distribution of discharge magnitude under DC+ voltage (T=0 °C, σ=80 μS/cm and d=5 cm)

Figure 6-1 (a) shows that at different DC+ voltage levels, the frequency distributions and standard deviations of discharge magnitude are slightly changed by the applied voltage. Generally, the frequency distributions appear more or less bell-shaped, and follow

approximately the normal distribution. When the applied voltage increases, the frequency distribution becomes sharper and sharper, which means that the standard deviation decreases and the discharge pulse becomes uniform. For example, the mean discharge magnitude is 575.2 pC and the standard deviation is 108.5 pC at 20.8 kV. However, when the applied voltage increases up to 22.5 kV, they are 531.2 pC and 38.2 pC respectively.

In order to precisely analyze the mean discharge magnitude and its standard deviation, the comprehensive frequency distribution of discharge magnitude corresponding to the applied voltage level, varying between 20.8 kV and 22.5 kV, is presented in Figure 6-1(b). Obviously, it follows the normal distribution with a mean discharge magnitude of 529.2 pC and a standard deviation of 66.4 pC.

6.2.2 Under DC- Voltage

For a given condition of T=0 °C, σ=80 μS/cm and d=5 cm, the frequency distributions of discharge magnitudes under DC- voltage are investigated and presented in **Figure 6-2**. Note that under DC- voltage, the frequency distribution of the discharge magnitude is significantly influenced by the applied voltage (**Figure 6-2**). At the low voltage levels of 21 kV and 22 kV, the frequency distribution follows the normal distribution, which is consistent with other investigations [20][122][123]. It transits into non-normal distribution (more than one peak) at slightly high voltage levels of 23 kV and 24 kV with a significantly large standard deviation. When the applied voltage is increased, the mean discharge magnitude and the standard deviation increase strictly which suggests that the discharge pulse becomes very

irregular at high voltage. At 21 kV, the discharge magnitude is 190.1 pC and the standard deviation is 29.3 pC. At 24 kV, they are 275 pC and 128 pC, respectively.

The overall frequency distribution of the discharge magnitude for the applied voltage ranging between 21 kV and 23 kV is presented in **Figure 6-2(b)**. The frequency distribution does not follow a normal distribution, as it has a mean value of 232.1 pC and the standard deviation of 68.8 pC.

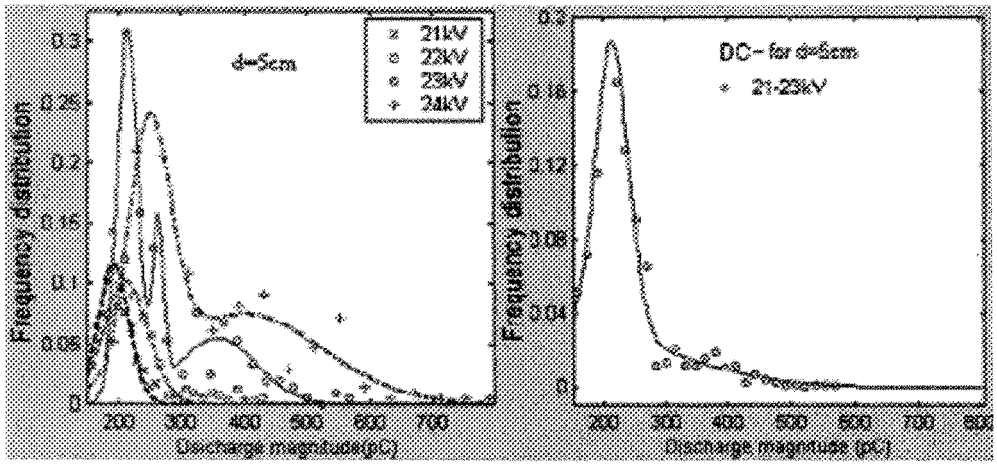

(a). Under various voltage levels (b). Voltage varying from 21-23kV

Figure 6-2 Frequency distribution of discharge magnitude under DC- voltage (T=0 °C, σ=80 μS/cm and d=5 cm)

6.2.3 Under Positive Half Cycle of AC Voltage

For a given condition of T=0 °C and σ=80 μS/cm as well as d=5 cm, the frequency distributions of discharge magnitude under the positive half-cycles of AC voltage are

presented in **Figure 6-3**. It is observed that under the positive half-cycles of AC voltage, the frequency distributions of discharge magnitude at low applied voltages follow approximately normal distribution. When the applied voltage increases, although the change of frequency distribution is significant, the mean discharge magnitude and the standard deviation increase slightly with an increase in the applied voltage. However, under the slightly higher applied voltage of 21 kV, this distribution no longer has the Gaussian shape and consequently, the discharge mode transits from corona into glow. At 18.4 kV, the mean discharge magnitude is 575.3 pC and the standard deviation is 43.5 pC. At 20 kV, they are 592.9 pC and 54.8 pC, respectively.

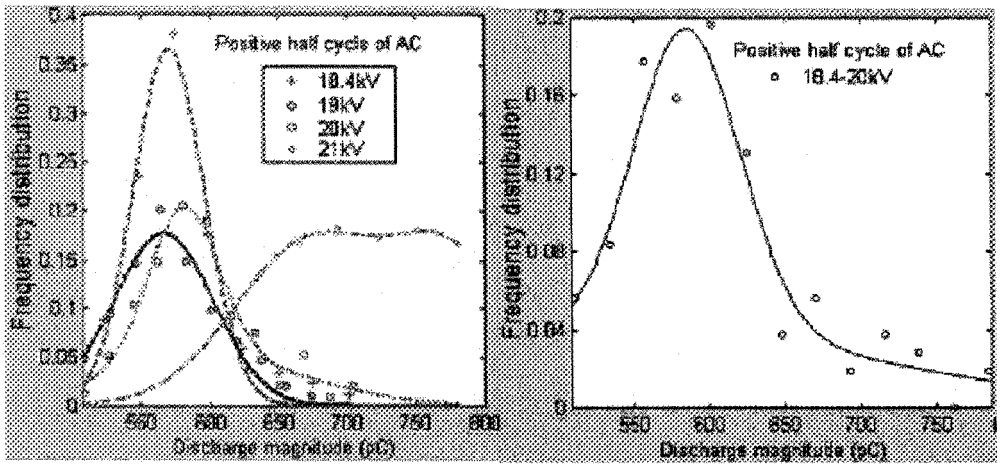

(a). under various voltage levels (b).Varying from 18.4-20 kV

Figure 6-3 Frequency distribution of discharge magnitude under the positive half cycle of AC voltage (T=0 °C, σ=80 μS/cm and d=5 cm)

The overall frequency distribution of the mean discharge magnitude for applied

voltages between 18.4 and 21 kV is shown in Figure 6-3(b). Apparently, this frequency distribution follows a normal distribution with the mean discharge magnitude of 600.2 pC and the standard deviation of 61.2 pC.

6.2.4 Under Negative Half Cycle of AC Voltage

In a given condition of T=0 °C and σ=80 μS/cm as well as d=5 cm, the frequency distributions of discharge magnitude are presented in **Figure 6-4** for the negative half-cycles of the AC voltage. It is found that under the negative half-cycle of the AC condition, the shapes of discharge magnitude distribution differ under various voltage levels. Under low voltage levels of 18.4 and 19 kV, these distributions follow the normal distribution. However, they are transited into non-normal distribution at high applied voltage levels of 20 and 21 kV. At 18.4 kV, the discharge magnitude is 215.9 pC and the standard deviation is 31.4 pC. At 20 kV, they are 259.8 pC and 105.7 pC, respectively.

The overall distribution of discharge magnitude for applied voltage ranging from 18.4 to 21 kV is presented in **Figure 6-4**(b). It is of Gaussian shape, but not a normal distribution, with the mean discharge magnitude of 232.6 pC and the standard deviation of 70.14 pC.

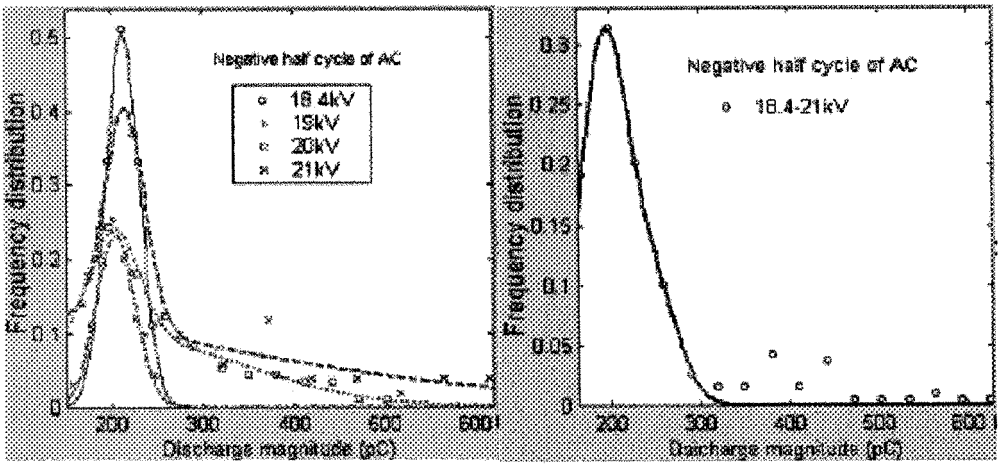

(a). under various voltage levels (b). Varying from 18.4-21kV

Figure 6-4 Frequency distribution of discharge magnitude under the negative half-cycle of AC voltage (T=0 °C, σ=80 μS/cm and d=5 cm)

6.3 ANALYSIS OF STATISTIC DISTRIBUTION OF DISCHARGE MAGNITUDE

From **Figure 6-1** and **Figure 6-3**, the frequency distributions of discharge pulse magnitude under DC+ voltage and the positive half-cycle of AC voltages are in agreement. Generally, the overall distributions under the DC+ and the positive half-cycle of AC voltage ranging from V_{inc} to $1.1V_{inc}$ follow normal distribution, and can be approximately expressed as the following equation:

$$P = \frac{1}{\sigma\sqrt{2\pi}} e^{-\frac{(q-\mu)^2}{2\sigma^2}} \quad \text{---------- (6-1)}$$

where P is the frequency distribution of discharge magnitude, σ^2 is variances, q is the discharge magnitude and μ is the mean discharge magnitude.

From **Figure 6-2** and **Figure 6-4**, it may be found that the frequency distributions of discharge pulse magnitude under DC- and the negative half-cycle of AC voltages are consistent. Both of them follow Gaussian distribution, and tend to transit from the normal distribution at low applied voltage into non-normal distribution at high voltage. The overall frequency distributions for a voltage of 1-1.1 V_{inc} are similar and can be expressed as the following equation:

$$P = \frac{1}{\sigma_1\sqrt{2\pi}} e^{-\frac{(q-\mu_1)^2}{2\sigma_1^2}} + \frac{1}{\sigma_2\sqrt{2\pi}} e^{-\frac{(q-\mu_2)^2}{2\sigma_2^2}} \quad \text{---------- (6-2)}$$

where P is the frequency distribution of discharge magnitude, σ_1^2 and σ_2^2 are variances, q is the discharge magnitude and μ_1 and μ_2 are the expectant value of discharge magnitude for the first and second peak, respectively.

The frequency distribution of discharge amplitude has been also investigated by other researchers. **Yicheng Wang** [126] demonstrated that the distribution of discharge amplitude under DC+ voltage follows the normal distribution. In addition, **R. J. Van Brunt et al.** [124] and **Al-Arainy et al.** [84] verified that the pulse amplitude distributions of the negative corona at the sharp-point metallic electrode also follow the normal distribution. He found that the discharge pulses had a very regular and well-ordered behavior. Meanwhile, he pointed out that under DC- voltage, a high rate of electron emission from the point cathode is a guarantee for normalization distribution of discharge magnitude. Obviously, the icicle electrode under DC- voltage was destroyed during the discharge process as explained in Section 5.4; this means that the sharp tip is missed and the electron emission is not well localized any more.

6.4 FACTORS AFFECTING DISCHARGE PULSE MAGNITUDE

Under a given condition of T=0 °C and σ=80 μS/cm, the relationship between the mean discharge magnitude, the standard deviation and the gap distance are investigated and the results are shown in **Figure 6-5**, **6-6**, **6-7** and **6-8**, respectively.

All above results show that the mean discharge magnitude and the standard deviation both decrease with an increase in gap distance, which means that the discharge magnitude becomes more uniform at a long gap distance.

Under DC+ voltage, **Figure 6-5** shows that when the gap distance increases from 3 cm to 9 cm, the mean discharge magnitude decreases from 568.8 pC to 253.3 pC. In percentage, it decreases almost 55.5%. The standard deviation decreases from 70.4 pC at 3 cm to 36.4 pC at 9 cm.

Under DC- voltage, **Figure 6-6** shows that when the gap distance increases from 3 cm to 9 cm, the discharge magnitude decreases from 330.8 pC to 209 pC, and the percentage of decrease is approximately 36.8%. In addition, the standard deviation decreases from 49.2 pC at 3 cm to 30.2 pC at 9 cm.

Under the positive half-cycle of AC voltage, **Figure 6-7** reveals that when the gap distance increases from 3 cm to 9 cm, the discharge magnitude decreases from 613.3 pC to 290.3 pC, and the percentage of decrease is approximately 52.7%. Meanwhile, the standard deviation decreases from 85.3 pC at 3 cm to 35.3 pC at 9 cm.

Under the negative half-cycle of AC voltage, **Figure 6-8** demonstrates that when the

gap distance increases from 3 cm to 9 cm, the discharge magnitude decreases from 243.0 pC to 195.3 pC, and the percentage of decrease is around 19.6%. Correspondingly, the standard deviation decreases from 76.8 pC at 3 cm to 30.2 pC at 9 cm.

Hence, the effect of gap distance on the discharge magnitude under DC+ voltage or under the positive half-cycle of AC voltages is more significant than those under DC- voltage and under the negative half-cycle of AC voltage.

To date, there have been no related investigations on the influence of the gap distance on the mean discharge magnitude. However, a similar relationship between the discharge pulse amplitude and the radius of the electrode was found [85]. The increase of the electrode radius will increase the amplitude of the discharge pulse. In order to reveal the relationship between the discharge magnitude and the gap distance, a form factor is introduced to express the influence of the gap distance on the electric field distribution of the air gap. This is presented as Equation (6-3) [39].

$$F = E_{mean} / E_{\max} = \frac{R}{R+d} \text{ ---------- (6-3)}$$

where R is the radius of electrode tip and d the gap distance.

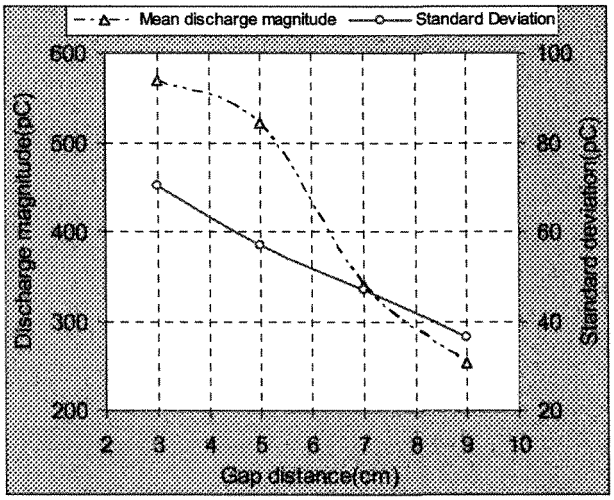

Figure 6-5 Mean discharge magnitude and the standard deviation vs. the gap distance under DC+ voltage (T=0 °C, σ=80 μS/cm)

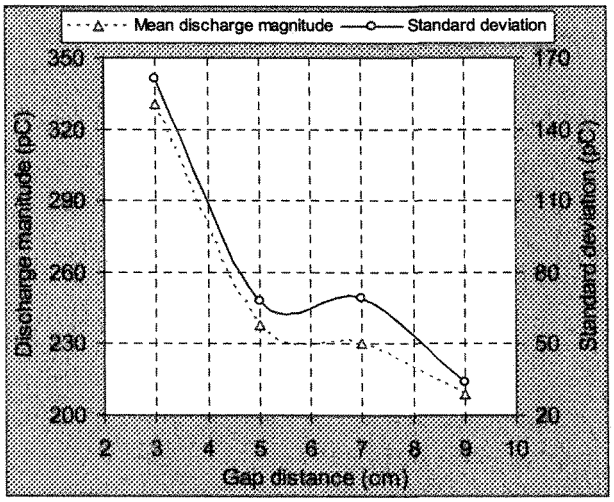

Figure 6-6 Mean discharge magnitude and the standard deviation vs. the gap distance under DC- voltage (T=0 °C, σ=80 μS/cm)

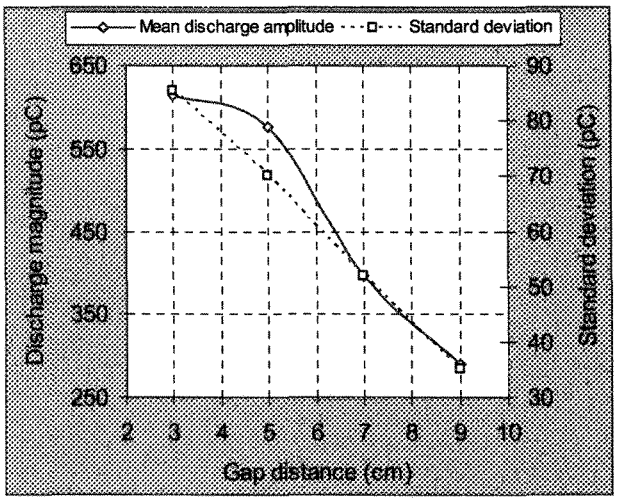

Figure 6-7 Mean discharge magnitude and the standard deviation vs. the gap distance under the positive half cycle of AC voltage (T=0 °C, σ=80 μS/cm)

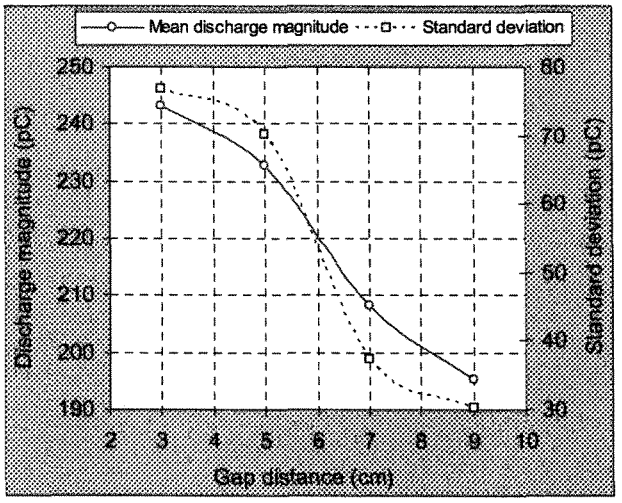

Figure 6-8 Mean discharge magnitude and the standard deviation vs. the gap distance under the negative half cycle of AC voltage (T=0 °C, σ=80 μS/cm)

From Equation 6-3, it may be concluded that the increase in the gap distance or the decrease in electrode radius will cause a decrease in the form factor of the gap space, *F*. Thus, the electrical field strength distribution becomes more non-uniform with increasing gap distance or decreasing electrode radius, which means that the discharge pulse magnitude decreases and become more and more uniform in long gap distance.

6.4.1 Environment Temperature

For a given condition of d=5 cm and σ=80 μS/cm, the effects of the environmental temperature on the mean discharge magnitudes under DC and AC voltage were investigated and are presented in **Figure 6-9** and **Figure 6-10** respectively. The discharge magnitude is evidently affected by the change of temperature. For the same conductivity, the mean discharge magnitudes at T=0 °C are evidently higher than those at T=-5 °C.

Under DC voltage (**Figure 6-9**), when the temperature increases from -5 °C to 0 °C, the mean discharge magnitude increases from 220.7 pC to 525.7 pC and from 173.0 pC to 215.3 pC for DC+ voltage and DC- voltage, respectively. The increase in percentage is 138.2% and 24.5% for DC+ voltage and DC- voltage, respectively.

Under AC voltage (**Figure 6-10**), when the temperature is raised from -5 °C up to 0 °C, the mean discharge magnitude increases from 334.0 pC to 576.4 pC and from 169.3 pC to 232.6 pC for the positive half-cycle of AC voltage and the negative half-cycle of AC voltage, respectively. The percentage of increase is 72.6% and 37.4%, respectively.

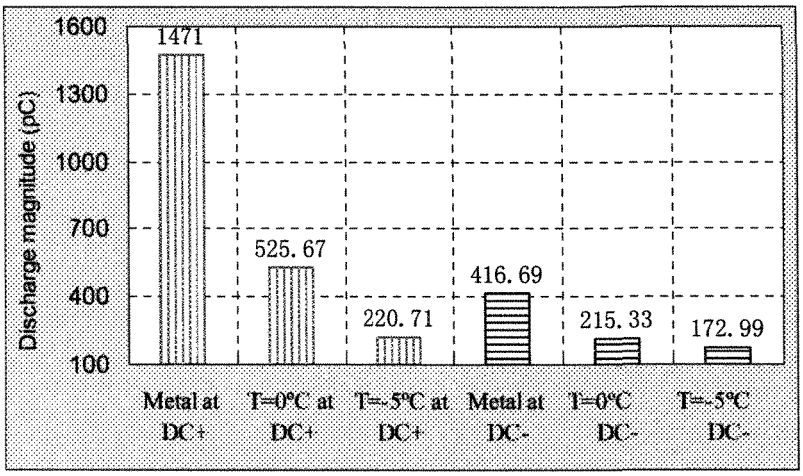

Figure 6-9 Effects of temperature on the discharge magnitude under DC voltage

(σ=8 0 μS/cm and d=5 cm)

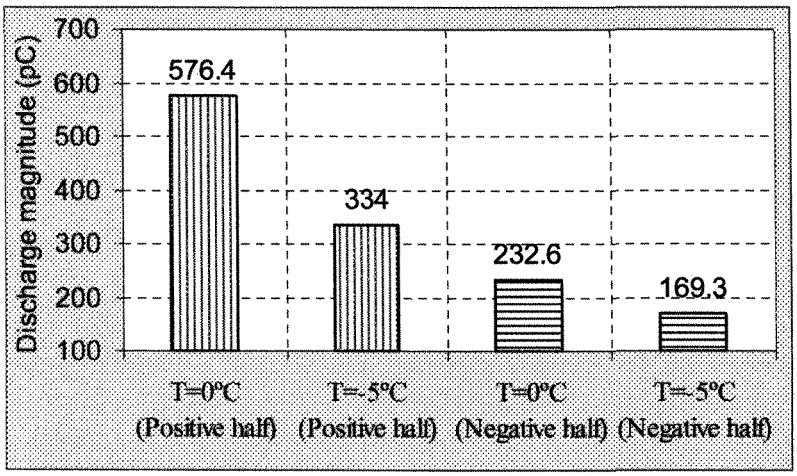

Figure 6-10 Effects of temperature on the discharge magnitude under AC voltage

(σ=80 μS/cm and d=5 cm)

In summary, the temperature has a more significant influence on the discharge

magnitudes under DC+ voltage and the positive half-cycle of AC voltage than those under DC- voltage and the negative half-cycle of AC voltage. Actually, the variation of temperature mainly changes the conductive property of the icicle electrode. Therefore, a metal electrode is used to study the difference between the discharge magnitude at the metallic electrode and the icicle electrode. The result under DC voltage is also presented in **Figure 6-9**. It has been found that the discharge magnitude at metal electrode is evidently bigger than those at icicle. The conductivity of the icicle at T=0 °C is higher than that at T=-5 °C, but not as good as the stainless steel electrode. Therein, the discharge magnitude is positively correlated with the electrode conductivity. Thus, the higher conductivity the electrode has, the bigger the discharge magnitude is.

The influence of the environmental temperature on the discharge magnitude is consistent with the results obtained in [45][100]. These investigations showed the discharge pulse amplitude is significantly larger at a water-droplet electrode than that at an icicle electrode.

Actually, the effects of temperature on the electrode properties are due to the following facts: at the boundary surface, the potential energy of electron approaches asymptotically to zero. The lowest energy required to remove an electron from a solid is called the work function ($e\varphi$). This energy can occur in various forms: thermal (phonons, kT), photons (hv), internal potential energy of the atoms and ions (eV*, eVi) and kinetic energy ($1//2Mv^2$). When the melting process may be regarded as a destruction of the lattice due, primarily, to a too-close approach of the singular hydrogen and H_3O_2 groups, resulting in a liquid, which is a mixture of mono- and di-hydro in temperature equilibrium [121]. The

melting, then, tends to reduce the interfacial free energy. This is also supported by the observation that the mechanical disturbance of an ice surface increases the surface conductivity since it produces many lattice defects and an electrically mobile ion state in the surface region. Because the impurities are non-volatile and insoluble in ice, small amounts of them can move to the surface to increase the surface conductivity and to decrease the activation energy [105].

6.4.2 Freezing Water Conductivity

At 0 °C, two different freezing water conductivities of 320 μS/cm and 80 μS/cm were chosen to reveal the influence of conductivity on the discharge magnitude. The results are shown in **Figure 6-11** and **Figure 6-12** for DC and AC conditions, respectively. It may be seen that the discharge magnitude increases slightly with an increase in conductivity.

Under DC+ voltage, the discharge magnitudes are 595.5 pC and 525.7 pC for 320 μS/cm and 80 μS/cm, respectively. However, under DC- voltage, they are 245.4 pC and 215.3 pC respectively. When the freezing water conductivity increases from 80 μS/cm to 320 μS/cm, the increase in percentage is 13.3% and 14.0% under DC+ and DC- voltage, respectively.

Under the positive half-cycle of AC voltage, the discharge magnitudes are 620 pC and 576.4 pC for 320 μS/cm and 80 μS/cm, respectively. However, under the negative half-cycle of AC voltage, they decrease to 243.9 pC and 232.6 pC, respectively. When the freezing water conductivity increases from 80 μS/cm to 320 μS/cm, the discharge magnitudes

are raised by 7.6% and 4.8% for the positive and the negative half-cycles of AC voltage, respectively.

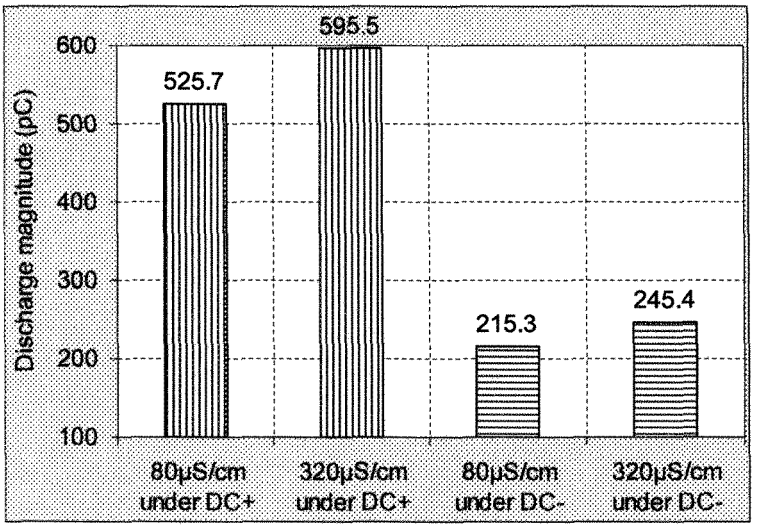

Figure 6-11 Effect of conductivity on the discharge magnitude under DC voltage

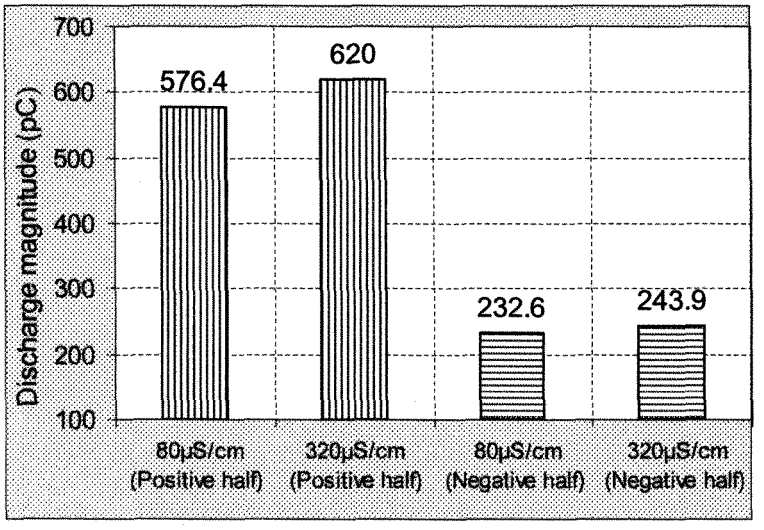

Figure 6-12 Effect of conductivity on the discharge magnitude under AC voltage

The above results are consistent with the result obtained by **Toshiyuki Sugimoto et al.** [125], who found that the magnitude of the initial and the final pulses in the first pulse series of each group increases linearly with the conductivity of water. In addition, compared with the influence of temperature, the variation of conductivity does not affect the discharge pulse magnitude as evidently as the temperature does.

6.4.3 Voltage Polarity

In a given condition of T=0 °C and σ=80 μS/cm, the discharge magnitude and the standard deviation under DC+ and DC- voltages are compared, and the results are presented in Figure 6-13. It is found that for various gap distances, the mean discharge magnitude under DC+ voltage is always higher than those under DC- voltage, and the difference decreases with an increase in the gap distance.

For example, when d=3 cm, the discharge magnitude is 568.8 pC under DC+ voltage and 330.8 pC under DC- voltage, and the difference between them is 238 pC. When d=9 cm, although the discharge magnitude under DC+ voltage decreases to 253.3 pC, it is still 52.4 pC higher than that under DC- voltage. In contrast, the standard deviation of discharge magnitude is smaller under DC+ voltage than that under DC- voltage under various gap distances, which means that the discharge pulse is relatively more uniform under DC+ voltage than that under DC- voltage. This is due to the change of the icicle tip under DC- voltage. Therefore, the initiatory electrode can not be localized exactly, which causes the discharge pulse become more irregular.

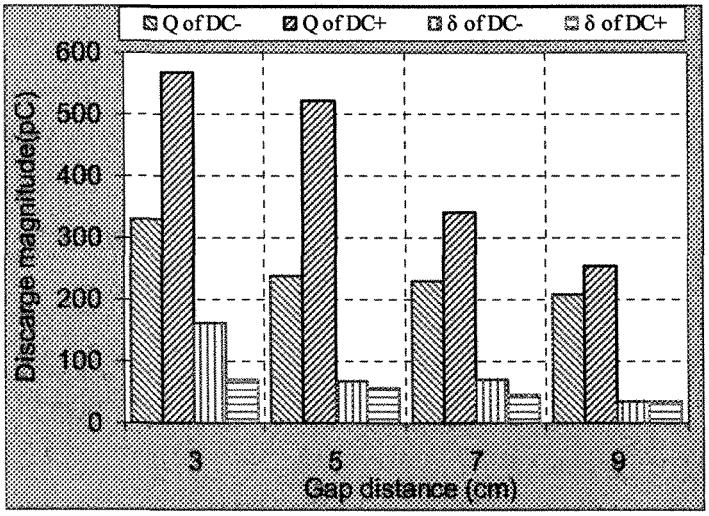

Figure 6-13 Discharge magnitude of various polarities under different gap distances

The effects of the voltage polarity on the amplitude of the discharge pulse have also been studied by **Malik et al** [82]. He found that the discharge pulse amplitude under DC- voltage is sensitive to the voltage level and less reproducible. In addition, the amplitude of discharge pulse is evidently larger under DC+ voltage than that under DC- voltage. Obviously, these results are consistent with this study.

6.4.4 Voltage Type

For a given condition of d=5 cm, σ=80 μS/cm and T=0 °C, the discharge magnitudes are determined under different voltage types and the results are shown in **Figure 6-14** and **Figure 6-15**. The discharge magnitude and the standard deviation are different under DC+

voltage and under the positive half-cycle of AC voltage, and they are both slightly lower under DC+ voltage than those under the positive half-cycle of AC voltage. At d=3 cm, the discharge magnitudes are 568.8 pC and 613.1 pC and the standard deviation is 70.4 pC and 85.3 pC for DC+ voltage and the positive half-cycle of AC voltage, respectively. The difference is 44.2 pC. However, at d=9 cm, the discharge magnitudes are 253.3 pC and 290.3 pC and the standard deviations are 35.3 pC and 36.4 pC for DC+ voltage and the positive half-cycle of AC voltage respectively, and the difference in the discharge magnitude is 37.0 pC.

The results presented in **Figure 6-15** show that the discharge magnitude and the standard deviation are both higher under DC- voltage than those under the negative half-cycle of AC voltage. When d=3 cm, the discharge magnitudes are 330.8 pC and 243.0 pC and the standard deviations are 161.0 pC and 76.8 pC, for DC- voltage and the negative half-cycle of AC voltage, respectively. The difference in discharge magnitude is 88.7 pC. When d=9 cm, the discharge magnitudes are 209 pC and 195.3 pC, and the difference is only 13.7 pC. Meanwhile, the standard deviations are 40.0 pC and 30.2 pC for DC- voltage and the negative half-cycle of AC voltage, respectively.

A similar investigation of the voltage type on the discharge magnitude at metallic electrodes has been carried out by **Al-Arainy et al.** [84]. He found that the discharge pulse amplitude under DC+ voltage is slightly higher than that under the positive half-cycle of AC voltage. However, the average pulse amplitude was somewhat higher for AC voltage as compared to DC- voltage. Therefore, there are some new statistical characteristics of discharge pulse at icicle electrodes, which suggests more studies at the icicle should be

carried out.

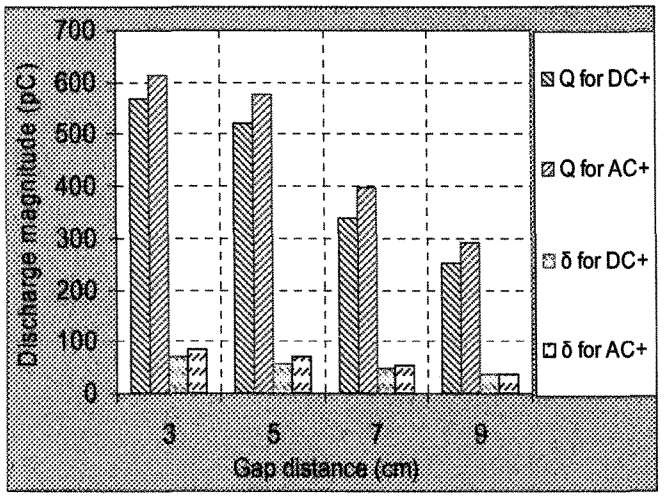

Figure 6-14 Discharge magnitude and standard deviation under DC+ and positive half cycle of AC voltage (d=5 cm, σ=80 μS/cm and T=0 °C)

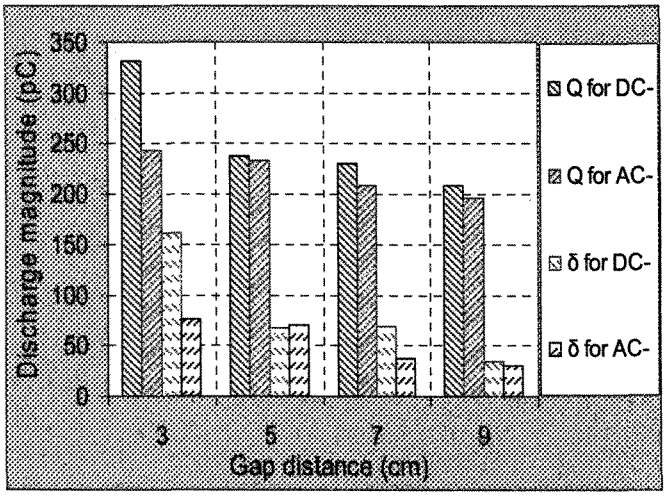

Figure 6-15 Discharge magnitude and standard deviation under DC- and negative half cycle of AC voltage (d=5 cm, σ=80 μS/cm and T=0 °C)

6.4.5 Atmospheric Pressure

When T=0 °C and σ=80 μS/cm, the influence of atmospheric pressure on the discharge magnitude is investigated and the results are presented in **Figure 6-16, 6-17,6-18** and **6-19** for DC+,DC-, the positive half cycle and negative half cycle of AC, respectively. It may be noticed that the atmospheric pressure has an observable effect on the discharge magnitude. The discharge magnitude does not increase or decrease linearly with the decrease in the atmospheric pressure. Inversely the maximum values of the discharge magnitude and the standard deviations occur consistently at the pressure of 80 kPa, corresponding to 2 km in altitude.

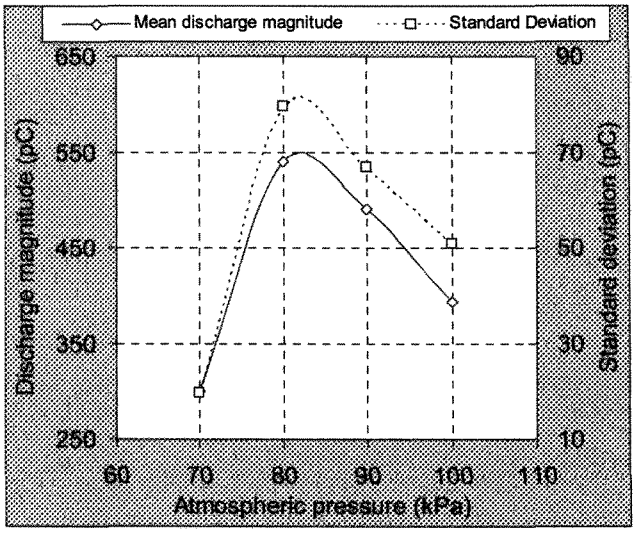

Figure 6-16 Relationship between the discharge magnitude and the atmospheric pressure under DC+ voltage (T=0 °C, σ=80 μS/cm and d=7 cm)

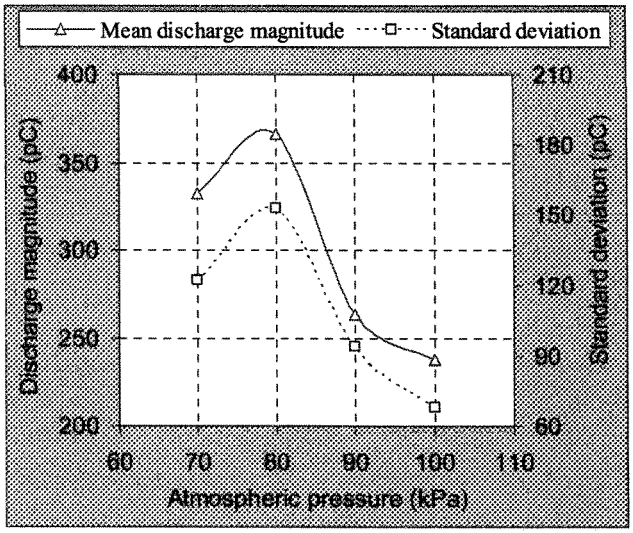

Figure 6-17 Relationship between the discharge magnitude and the atmospheric pressure under DC- voltage (T=0 °C, σ=80 μS/cm and d=7 cm)

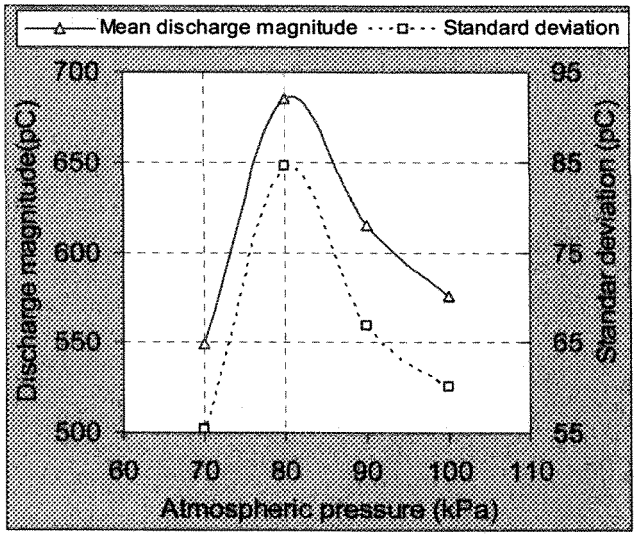

Figure 6-18 Relationship between the discharge magnitude and the atmospheric pressure under positive half-cycle of AC voltage (T=0 °C, σ=80 μS/cm and d=5 cm)

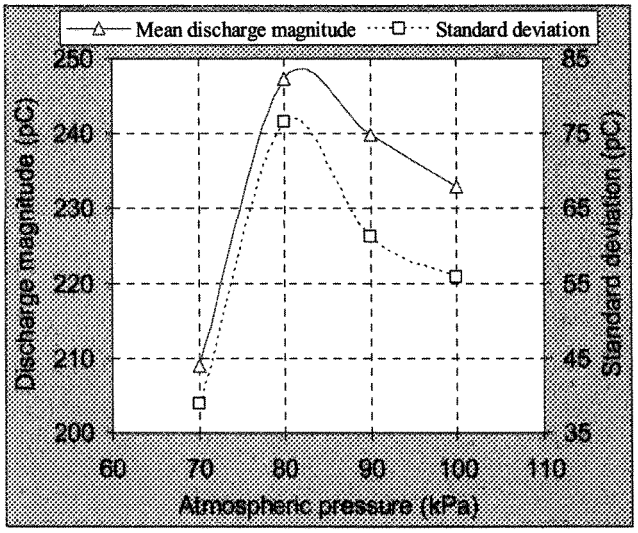

Figure 6-19 Relationship between the discharge magnitude and the atmospheric pressure under negative half-cycle of AC voltage (T=0 °C, σ=80 μS/cm and d=5 cm)

The results under DC+ voltage as presented in Figure 6-16 show that the discharge magnitudes are 339.6 pC at 100 kPa and 539.2 pC at 80 kPa. It decreases to 248.8 pC at 70 kPa. The results under DC- voltage shown in Figure 6-17 illustrate that the discharge magnitudes are 215.3 pC and 287.3 pC at 100 kPa and 80 kPa respectively. When the atmospheric pressure decreases to 70 kPa, the discharge magnitude reduces to 248.6 pC. Meanwhile the variation of standard deviation is consistent with the change of discharge magnitude. When the atmospheric pressure decreases from 100 kPa to 80 kPa, the percentage of increase is 59.7% under DC+ voltage and 33.4% under DC- voltage, respectively.

Figure 6-18 shows that under the positive half-cycle of AC conditions, the discharge magnitude increases from 576.1 pC to 672.3 pC, when the pressure decreases from 100 kPa to 80 kPa, and then it decreases to 550.5 pC as the pressure decreases further to 70 kPa. The

results under the negative half-cycle of AC voltage as presented in **Figure 6-19** show that the discharge magnitude increases from 232.9 pC to 247.2 pC when the pressure decreases from 100 kPa to 80 kPa and then decreases to 209.0 pC at 70 kPa. When the pressure decreases from 100 kPa to 80 kPa, the increases in percentage are 16.7% and 6.1% respectively for the positive and the negative half-cycle of AC voltages.

The above results show that the corona discharge is the most serious at the pressure of 80kP compared to other pressures, which should be paid attention. In general, the discharge magnitude can be expressed as the following equation (6-5):

$$Q = n_0 e \cdot e^{\alpha \cdot x} \text{ ---------- (6-5)}$$

Where Q is the discharge magnitude, n_0 is the initiatory electrons, e is the charge of the electron, x is the length of the avalanche, and α is the ionization coefficient of air and can be expressed as [105]:

$$\alpha = APe^{-BP/E} \qquad (6\text{-}6)$$

Where A=11.11 cm·kPa and B=275 V/cm·kPa.

In order to understand the discharge process in gas, a ratio of $\boldsymbol{\alpha/E}$ is introduced since it physically represents the number of ions produced by electron collisions per unit of electric potential drop [20]. This ratio is defined as the ionization efficiency, $\boldsymbol{\eta}$ and given by:

$$\eta = \frac{\alpha}{E} = \frac{A}{E} Pe^{-BP/E} \qquad (6\text{-}7)$$

Therefore, $\boldsymbol{\eta}$ is a function of $\boldsymbol{E/P}$, and the relation between them is illustrated in **Figure 6-20**. From **Figure 6-20**, it may be noted that $\boldsymbol{\eta}$ shows a maximum value and the maximum value may be obtained by differentiating Equation (6-7) and setting the derivative

equal to zero, i.e.,

$$\frac{d\eta}{d(E/p)} = \frac{AB}{(E/P)^3} e^{-Bp/E} - \frac{A}{(E/p)^2} e^{-Bp/E} = 0 \quad (6\text{-}8)$$

Hence, the maximum value of η occurs at:

$$\frac{E}{p} = B \qquad (6\text{-}9)$$

For a given electric field configuration, the variation of η is consistent with α, when η reaches its maximum value. Meanwhile, the coefficient, α, and the consequent discharge quantities also reach the maximum values. It may be observed from the above curves that their shapes are in similar agreement.

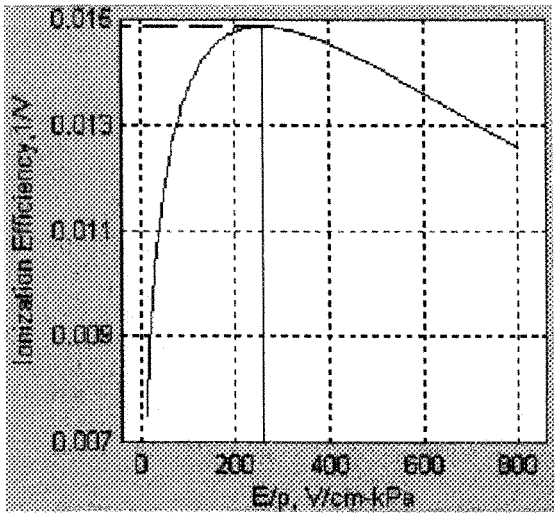

Figure 6-20 Relationship between η and E/P

Based on the experimental result of V_{inc}, and Equation 6-9, the Electric field strength at the icicle tip and its corresponding B are calculated for pressure of 80 kPa, respectively,

and the calculated values are listed in **Table 6-1**. The value of ***B*** is very close to the theoretical values; however, more tests should be carried out in the future.

Table 6-1 Calculated electric field strength and corresponding the value of B

	DC+	DC-	Theoretical value[10][20]
E (kV/cm)	23.8	25.6	25
B (V/cm·kPa)	295	283	275

6.5 CONCLUSIONS

1). The distributions of discharge magnitudes under DC and AC voltage follow Gaussian distribution. However, the distribution shapes are affected by voltage polarities of DC or AC voltages. The distribution may be expressed as follows:

$$P = \frac{1}{\sigma\sqrt{2\pi}} e^{-\frac{(q-\mu)^2}{2\sigma^2}}$$ for DC+ voltage and positive half-cycle of AC voltage

$$P = \frac{1}{\sigma_1\sqrt{2\pi}} e^{-\frac{(q-\mu_1)^2}{2\sigma_1^2}} + \frac{1}{\sigma_2\sqrt{2\pi}} e^{-\frac{(q-\mu_2)^2}{2\sigma_2^2}}$$ for DC- voltage and negative half cycle of AC voltage

2). The discharge magnitude and the standard deviation decrease with an increase in gap distance. The gap distance has an evident influence on discharge magnitude under DC+

and positive half-cycle of AC voltage than those under DC- and negative half-cycle of AC voltage.

3). The discharge magnitude at 0 °C is evidently larger than that at -5 °C. However, the change of conductivity affects the discharge magnitude slightly when the temperature stays constant.

4). The voltage polarity and type both have an influence on the discharge magnitude and the standard deviation. Under DC voltage, the discharge magnitude under DC+ voltage is higher than that under DC- voltage. In addition, the discharge magnitude under DC+ voltage is slightly lower than those under the positive half-cycle of AC, but is higher under DC- voltage than that under the negative half-cycle of AC voltage.

5). The atmospheric pressure has an obvious effect on the discharge magnitude. The discharge magnitude first increases and then decreases with a decrease in pressure. The maximum discharge magnitude appears at 80 kPa, corresponding to 2 km in altitude.

CHAPTER 7

SPACE CHARGE BEHAVIORS AND THEIR INFLUENCE ON SEQUENTIAL DISCHARGE PULSE STATISTICAL ANALYSIS OF DISCHARGE PULSE MAGNITUDE

CHAPTER 7

SPACE CHARGE BEHAVIORS AND THEIR INFLUENCE ON SEQUENTIAL DISCHARGE PULSES

7.1 INTRODUCTION

It is well-known that corona discharge is a kind of pulsating discharge phenomenon. This discharge pulse generally has a significant statistical variability. These pulses are also not completely random in some sense, and they are potentially determined by the effects of space charge behaviour, whereby, the residual space charges left behind will influence the probabilities for initiation and development of subsequent discharge activities.

The occurrence of corona discharges at icicle tips is the first stage of the flashover process, and will produce a large quantity of space charges around the icicles. In turn, these space charges will affect the electrical field distribution around the icicles, and, consequently, affect the successive discharge activities and their development. Therefore, the corona discharges at the icicle tips play an important role in the formation of the initial arcs and even in the flashover process.

Although studies of corona discharge have been widely carried out [79][86][89][98],

very few studies on the corona discharges at icicle tips [45][48] were focused on and the space charge produced by the corona discharge is often ignored in the studies on the discharge development processes and the simulation of electric field distribution around the ice-covered insulators [43][53].

In order to better explore these stochastic discharge processes and advance our fundamental knowledge of corona discharge, the space charge behaviour during discharge activities will be mainly discussed and analyzed in detail in this chapter.

7.2 DISCHARGE PULSE SEQUENCE AT ICICLE ELECTRODE

7.2.1 Sequential Discharge Pulse under DC+ Voltage

For a given condition of d=7 cm, T=0 °C and σ=320 μS/cm, a positive DC voltage was applied to the icicle electrode and the corona discharges at the icicle tip were recorded and observed. **Figure 7-1** shows the corona discharge pulse sequence for 50 ms at positive DC voltages of 22.5, 23, 24 and 25 kV, respectively.

At a low applied voltage of 22.5 kV, every discharge pulse with a large charge magnitude is followed by one discharge pulse with a small charge magnitude. After a short period, called a dark period, without discharge pulse generation, another discharge pulse with large discharge magnitude occurs again. The discharge pulse series is severely non-uniform and the difference between large magnitudes and small magnitudes is significant. This phenomenon can be still observed at an applied voltage of 23 kV, but is not as obvious as those under 22.5 kV. If the applied voltage is increased further up to 24 kV or 25 kV, the

discharge frequency increases significantly and the time interval decreases. Meanwhile, the aforementioned phenomenon does not appear any more. Moreover, the discharge pulses tend to be more uniform.

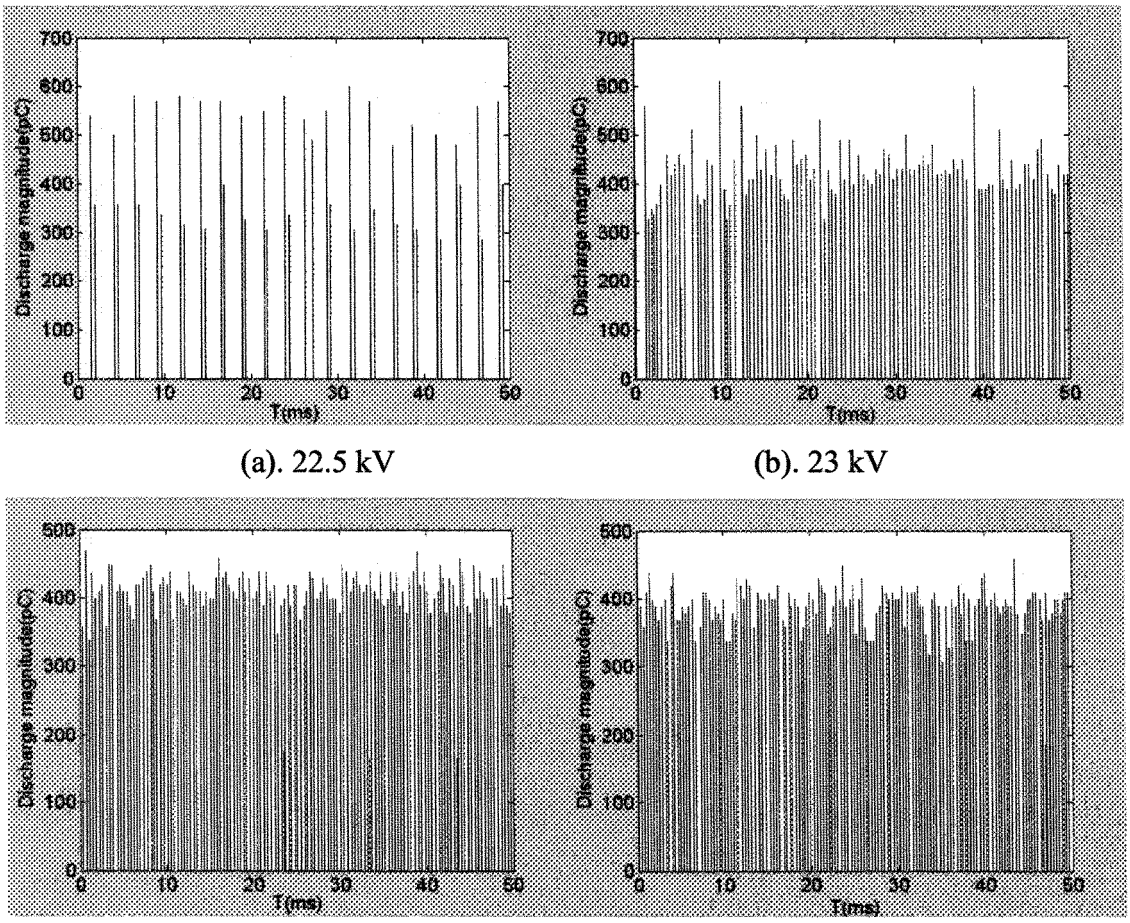

(a). 22.5 kV (b). 23 kV

(c). 24 kV (d). 25 kV

Figure 7-1 Discharge pulse sequence at various DC+ voltage levels at icicle

(T=0 °C, σ=320 μS/cm and d =7 cm)

7.2.2 Sequential Discharge Pulses under Different DC- Voltage

For a given condition of d=5 cm, T=0 °C and σ=80 μS/cm, a negative DC voltage was applied to the icicle electrode and the corona discharge magnitude at the icicle tip were recorded and observed. **Figure 7-2** shows the corona discharge pulse sequence for 50ms at negative DC voltages of 21, 22, 23 and 24 kV, respectively.

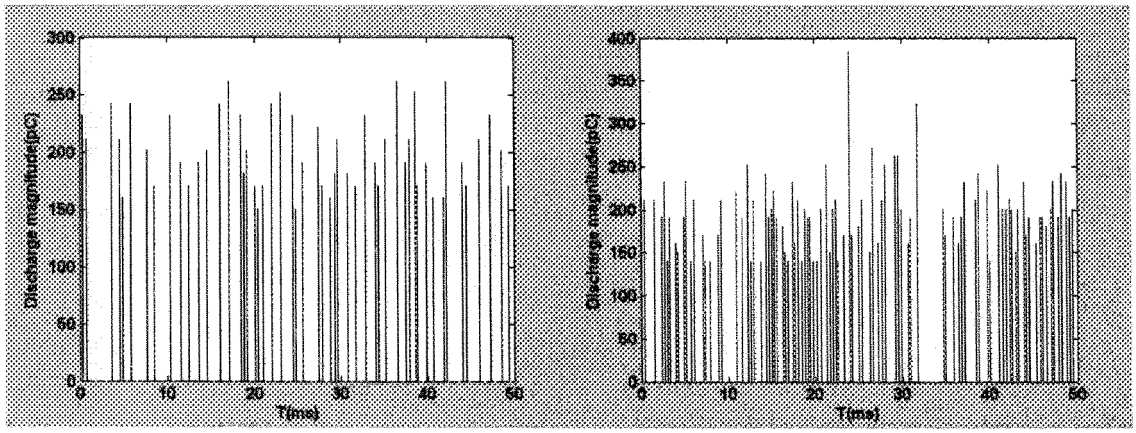

(a). 21 kV (b). 22 kV

(c). 23 kV (d).24 kV

Figure 7-2 Discharge pulse sequence at various DC- voltage levels at icicle

(T=0 °C, σ=80 μS/cm and d =5 cm)

It can be observed that the discharge pulses are not uniform at all applied voltage levels and these discharge pulse are completely random. For example, most of the magnitudes of discharge pulse are small and less than 250 pC at 21 kV and 300 pC at 24 kV. They do not like the discharge pulses under DC+ voltage, which is every discharge pulse with a large charge magnitude is followed by one discharge pulse with a small charge magnitude. In addition, the discharge pulses become more and more non-uniform with an increase in applied voltage, but the maximum discharge pulse increases evidently.

7.2.3 Sequential Discharge Pulses under the Positive Half Cycle of Different AC Voltage

For a given condition of T=0 °C, σ=320 μS/cm and d =7 cm, AC voltage is applied to the icicle electrode and the corona discharge pulses were recorded by the current pulse measurement system. **Figure 7-3** shows the corona discharge pulses for 40 ms at AC voltages of 18.4 kV and 19 kV, respectively.

Figure 7-3 shows that the discharge pulse sequence occur cyclically. In addition, the period in which the discharge pulse occurs is significantly shorter compared to the DC voltage. The repetition rate of discharge pulses is much lower than that under DC+ voltage. There is only one cluster of discharge pulses in every voltage period, and the first discharge pulse is always the largest. After that, they are followed by several discharge pulses of small magnitude, and the discharge pulse magnitude tends to decrease one by one and completely disappear. After a long period, the discharge pulse series are generated again in

the next period.

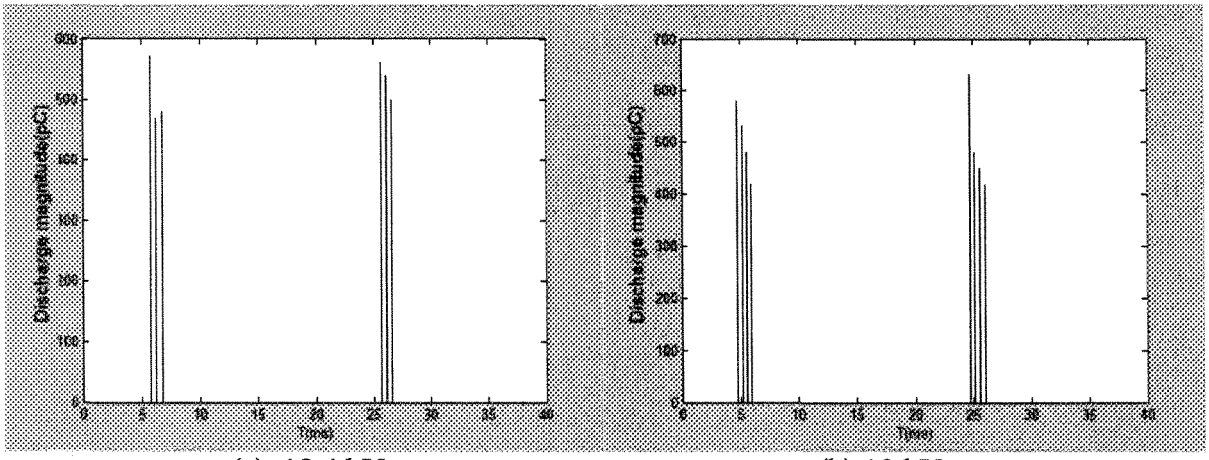

(a). 18.4 kV (b).19 kV

Figure 7-3 Discharge pulse sequence at positive half cycle of AC voltage at icicle (T=0 °C, σ=320 μS/cm and d =7 cm)

7.2.4 Influence of Applied Voltage on the Discharge Magnitude

The statistical results of the corona discharge magnitude are analyzed at different applied voltage levels and the result is presented in **Figure 7-4**. The maximum value and the standard deviation of discharge pulse magnitude both significantly decrease with an increase in the applied voltage, which indicates that the corona discharge pulses tend to become more and more uniform as the applied voltage increases. However, the mean discharge magnitude fluctuates slightly with the change of applied voltage, and it does not increase with an increase in the applied voltage. For example, the mean discharge magnitudes are 422.7 pC, 426.7 pC, 386.5 pC and 398.2 pC corresponding to the applied

voltage of 22.5 kV, 23 kV, 24 kV and 25 kV, respectively. **Figure 7-4** (b) shows that the mean discharge magnitude and the standard deviation both increase with an increase in applied voltage under AC voltage. That is because the influence of previous discharge pulse on the sequential discharge pulse is not as evident as that under DC voltage due to too few discharge pulses.

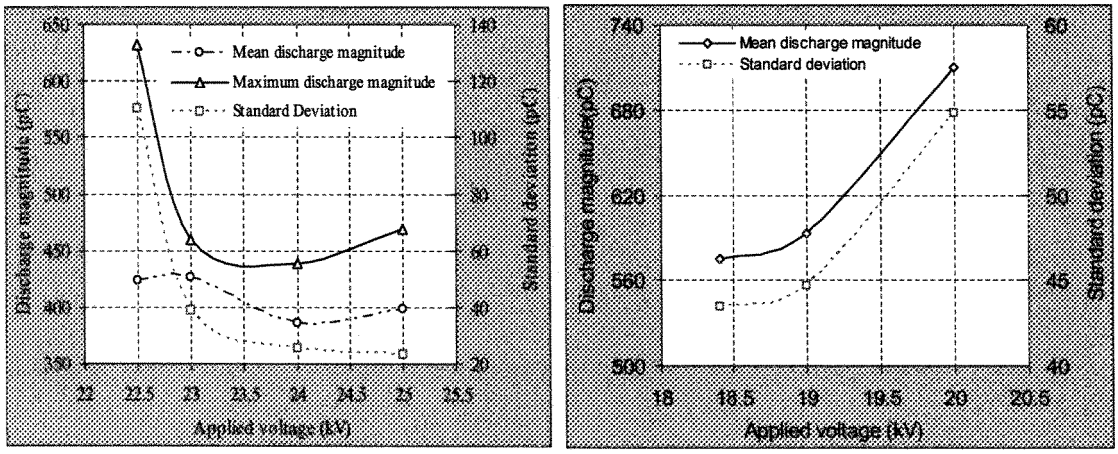

(a). DC+ voltage (b). AC voltage

Figure 7-4 Influence of the applied voltage on the discharge magnitude

7.2.5 Influence of Applied Voltage on the Time Interval of Discharge Pulse

According to **Figure 7-1** and **Figure 7-3**, the effect of the applied voltage on the time interval is shown in **Figure 7-5**.

The relationship between the applied voltage of DC+ and the time interval as presented in **Figure 7-5**(a) shows that the maximum time interval and the mean time interval both decrease with the applied voltage, which means that the discharge frequency

increases in high applied voltage. However, the minimum value of the time interval does not decrease strictly with an increase in applied voltage. The minimum time interval represents the minimum time required for the electric field to reactivate the next discharge pulse. It depends on the time constant of the capacitance of the gap in series with the resistance of the icicle, as well as on the disappearance of the space charge, which is influenced by the applied voltage level and the magnitude of the previous discharge pulse.

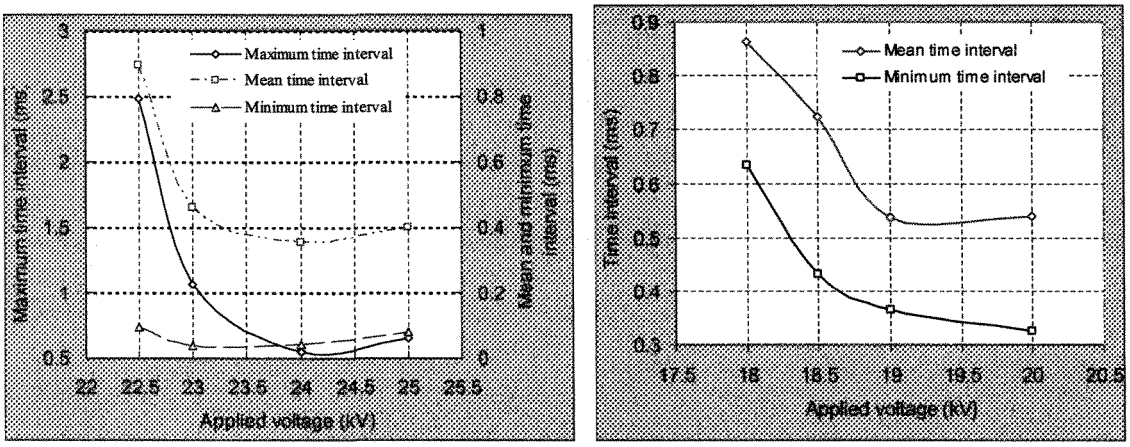

(a). DC+ voltage (b). AC voltage

Figure 7-5 Influence of applied voltage on the time interval

Figure 7-5 (b) shows that under AC voltage, the mean time interval and the minimum time interval both decrease with an increase in applied voltage. The mean time interval and the minimum time interval are evidently bigger than those under DC+ voltage. In special, the minimum time interval of AC voltage is slightly smaller than the mean time interval of DC voltage. Therefore, under AC voltage the influence of the previous discharge pulse on the sequential discharge pulse is not evident any more.

7.2.6 Distribution of Time Interval

The frequency distributions of the time interval of the discharge pulses shown in **Figure 7-1** during 200 ms are presented in the **Figure 7-6** according to different voltage levels. At low voltage level of 22.5 kV, although the time interval is mainly concentrated at around 0.5 ms, the statistical result of time interval does not follow the normal distribution as shown in red line. However, as the applied voltage increases, this distribution tends to follow a normal distribution as shown in red line, especially at high voltage level of 25 kV. This means that although the time intervals to occur the discharge pulses seem random, it follow a certain mechanism due to the existence of space charge, which is in agreement with the statistical result in [126].

Figure 7-7 shows the probability density distribution of time intervals corresponding to **Figure 7-6**. Obviously, the probability density distribution of time intervals is evidently influenced by the applied voltage. In particular, under low voltage level of 22.5 kV, its distribution range is wide. Whereas under high voltage levels of 24 kV or 25 kV, the probability density distributions become more and more narrow and follow an approximately normal distribution. Meanwhile, the standard deviation reducing at high applied voltage means that the time interval becomes more uniform at high applied voltage compared to that at low voltage.

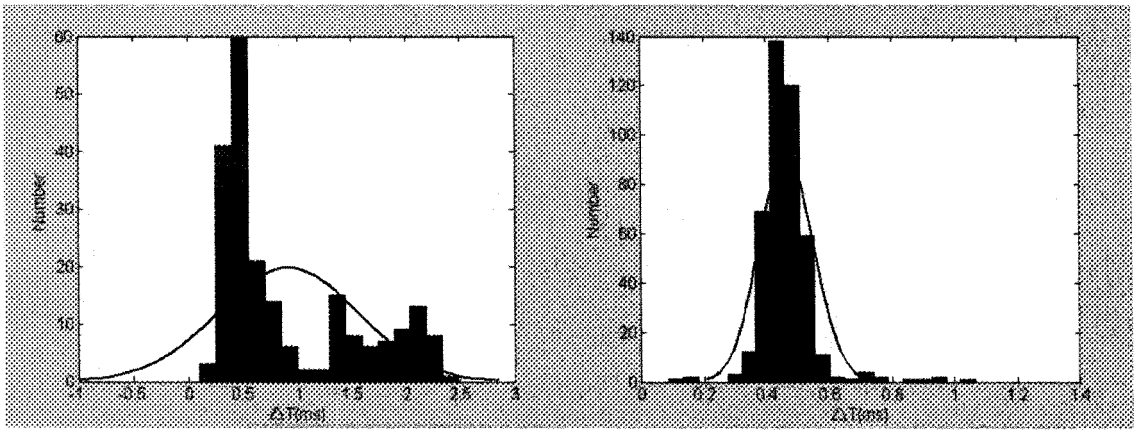

(a).22.5 kV (b).23 kV

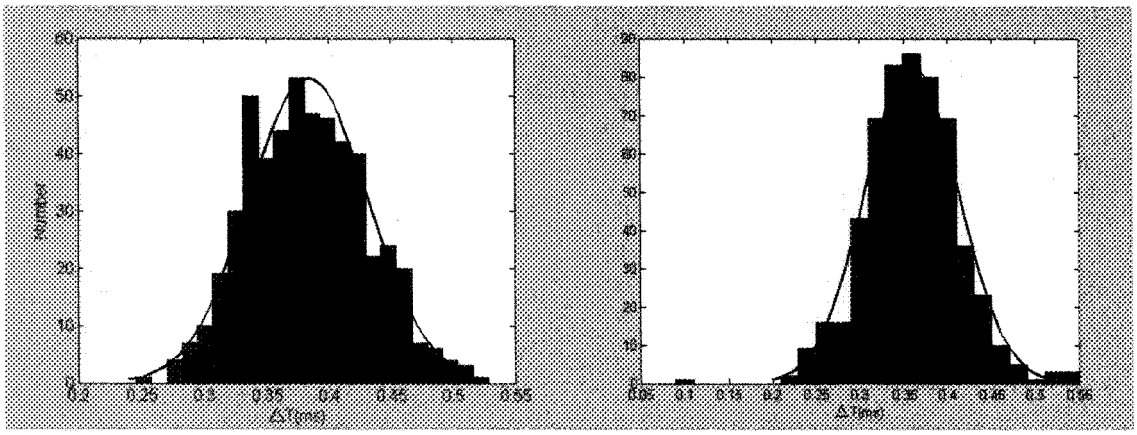

(c).24 kV (d).25 kV

Figure 7-6 Statistical result of frequency for discharge time interval

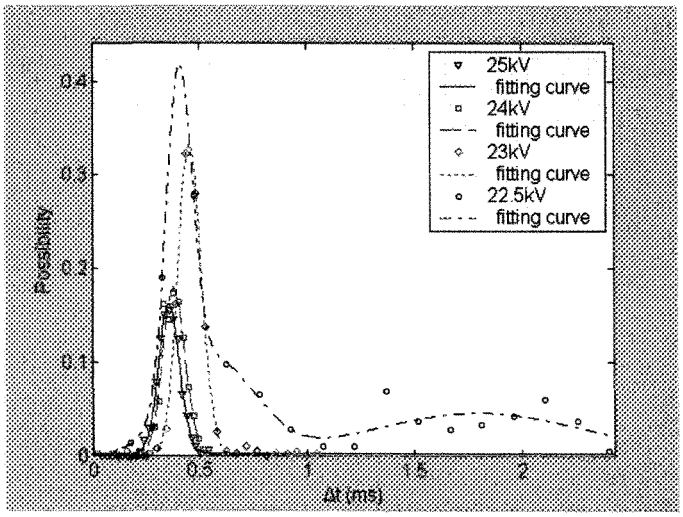

Figure 7-7 Probability density distribution of time interval

7.3 INFLUENCE OF PREVIOUS DISCHARGE PULSE ON SEQUENTIAL DISCHARGE PULSE

7.3.1 First Discharge Pulse Magnitude and Second Discharge Pulse Magnitude

The generation mechanism and definition of the first and the second discharge pulses are shown schematically in **Figure 7-8**. The discharge pulse, which occurs after a long time interval and have a high magnitude, are defined as the "first pulse", and those with a small magnitude and the closest to the "first pulse" are defined as the "second pulse" [83].

In order to understand how the space charge influences the sequential in a cluster of discharge pulse sequence, the first and second discharge pulse magnitude and their corresponding time intervals are extracted under DC+ voltage level of 22.5 kV and AC voltage level of 19 kV, respectively, and the relationship between the discharge magnitudes

and the time intervals is illustrated in **Figure 7-9**.

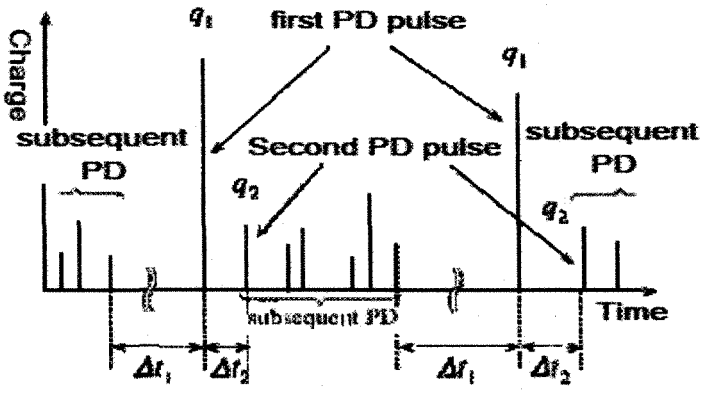

Figure 7-8 Definition of the first and the second discharge pulse

As seen in **Figure 7-9**(a), under DC+ voltage, although all discharge magnitudes are scattered, the first and second discharge pulses can be obviously distinguished by the time interval and the discharge magnitude, Q. Generally, the time interval to activate the first discharge pulse is longer than 1 ms and the first discharge pulse magnitudes seem to be random and bigger than 500 pC. The time interval to generate the second discharge pulse is normally shorter than 0.9 ms. Moreover, all second discharge pulse magnitudes are less than 500 pC. The second discharge pulse magnitudes are evidently dependent on the previous time interval and increase with an increase in the time interval.

Figure 7-9 (b) shows that under a positive half-cycle of AC voltage the first and the second discharge pulse magnitude are completely separated. The time interval of first discharge pulse is long, up to almost 20 ms, and all discharge magnitudes are above 500 pC, which means only one first discharge pulse is generated in every applied voltage period.

The time interval to activate the second discharge pulse is relatively small and meanwhile its discharge amplitude is slightly smaller compared to the first one. Despite the fact, some magnitudes of the second discharge pulse are also larger than 500 pC; half of them are less than 500 pC.

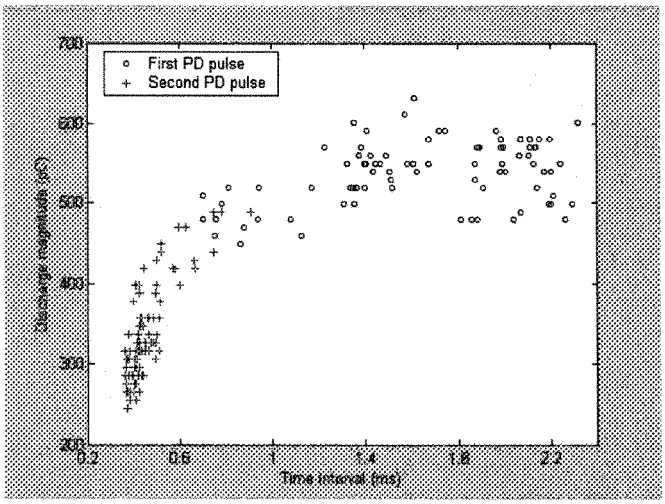

(a). DC+ voltage level of 22.5 kV

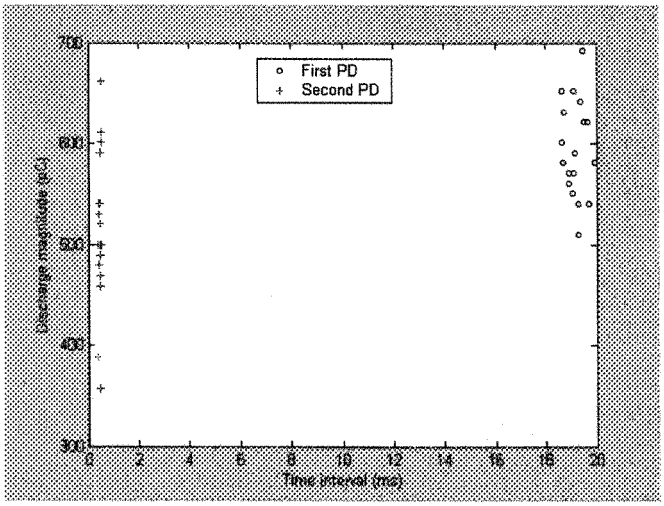

(b). AC voltage level of 19 kV

Figure 7-9 Relationship between the first discharge pulse and the second discharge pulse

7.3.2 Relationship between the Discharge Magnitude and the Time Interval under DC+ voltage

The relationship between the subsequent discharge pulse magnitude and the time interval under positive DC voltage is shown in **Figure 7-10** for various voltage levels. Each plot corresponds to a pair of sequential discharge pulses in a period of 200 ms.

Figure 7-10(a) and (b) show that at low voltage levels of 22.5 kV or 23 kV, the discharge magnitude, Q, increases with an increase in the time interval Δt, up to a certain time interval by approximate linearity defined as the critical time interval [24]. When the time interval is above that, this increase in Q is not significant. That is, when the time interval is longer than the critical time interval, Q is not influenced by Δt and is kept around 550 pC. The critical time interval is different for different applied voltage levels. It is approximately 1.41 ms at 22.5 kV and 1.1 ms at 23 kV.

However, at high voltage of 24 kV or 25 kV, the above-mentioned linear relationship between Q and Δt does not exist. In this case, almost all time intervals are less than 0.6 ms and almost all discharge magnitude is higher than 300 pC but lower than 500 pC, and it is unlike the phenomenon under low applied voltage, in which some discharge magnitude is lower than 300 pC and some is higher than 600 pC. This is because all the discharge activities occur under the strong influence of the space charge.

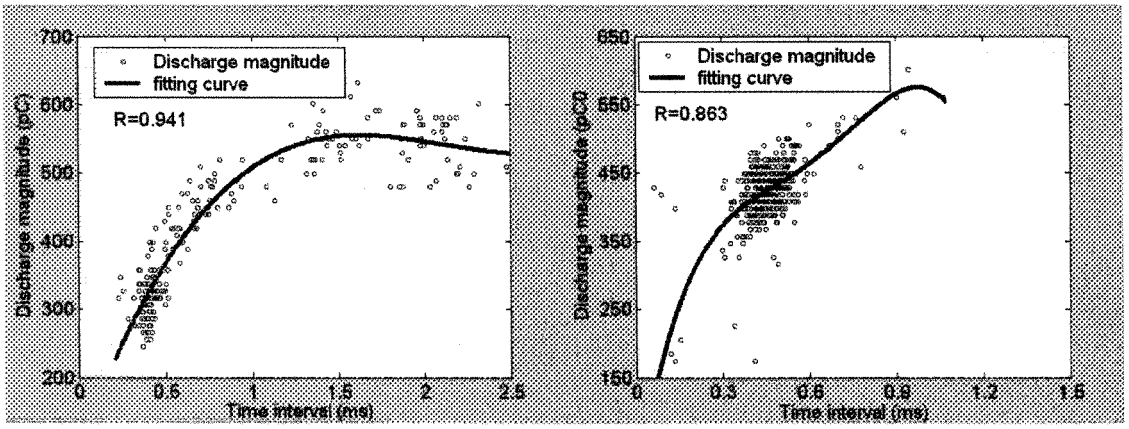

(a). 22.5 kV (b). 23 kV

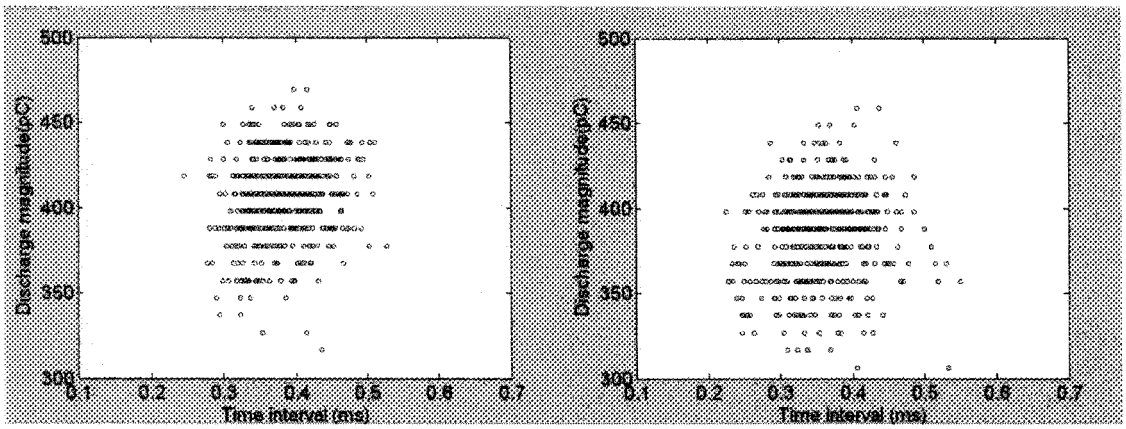

(c). 24 kV (d). 25 kV

Figure 7-10 Relationship between discharge amplitude and time interval under different DC+ voltage levels (T=0 °C, σ=320 μS/cm and d =7 cm)

7.3.3 Relationship between the Discharge Magnitude and the Time Interval under DC- voltage

The relationship between the subsequent discharge pulse magnitude and the time interval under negative DC voltage is shown in **Figure 7-11** for various voltage levels. Each

plot corresponds to a pair of sequential discharge pulses in a period of 100 ms. it can be noted that although the time interval of discharge pulse reduces, the discharge pulse magnitudes are random. No evident relationship between Q and Δt may be found. For example, according to the same time interval of 0.4 ms at 23 kV, some discharge magnitudes are as low as around 150 pC and some magnitudes are higher than 450 pC.

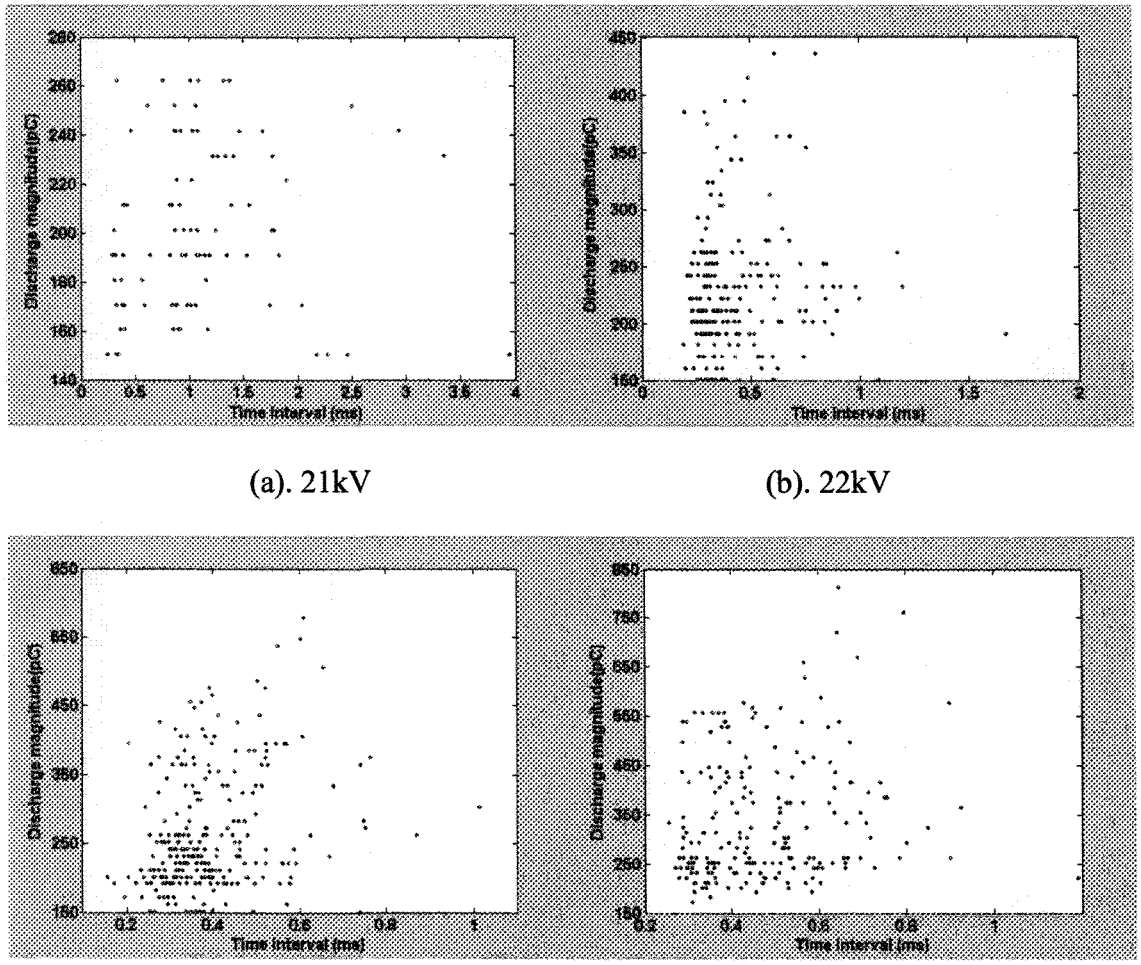

(a). 21kV (b). 22kV

(c). 23kV (d). 24kV

Figure 7-11 Relationship between discharge amplitude and time interval under different DC- voltages (T=0 °C, σ=80 μS/cm and d=5 cm)

7.4 DISCHARGE ACTIVITIES AT METAL ELECTRODE

7.4.1 Sequential Discharge Pulse under DC Voltage

For d=5 cm, a positive or negative DC voltage was applied to the metal electrode and the corona discharges were recorded and observed. **Figure 7-12** shows the corona discharge pulses for 50 ms at different positive DC voltage levels of 14, 15, 16 and 18 kV, respectively. **Figure 7-13** presents the corona discharge pulses for 50 ms at different negative DC voltage levels of 15, 16, 18 and 21 kV, respectively.

Under DC+ and DC- voltages, at a low applied voltage level, every discharge pulse with a large charge magnitude is followed by one discharge pulse with a small charge magnitude. After a relatively long period without discharge pulse generation, another discharge pulse with large discharge magnitude occurs again. The discharge pulse series is severely non-uniform and the difference between large magnitudes and small magnitudes is significant. For example, at the positive applied voltage levels of 14, 15, 16 kV, and at the negative applied voltage levels of 15, 16, 18 kV, the aforementioned phenomenon always exists. However, as the applied voltage increases up to 18kV under DC+ and to 21kV under DC- respectively, the discharge frequency increases significantly and the time interval decreases. Meanwhile, the aforementioned phenomenon no longer appears. Moreover, the discharge pulses tend to be more uniform.

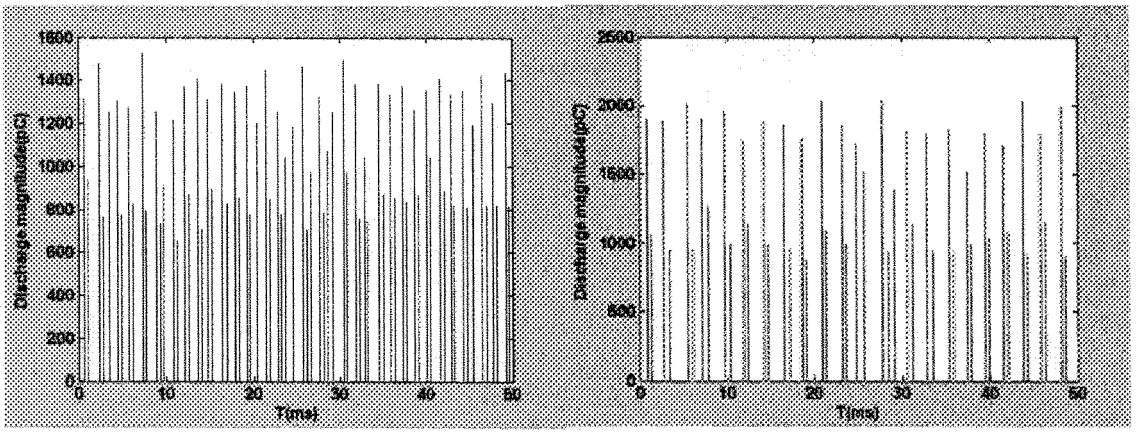

(a).14kV (b).15kV

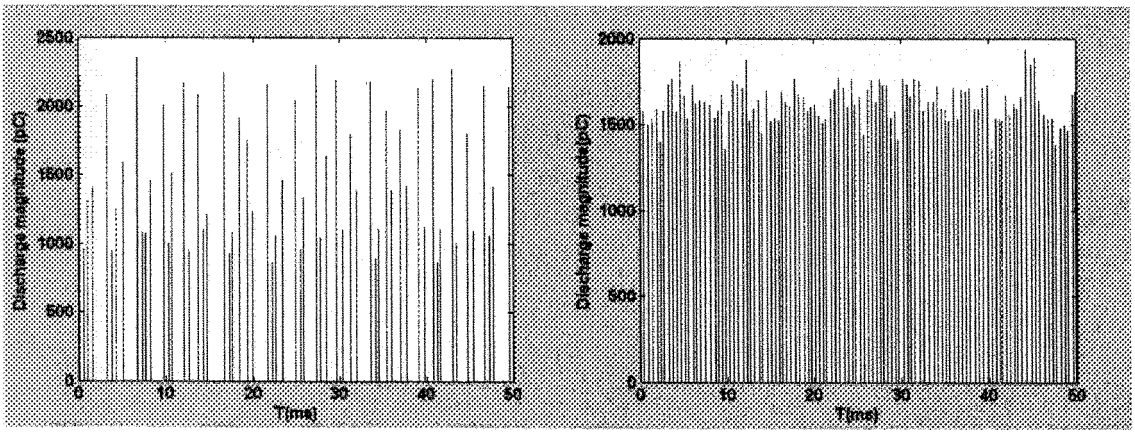

(c).16kV (d).18kV

Figure 7-12 Discharge pulses at different DC+ voltage levels for metal electrode (d=5 cm)

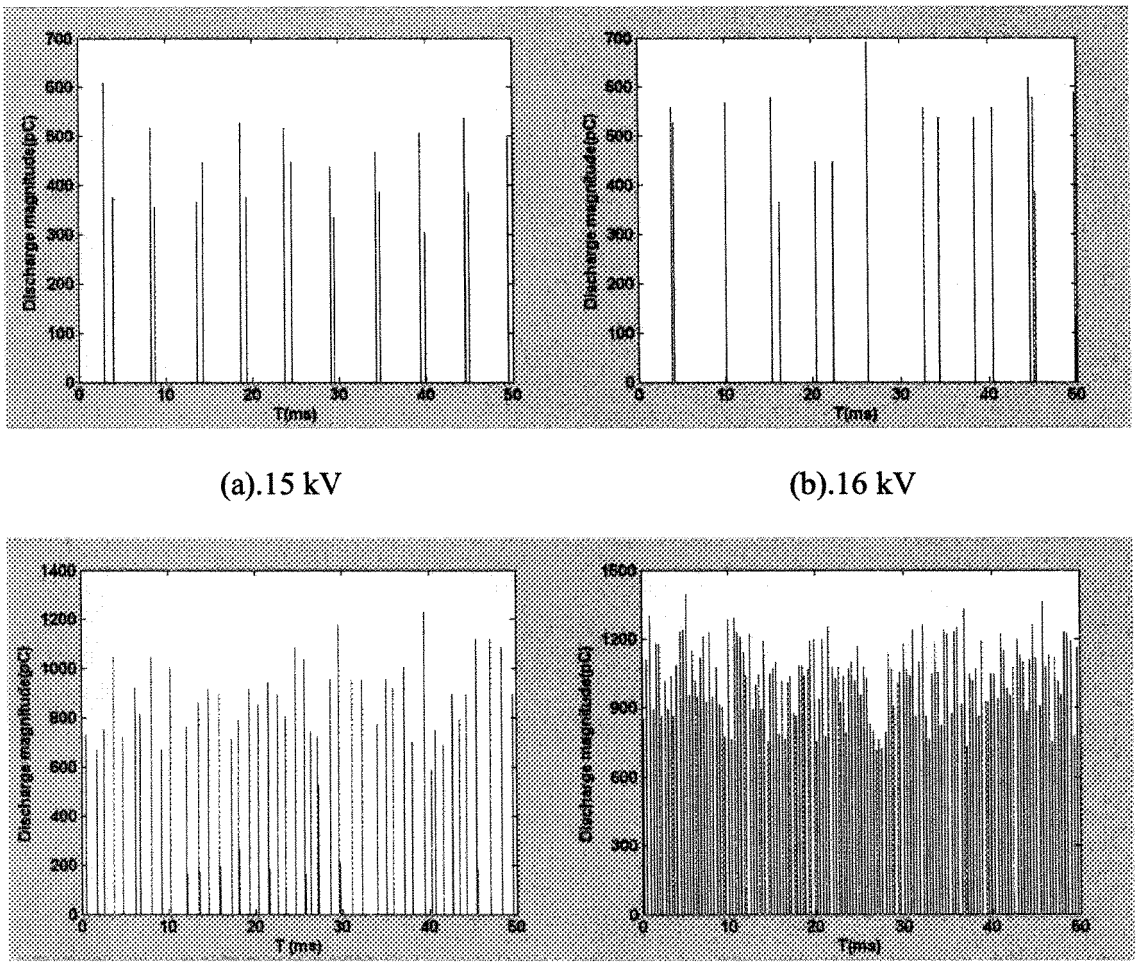

(a).15 kV (b).16 kV

(c). 18 kV (d).21 kV

Figure 7-13 Discharge pulses at different DC- voltage levels for metal electrode (d=5 cm)

7.4.2 Relationship between the Discharge Magnitude and the Time Interval under DC+ voltage

Under positive DC voltage and d=5 cm, the relationship between the subsequent discharge pulse magnitude and the time interval at the metal electrode is shown in **Figure**

7-14 for various voltage levels. Each plot corresponds to a pair of sequential discharge pulses in a period of 200 ms.

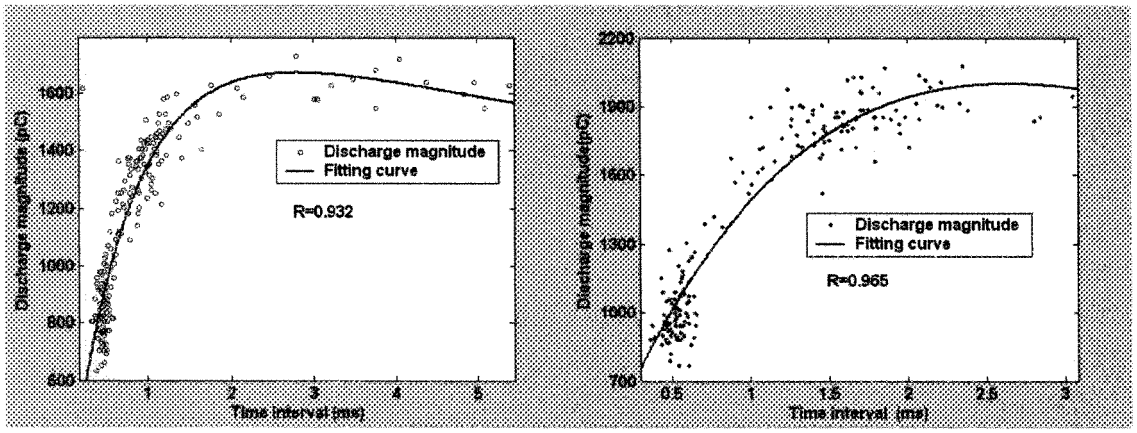

(a).14 kV (b).15 kV

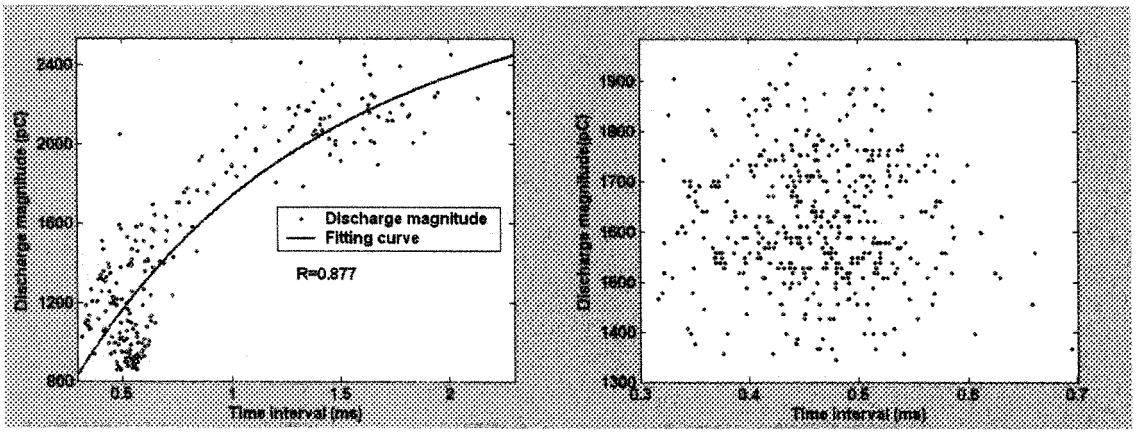

(c).16 kV (d).18 kV

Figure 7-14 Relationship between the discharge amplitude and the time interval under different DC+ voltages for the metal electrode

Figure 7-14 (a), (b) and (c) show that at the low voltage levels of 14, 15 and 16 kV, the discharge magnitude, Q, increases with an increase in the time interval Δt, up to the

critical time interval. When the time interval is above that value, this increase in Q is no longer significant. That is, when the time interval is longer than the critical time interval, the discharge pulse magnitude, Q, is not influenced by Δt and is slightly influenced by an increase in the applied voltage. The critical time interval decreases slightly from approximate 2.5 ms at 14 kV to around 1.5 ms at 16 kV. When the applied voltage increases to 18 kV, the aforementioned linear relationship between Q and Δt does not exist any longer. It can be observed that all the time intervals are less than 0.7 ms; meanwhile, all the discharge magnitude is almost higher than 1300 pC, but lower than 1900 pC. This is different from the phenomenon at low applied voltage, in which some discharge magnitudes are lower than 800 pC at 14 kV and some of them are higher than 2400 pC at 16 kV. This is because all the time interval of discharge pulse is less than the critical time interval, and therefore the all the discharge activities occur under strong influence of the space charge.

7.4.3 Relationship between the Discharge Magnitude and the Time Interval under DC- voltage

Under negative DC voltage and d=5 cm, the relationship between the subsequent discharge pulse magnitude and the time interval at the metal electrode is shown in **Figure 7-15** . Each plot corresponds to a pair of sequential discharge pulses in a period of 200 ms.

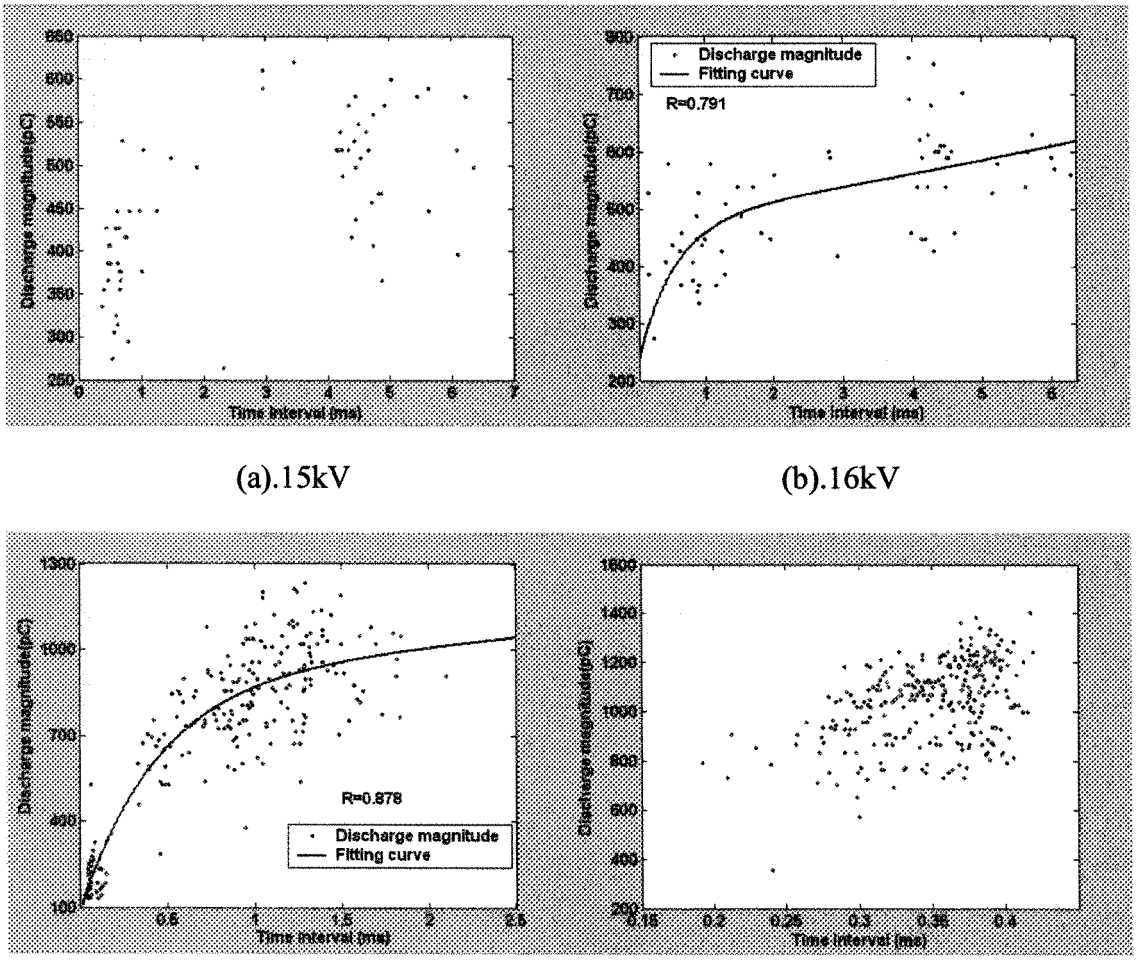

(a).15kV (b).16kV

(c). 18kV (d).21kV

Figure 7-15 Relationship between discharge amplitude and time interval under DC- voltage for metal electrode

Figure 7-15 (a) show that at low voltage level of 15 kV, the discharge magnitudes, Q, are separated by different time intervals. The discharge magnitude with a large time interval is relatively larger than those with a small time interval. When the applied voltage increases slightly, to 16 kV, it can be found that the discharge pulse magnitude increases with an increase in the time interval, Δt, to a critical time interval, and this tendency

becomes more evident under a slightly higher voltage level of 18 kV. The critical time interval decreases with an increase in applied voltage, and the discharge magnitude corresponding to the critical time interval is around 600 pC and 800 pC for 16 and 18 kV, respectively.

When the applied voltage is increased further and reaches 21 kV, the aforementioned relationship between Q and Δt does not exist. These discharge activities seem random as those observed under DC+ voltage, and almost all time intervals are less than 0.45 ms and almost all discharge magnitudes are higher than 600 pC but lower than 1400 pC. Evidently, all the discharge activities occur under the strong influence of the space charge, and this result is in quite agreement with the studies in [20] [105].

7.5 DISCUSSION

7.5.1 Occurrence of Discharge Pulse Series

As can be seen from **Figure 7-1** and **Figure 7-3**, the discharge pulse series is not consecutive, and the pulse amplitude and the time separation between two adjacent pulses are both varied. These non-consecutive discharge pulses have been found in other investigations [70] [125].

Basically, two conditions must be satisfied to form corona discharge: (1) one volume must have an Electric field strength (E) to gas density (N) ratio, E/N, greater than the critical value, $(E/N)_c$, at which the gas ionization coefficient η equals the electron attachment coefficient η_a, called critical volume; (2) some initiatory electrons must exist in

above critical volume. For example, the initial electrons result from the field emission from the electrode surface for DC- voltage and from the ionization of gas molecules for DC+ voltage, except that the discharge mechanism is the same. Therefore, in the following discussions and analysis, only the positive polarity will be discussed. The critical volume and the initial position of corona discharge for DC+ are shown in **Figure 7-16** (a) and (b), respectively.

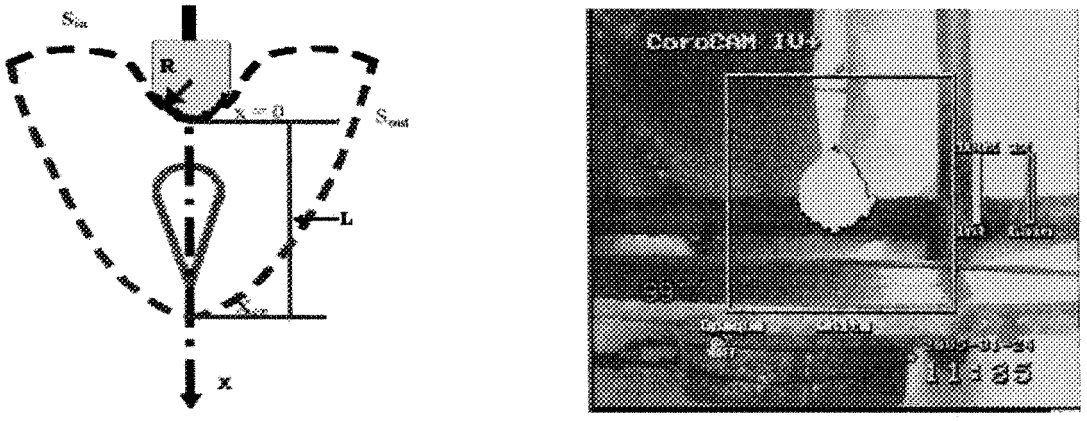

(a).Representation of critical volume, (b).Initial position of corona discharge

Figure 7-16 Corona discharge volume and inception position

Where S_{in} and S_{out} are the inner curve surface and outer curve surface of critical volume, and they are defined as:

$$S_{in}: X = 0 \text{ and } \bar{n}_e = n_0 \cdot \exp[\int_l \alpha_i(x) - \eta_\alpha(x)]dl(x)$$

$$S_{out}: X = X_{cr} \text{ and } E = E_{cr}, \eta_i = \eta_\alpha$$

Where $l = X_{cr} - X_0$ represents the path followed by the electron avalanche in the gas gap

in which $E/N > (E/N)_c$; X is the boundary of critical volume, x distance of point away from icicle electrode and $dl(x)$ is an element of path length; n_0 is initiatory electrons; η_i and η_α are ionization efficient and detachment efficient, respectively.

At the vicinity of the electrode point, numerous ionizations are produced in the region of intensive field. Because the free electrons are very mobile, an immobile positive ionic is left behind to form a space charge cloud (DC+ voltage). In fact, the discharge activities of coronas are restricted to a certain volume, where the overall Electric field strength, $\vec{E}$, is high enough to allow ionization. The Electric field strength $\vec{E}$ is determined by the external field, $\vec{E}_{app}$, and the electric field of space charge cloud, $\vec{E}_s$.

$$\vec{E} = \vec{E}_s + \vec{E}_{app} \text{ ---------- (7-1)}$$

The electrical field stress of the space charge cloud, $\vec{E}_s$ at the vicinity of electrode point with a known charge magnitude, Q, could be calculated approximately as follows:

$$\vec{E}_s = Q \Big/ (4\pi\varepsilon\rho^2) \text{ ---------- (7-2)}$$

Where ε is the permittivity of free space and ρ is the distance of the center of the space charge from the electrode point.

Because the initial growth of a discharge pulse depends exponentially on the local field strength [127], it can be expected that the 'size' of a discharge pulse as measured, for example, by its amplitude or integrated charge, will be sensitive to the small reductions in the field stress at the vicinity of the electrode point due to the existence of the space charge cloud. The subsequent discharge pulse occurs only after the space charge cloud moves

sufficiently far away from the electrode to allow the restoration of local field stress.

It is well known that these stochastic characteristics of the discharge activities are caused by the remaining space charge created by the discharge pulse. The space charge may reduce the local electric field strength near the point electrode to a level that eventually quenches the discharge activities. As long as the charge carriers are close to the initiation point of the avalanche, they will reduce the local field strength and thus finally stop the continuation of the avalanche.

The variability results in part from where and when the seed electron that initiates an electron avalanche appears. If the seed electron appears too far from the stressed electrode in a region where attachment dominates, the electron avalanche cannot form. However, if the electron is too close to the electrode inside the critical volume, the avalanche strikes the electrode before it can reach the critical size of 10^8 to form a detectable discharge pulse [130]. The seed electrons are delivered by negative ions of O_2^-. Negative ions can detach their extra electrons through a collision near the point electrode where the local Electric field strength is high enough [131].

7.5.2 Discussion on the Discharge Pulse Sequence under Different Voltage Polarities and Electrode Materials

At the icicle electrode, it is easy to find the difference between discharge pulses under different voltage types. Under positive DC voltage, every discharge pulse with a large charge magnitude is followed by one discharge pulse with a small charge magnitude

at low applied voltage, and the discharge magnitude, Q, increases with an increase in the time interval, Δt, up to a certain time interval. Only at high-applied voltage, the discharge pulse magnitudes seem random and irregular. However, under negative DC voltage, the discharge pulse magnitudes always appears randomly, and there is no similar relationship between the discharge magnitude and the time interval found at low or high-applied voltage levels. In addition, in a comparison of discharge pulses between the icicle electrode and the metal electrode, it is well known that at the metal electrode, a relationship between the discharge magnitude and the time interval may be obtained at the low levels of positive or negative DC voltage. Under DC+ voltage, comparing the discharge pulse occurring at the metal electrode with those at the icicle electrode, it is found that at the metal electrode there need a bigger variation of the applied voltage to transit the non-discharge pulses into the relative uniform discharge pulses.

Therefore, under negative DC voltage, the discharge at the icicle electrode is obviously different from that under other conditions. This may be due to the damage of icicle tip. The melting process of the icicle will cause a change in the source to emit the first electron. A sharp-point electrode is a guarantee to investigate the existence of space charge and its influence [20] [105].

In addition, **Loeb et al** [100] stated that at the water droplet electrode, there is no true corona occurrence because of its feeble luminosity. There are several numerical models proposed to explain the appearance of discharge pulses. **Morrow** [128] proposed that the secondary photon emission is dominant for the peak current of discharge pulse. The **Reess and Pailol's** model [132] explains that the field-effect emission is essential for the first rise

time of Trichel pulse. These theories suggest that the Trichel pulse never occurs at water or ice surfaces. However, a new quasi-one-dimensional model, taking into account only the secondary ion emission, shows a good agreement with the shape of the pulse and other characteristics [133]. According to this model, the discharge current pulse can occur not only from metal electrodes but also from water and ice surfaces. The related experiment results have also been verified by **Toshiyuki Sugimoto et al** [125] at water electrodes and **H.W. Bandel** [45] at water and ice points. However, more experimental and theoretical research using undamaged icicle tip is necessary to confirm these discharge pulses and their appearance to reveal the existence of space charge.

7.5.3 Space Charge Behavior Under DC+ Voltage

7.5.3.1 Space Charge Behavior and Discharge Pulse Generation

In order to explain this consecutive discharge pulse sequence in **Figure 7-1**, the corona stabilization and the space charge behaviors under DC+ voltage are proposed and illustrated in **Figure 7-17**. At first, once discharge pulse occurs as shown in **Figure 7-17** (I), because electrons move at least 100 to 1000 times faster than positive space charges, the residual space charges will form around the electrode point, as shown in **Figure 7-17** (II). The residual space charge ions will distort the Electric field strength and suppress the corona discharge occurrence, and this period without discharge activities is called a dark period. If the space charge cloud cannot suppress the generation and extension of discharge activities, and meanwhile, some initial electron are generated in the critical volume where

the Electric field strength is higher than the critical Electric field strength, a discharge pulse occurs as shown in **Figure 7-17** (II-a). During a small time interval period like **Figure 7-17** (II) and (II-a), the discharge pulse magnitude becomes relatively large in a short time interval. In general, this phenomenon occurs only at high voltage.

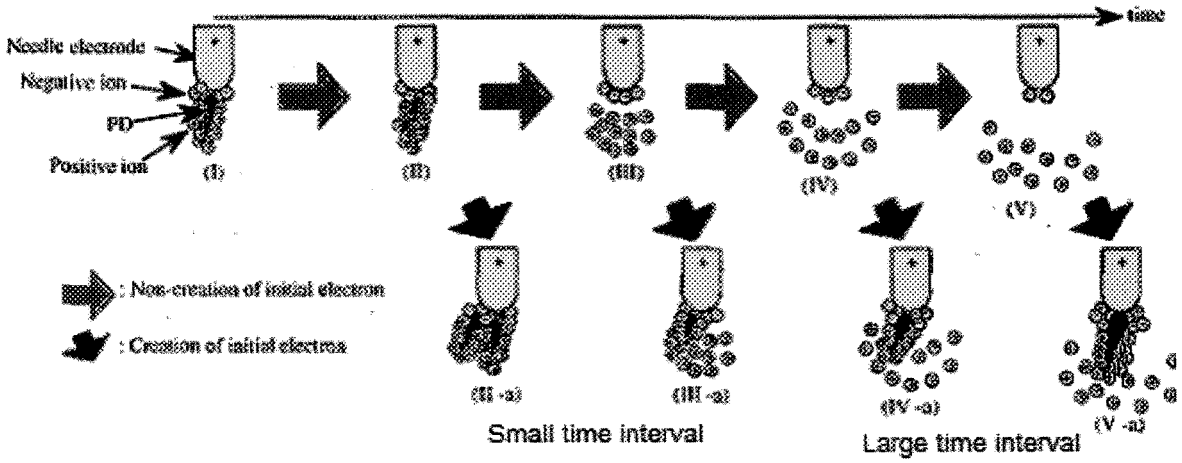

Figure 7-17 Schematic illustration of space charge behaviour and discharge generation

If the Electric field strength produced by the space charge cloud is strong enough to suppress the corona discharge activities, as the time increases, the space charge cloud will drift away from the anode. When the time interval is not very long and the space charge cloud does not drift very far from the anode, the original Electric field strength is not restored completely. At this moment, if a free electron is created in the critical volume to form an avalanche, a discharge pulse will be formed as shown in **Figure 7-17** (III) and (IV). The discharge magnitude depends on the time interval of the discharge pulse. The longer the time interval is, the larger the discharge pulse magnitude is.

If the time interval is longer than the critical time interval as shown in **Figure 7-17** (V), the space charge cloud will drift far away from the anode and will disappear at the cathode. The original field around the anode will be restored completely. Once a free electron is created, the discharge activity will occur and the pulse magnitude will be large. This is known as the "first pulse".

During discharge processes, the positive space charge generally reduces the local Electric field strength near the point electrode to a level that eventually quenches the discharge activities. Meanwhile, while the electrons drift and diffuse, numerous electrons are captured by molecules to form negative space charges. In turn, the negative space charge will provide the first free electrons to form the next pulsating discharge in the critical volume. However, how long the space charge can keep inhibiting the next discharge pulse cannot be clearly described by a single number. The space charge occupies a certain volume and contains a variety of ionic species, which in general have different mobility, and the next discharge pulse may occur before the space charge completely dissipates.

In addition, a similar discharge phenomenon between the discharge magnitude and the time interval of discharge pulse has been verified in SF_6 [83] and air [24], respectively.

7.5.3.2 Space Charge Behavior at Low Applied Voltage

Figure 7-10 shows that the relationship between the discharge magnitude and the time interval is influenced by the applied voltage, and this change is potentially determined by the existence of space charge.

The schematic illustration of the discharge pulse mechanism at low voltage is shown in **Figure 7-18**. This phenomenon mainly occurs at the applied voltage of 22.5 kV and 23 kV, when d=7 cm. At voltage levels slightly higher than that of the corona inception (22.5 or 23 kV), the Electric field strength produced by the applied voltage is low. Consequently, the discharge frequency is low, which means that the time interval between two discharge pulses is long. The discharge process is shown in **Figure 7-17** (III) and (IV). The discharge magnitude increases with an increase in the time interval.

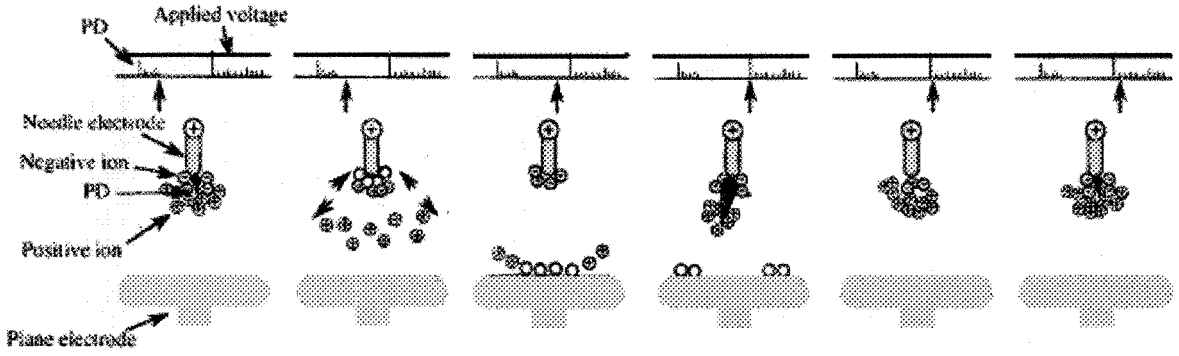

Figure 7-18 Schematic illustration of discharge mechanism at low voltage

The critical time interval, at which the discharge magnitude begins to stop increasing, depends on the voltage levels. The critical time interval at 23kV is less than that at 22.5 kV. This is because the space charge cloud moves faster in the stronger Electric field strength, and consequently, it takes less time for the space charge to drift.

When the time interval is higher than the critical value, it is sufficiently long to let all residual space charges clear completely before the next pulse starts. The influence of the space charge on the original Electric field strength is negligible. The influence of space

charge on the original field stress is very weak and thus ignorable. Thus, the discharge activities are not strongly influenced by the space charge cloud and the discharge pulse is only voltage dependence. The aforementioned correlation between the discharge magnitude and time interval vanishes. This discharge pulse is called the first discharge pulse and shown in **Figure 7-1** (a) and **Figure 7-8**. After that, the negative ions and electrons will increase discharge probability; however, the positive ions activate the corona stabilization effect. Hence, some discharge activities with small charge magnitude occur in the short time interval and they are called the second discharge pulse or sequential discharge pulse as shown in **Figure 7-1** and **Figure 7-17** (IV), respectively. During this discharge process, because the time interval is shorter than the critical value, the following discharge pulse magnitudes are proportional to the previous time interval.

7.5.3.3 Space Charge Behavior in High Applied Voltage

The schematic illustration of a discharge pulse generation mechanism at high voltage is shown in **Figure 7-19**. At a high voltage of 24 or 25 kV, the critical volume is large and the appearance of an initial free electron is very likely. Therefore, the discharge can be generated more easily than at the lower voltage levels of 22.5 or 23 kV. This will cause the time interval to reduce, which means the space charge cloud cannot move far away enough. This causes the activated the corona stabilization as shown in **Figure 7-17** (II-a), then the discharge magnitude of the subsequent discharge pulse becomes small. It is found from **Figure 7-10** (c) and (d) that the maximum time interval is 0.51 ms at 24 kV and

0.55 ms at 25 kV respectively. This means that all time intervals of discharge pulses are shorter than the critical time intervals of 1.3 ms and 1.0 ms under voltages of 22.5 kV and 23 kV respectively. Thus, all discharge activities occur under the effect of corona stabilization as shown in **Figure 7-17** (II). Therefore, the magnitude of subsequent discharge pulse is relatively small due to the corona stabilization effect from numerous positive ions derived from the previous discharge activities as shown in **Figure 7-17** (II) to (IV).

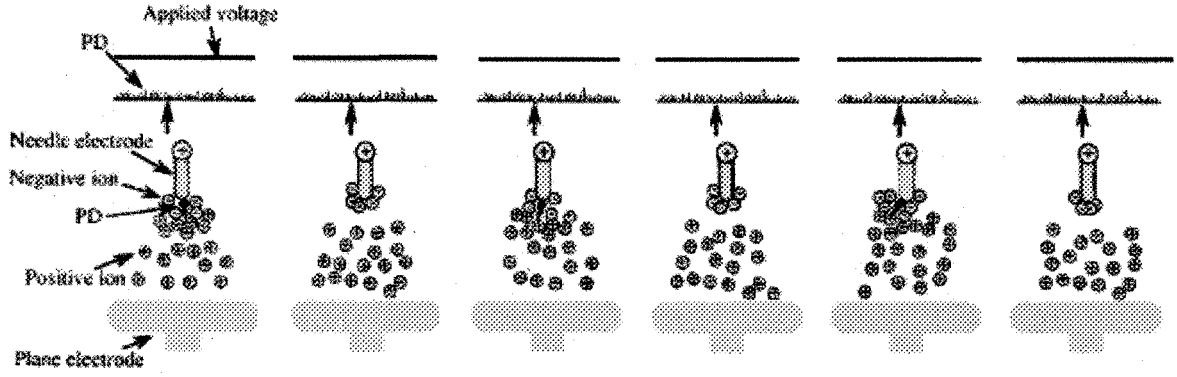

Figure 7-19 Schematic illustration of discharge mechanism at high voltage

7.5.4 Space Charge Behaviors under AC Voltage

The schematic illustration of discharge pulse generation mechanism at AC voltage is shown in **Figure 7-20**. The behaviors of space charge are more complicated under AC voltage than those under DC voltage, due to the change of external field. Therefore, the characteristics of space charge memory effects cannot be measured for the entire consecutive corona pulse series except for those with time intervals shorter than the critical

time interval. The ions generated by discharge activities in the previous negative half cycle drift away. The residual ions in one polarity will reduce electrical field stress and suppress discharge activities, whereas, after a switch of polarity, they may contribute to the generation of discharge activities in the sequential half cycle. Many investigations [134] revealed that discharge activities are mainly concentrated along the rise front of the sinusoidal waveform. Generally, the first discharge magnitude is proportional to the instantaneous voltage and the scatter of V_{inc} is related to the probability of generation of an initial electron.

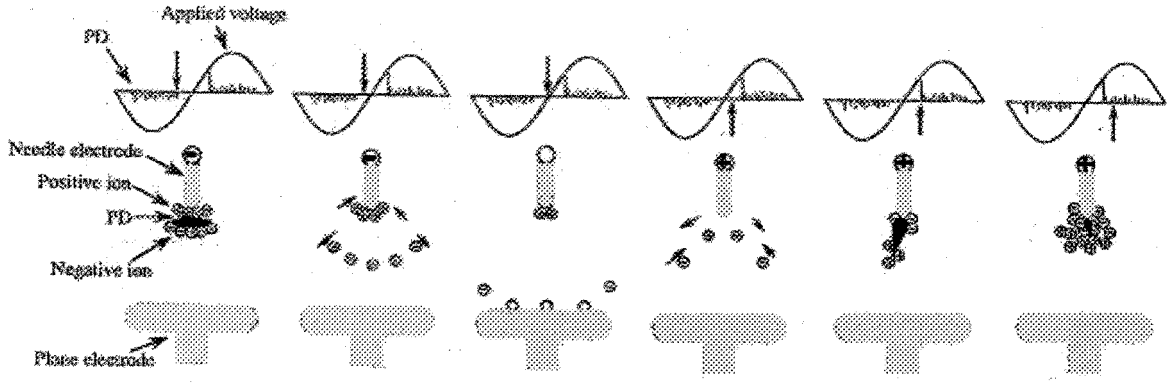

Figure 7-20 Schematic illustration of space charge behaviour under AC voltage

Figure 7-3 shows that the sequential discharge pulse magnitude is evidently smaller than the first one, although the external applied voltage still increases. **Figure 7-6** shows that the mean time interval in one cluster is less than the critical time interval. Therefore, before the sequential discharge pulses occur, the influence of space charge on the sequential discharge pulse still exists. This will cause the discharge pulse decrease and to be

independent of instantaneous voltage.

7.6 CONCLUSIONS

1). At different applied voltage levels, both the magnitude and repetition rates of the corona discharge pulses are different. At a voltage slightly higher than V_{inc}, each corona discharge pulse of larger magnitude is consistently followed by another pulse of lower discharge magnitude. At a high voltage, this phenomenon disappears. The repetition rates of the corona discharge pulses increases and the discharge pulse magnitudes become very uniform.

2). The time interval before the first pulse discharge is generally larger than that before the second pulse discharge. Although, the maximum time interval and the mean time intervals both decrease with an increase in applied voltage, the minimum time interval under DC voltage does not decrease strictly with an increase in applied voltage. The minimum time interval of AC voltage is slightly smaller than the mean time interval of DC voltage. Therefore, under AC voltage the influence of the previous discharge pulse on the sequential discharge pulse is not as evident as that under DC voltage.

3). The discharge pulses magnitude is influenced by the time interval between them. At voltages slightly higher than V_{inc}, the discharge magnitude, Q, increases with an increase in the time interval Δt, when Δt is small. Whereas, when Δt reaches a certain critical time interval, this increase in Q is not significant any more. At high voltages, the above relationship between Q and Δt does not exist.

4). The space charge will distort the electric field distribution and consequently affect the next discharge. Depending on the applied voltage and other conditions, if the Electric field strength produced by the space charge cloud is not strong enough to suppress the corona discharge, the next discharge will occur and a discharge pulse will be formed after a short time interval. If the Electric field strength produced by the space charge cloud is strong enough to suppress the corona discharge, the next discharge will occur when the space charge cloud drifts away from the anode, the discharge magnitude being dependent on the time interval. If the time interval is longer than the critical time interval, the space charge cloud will drift far away from the anode and has no effects on the next discharge. Therefore, another first pulse discharge will occur.

5). The influence of space charge on the sequential discharge pulse is more complicated under AC voltage due to the switch of voltage polarity compared to DC voltage. Under AC voltage, the residual ions suppressing the sequential discharge occurrence in previous half cycle may contribute to the generation of discharge activities in a sequential half cycle.

6). At metal electrode, the influence of space charge under DC voltage on the sequential discharge pulse can be obviously observed, and this phenomenon is in consistence with that found at icicle tip under DC+ voltage.

7). The discharge at icicle tips under negative DC voltage is different from those found under other voltage polarity and types, therefore, more experimental and theoretical research based on the undamaged icicle tip is necessary to confirm these discharge

pulses and their appearance from icicle and water tips to reveal the existence of space charge.

CHAPTER 8

SPACE CHARGE DIFFUSION AND DRIFT

CHAPTER 8

SPACE CHARGE DIFFUSION AND DRIFT

8.1 INTRODUCTION

The occurrence of corona discharge pulse is due to the existence of space charge, and this discharge is based on the generation of successive secondary avalanches producing breakdown.

At a sufficiently high field stress, the free electrons are likely to ionize a gas molecule by simple collision resulting in two free electrons and a positive ion. These two electrons will be able to cause further ionization by collision leading in general to 4 electrons and 3 positive ions. The process is cumulative, and the number of free electrons will increase as they continue to move in the electric field. The swarm of electrons and positive ions produced in this way is called an electron avalanche. Because the electrons move 10^2 to 10^3 times faster than positive ions, when electrons move away, the positive ions are still left behind, and the shape of a cone in space occurs. This is called the space charge.

In order to understand the space charge behaviour and its influence on the discharge process, the diffusion and the drift of the space charge cloud are studied in detail in this chapter and some simulated results will be presented as well.

8.2 SPACE CHARGE CLOUD

The existence of space charge will distort the original electric field and suppress the discharge activities. Meanwhile, the space charge cloud drifts away from the electrode tip to restore the Electric field strength. If there is no other discharge activities during its diffusion and drift, the diffusion and drift of the space charge cloud can be expressed as follows:

$$\frac{\partial n}{\partial t} + v \times \nabla n - D\nabla^2 n = 0 \text{ ---------- (8-1)}$$

Where n is the ion density, v the drift velocity of ion, and D the diffusion coefficient of ions.

Equation 8-1 is too difficult to be solved. Therefore, a new simplified method is proposed to consider the diffusion and drift of the space charge cloud; the space charge cloud is divided into limited small-spheres, in which the ion density is uniform and the Electric field strength is equivalent in the space charge sphere.

The process of diffusion and drift is based on the following assumptions:

- The electron flight between collisions is always rectilinear.
- Collisions produce abrupt changes in the direction of flight.
- The time of collisions will be considered negligible compared with the time of flights.

8.3 ION DIFFUSION

8.3.1 Ions Diffusion in the Space Charge Sphere

Supposing an ion sphere with the initial ion density n_0 and r_{eq} in radius, its propagation can be described by Equation 8-2, when $t > 0$ [135].

$$\frac{1}{r}\frac{\partial^2}{\partial r^2}(rn) = \frac{1}{D}\frac{\partial n}{\partial t} \qquad 0 \le r < r_{eq}, t > 0 \quad \text{---------- (8-2)}$$

Where n is the ion density in the sphere. It is supposed that ions diffuse uniformly in all directions; hence the number of ions crossing a unit area in the unit time is [105]:

$$J = -D\frac{\partial n}{\partial r} \quad \text{---------- (8-3)}$$

Because J can be also expressed as:

$$J = nv \quad \text{---------- (8-4)}$$

Combining Equation 8-3 and 8-4, Equation 8-2 can be written as:

$$\frac{\partial n}{\partial r} + \frac{v}{D}n = 0 \quad \text{---------- (8-5)}$$

Consider the space charge ions in a solid sphere $0 \le r \le r_{eq}$, with ion generation and subject to the non-homogeneous boundary condition of Equation (8-5), Therefore, the diffusion of ions in the space charge sphere can be concluded mathematically as follows:

$$\begin{cases} \dfrac{1}{r}\dfrac{\partial^2}{\partial r^2}(rn) = \dfrac{1}{D}\dfrac{\partial n}{\partial t} & \text{in} \quad 0 \le r < r_{eq}, t > 0 \\ \dfrac{\partial n}{\partial r} + \dfrac{v}{D}n = 0 & \text{at} \quad r = r_{eq}, t > 0 \quad \text{----------(8-6)} \\ n = n_0 & \text{for} \quad 0 \le r \le r_{eq}, t = 0 \end{cases}$$

When this problem is transformed by the transformation $U(r,t) = rn(r,t)$, the transformed system becomes:

$$\begin{cases} \dfrac{\partial^2 U}{\partial r^2} = \dfrac{1}{D}\dfrac{\partial U}{\partial t} & \text{in} \quad 0 \le r < r_{eq}, t > 0 \\ U = 0 & \text{at} \quad r = 0, t > 0 \\ \dfrac{\partial U}{\partial r} + (H - \dfrac{1}{b})U = 0 & \text{at} \quad r = r_{eq}, t > 0 \\ U = rn_0 & \text{for} \quad 0 \le r \le r_{eq}, t = 0 \end{cases} \text{----------(8-7)}$$

This is a homogeneous ion conduction problem for a slab $0 \le r \le r_{eq}$. After the transformation of the solution from $U(r,t)$ to $n(r,t)$, we obtain:

$$n(r,t) = \frac{2}{r}\sum_{m=1}^{\infty} \exp(-2t\beta_m^2) \frac{\beta_m^2 + k^2}{r_{eq}(\beta_m^2 + k^2) + k} \sin(r\beta_m) \int_{r'=0}^{r_{eq}} r' n_0 \sin(r'\beta_m) dr' \text{ ----- (8-8)}$$

Where

$$k \equiv \frac{v_d}{D} - \frac{1}{r_{eq}} \text{ ---------- (8-9)}$$

and the β_m value are the positive roots of

$$\beta_m r_{eq} \cot(\beta_m r_{eq}) + r_{eq} k = 0 \text{ ---------- (8-10)}$$

The roots of this transcendental equation are real if $r_{eq}k > -1$. When the value of k as defined above is introduced into inequality we find $(r_{eq}\frac{v}{D} - 1) > -1$, which implies $\frac{v}{D} > 0$. This result is consistent with the requirement on the physical grounds that in the original sphere problem we should have $\frac{v}{D} > 0$. Therefore, in the

psedoproblem, the coefficient $(r_{eq}\frac{v}{D}-1)$ may be negative, but the quantity $r_{eq}\frac{v}{D}$ is always positive.

8.3.2 Ions Diffusion out of the Space Charge Sphere

We now consider the problem of the ion diffusion in hollow sphere $a \le r \le b$. Based on the assumption proposed by McDaniel [136]:

- Ions are distributed uniformly in one plane whose radius is r_0 with a surface density of s;
- Ions diffuse towards unlimited space under a constant electrical field stress;
- Depleting reactions happen between ions and neutral molecules.

One solution of Equation 8-1 has been given as follows:

$$n(r,z,t)=\frac{s}{(4\pi D_L)^{1/2}}\exp[-\alpha t-\frac{(z-tv)^2}{4tD_L}]\times$$
$$[1-\sum_{m=0}^{\infty}\sum_{i=0}^{m}\frac{1}{m!i!}(\frac{r^2}{4tD_T})^m(\frac{r_0^2}{4tD_T})^i\exp(-\frac{r_0^2+r^2}{4tD_T})] \quad \text{---------- (8-11)}$$

Where D_L and D_T are diffusion coefficients in horizontal and vertical directions, respectively.

Supposing no ionizations due to collisions occur during dark duration,

$$\alpha = 0 \quad \text{---------- (8-12)}$$

If the plane with radius of R becomes one point, $r_0 \to 0$, and

$$b = s(\pi r_0^2) \quad \text{---------- (8-13)}$$

If b is the total number of ions, by L'Hospital's rule, the Equation can be expressed by

Where Q is the charge magnitude, E is the Electric field strength, and m is the mass of the particle. v is known as the drift velocity. The ratio of the velocity in field direction to the magnitude of field intensity, or the drift velocity per unit applied field, is expressed as:

$$k = \frac{v}{E} \text{----------(8-18)}$$

Where $\boldsymbol{k}$ is the mobility of ions.

When ions are moving in a gas in an electric field, they will collide with other articles according to the kinetic theory of gases and exchange energies.

Because the electric field of an air gap is not uniform, the drift of space charge clouds is a very complicated. Based on the methods proposed in [137] and previous assumptions in Section 8.2, the space charge cloud can be considered a point, and its drift is as follows:

$$\rho = k \cdot \vec{E} \cdot t \text{---------- (8-19)}$$

Where ρ is the drifting distance of space charge cloud away from the electrode tip, $\vec{E} = \vec{E}_{app} + \vec{E}_s$, $\vec{E}_{app}$ is external applied Electric field strength and $\vec{E}_s$ is the space charge Electric field strength.

8.5 RE-IGNITION OD CORONA DISCHARGE

With the time increase, the space charge sphere becomes bigger due to diffusion and drifts farther and farther away from the electrode because of the electric field. Thus, the Electric field strength at the vicinity of electrode tip will be restored. If the local field stress is restored to above a certain value, a sequential discharge pulse will occur.

Actually, the re-inception field tress of discharge activity in a fix electrode configuration is a constant, and this value is different and not related to the inception electric field of the first discharge [138]. Supposing the mechanism of sequential discharge pulse is similar to the first discharge pulse, based on the investigation [139], the equation of the re-inception field stress can be expressed as follows:

$$\vec{E}_r = 6.18\times10^5(1+\frac{1}{\sqrt[3]{100R_r}}) \text{ ---------- (8-20)}$$

Where $R_r=U/E_{max}$, U and E_{max} are the applied voltage and the maximum electric field at the vicinity of the electrode. Once the electrical field stress is higher than E_r, the second discharge activities will start again.

8.6 SIMULATION OF ION DIFFUSION AND DRIFT

For a quantitative understanding of the space charge behaviour, the space charge behaviour is theoretically calculated in consideration of (a) ion diffusion and (b) ion drift after discharge generation, respectively.

8.6.1 Ion Diffusion

Experimental evidence, based mostly on short gap measurements [140] has shown that the streamers which form the corona are essentially comprised of two regions: (1) the streamer head, or active region, where the luminosity generated in the tip flows to the H.V. electrode and remains attached to the electronegative molecules. The streamer head has the following characteristics:

1) It contains a net electric charge;

2) The temperature of the surrounding gas is 273 K;

3) The maximum temperature at the central axis of the corona channel is 1200 K [141] [142].

4) The half width of the temperature distribution is 10 μm, which corresponds to the radius of the corona channel [143] [144].

5) The temperature distribution is independent of time.

During calculation of the positive ion distribution with consideration of ion diffusion in the radial direction of the icicle electrode, the ion diffusion coefficient, D, is given as follows based on the aforementioned characteristics:

$$D = \frac{KT}{e} k^{+} \text{ ---------- (8-21)}$$

Where K is the Boltzmann constant ($1.38\ 10^{-23}$ JK^{-1}), k^{+} is the mobility of positive air ions, and T is assumed a Gaussian temperature distribution in or around a corona channel and expressed [145] as:

$$T = 927 \exp\{-(\frac{{d_c}^2}{10 \times 10^{-6}})^2\} + 273 \text{ ---------- (8-22)}$$

Where d_c is the distance in the radial direction from the central axis of the corona channel.

The distribution of the positive ion density along one axial direction can be calculated by the following:

$$\frac{n}{n_0} = -\frac{1}{\sqrt{4\pi Dt}} \exp(-\frac{r^2}{4Dt}) \text{ ---------- (8-23)}$$

where n is the ions density at the time of t after discharge pulse generation, the distance, r is the radius of the space charge cloud and n_0 is the number of ions at t=0 and d=0.

The calculated results based on the above characteristics for different times after discharge activity occurrence are shown by the full curves in Figure 8-1. As time proceeds, the number of ions in the axial direction decreases drastically, while the width of the ion distribution radically increases in the radial direction of the electrode. This means that the ion density declines drastically.

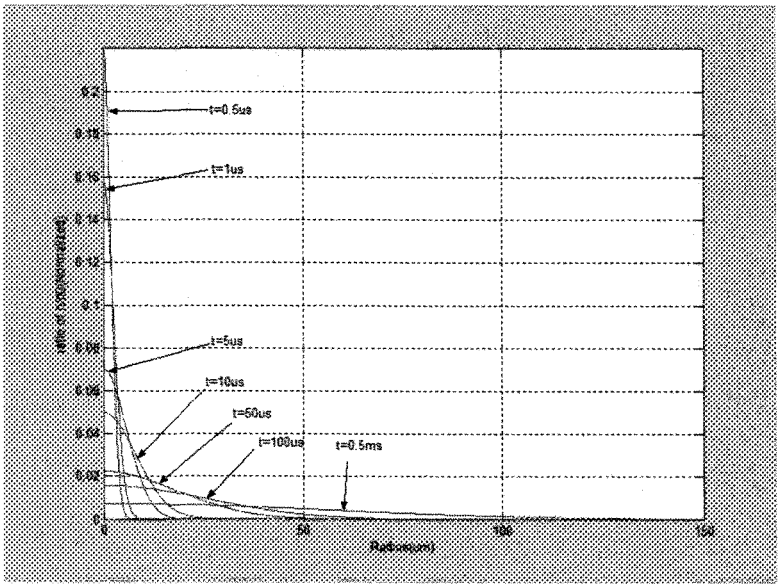

Figure 8-1 Positive ion distribution due to ion diffusion

8.6.2 Ion Drift

During calculation of ion drift, the following assumptions are proposed:

1) Discharge activities occur once discharge pulse is observed and discharge pulse duration is 600 ns[146], which accords to the duration of discharge pulse;
2) Ion mobility, k^+ is considered to be $1.36\times10^{-4}\ m^2V^{-1}s^{-1}$[105];
3) Collision between positive ions and other particles are neglected;

4) The influence of space charge is considered a charged sphere.

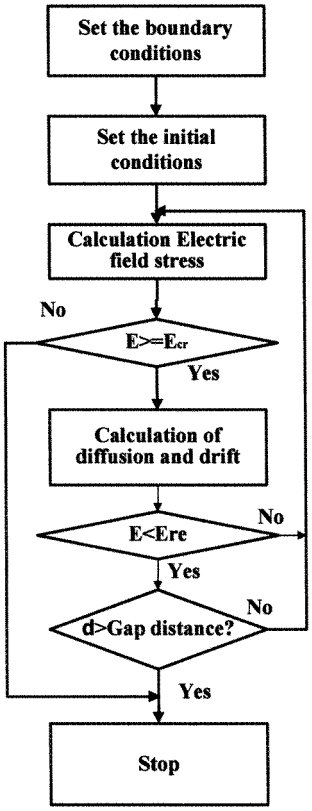

Figure 8-2 Flow chart for calculating the drift and diffusion of space charge sphere

The whole calculation flow chart is present in **Figure 8-2**. The drift condition of space charge positive ions at V_{app}=22.5 kV and d=7 cm was calculated and the result is presented in **Figure 8-3**. The whole diffusion and drift process of the space charge cloud before the next discharge was generated is illustrated and hatched in red. It was found that the radius of the space charge is enlarged and the distance between the space charge cloud and electrode tip increases with time. The influence of a space charge will last for 1.63 ms, when the sequential discharge pulse appears. The space charge does not reach completely to the electrode plane. This calculation result means that when the

influence of space charge is eliminated, the space charge ions have not arrived to plate or been absorbed as mentioned in [20][85]. In addition, the calculation result is in fair agreement with the experimental result simulated by **R. Morrow et al** [147], in which the streamer in the conditions of 20 kV and 50 mm gap is predicted to cease propagation after it has traversed 3.5 cm.

In addition, the corona discharge does not initiate directly from the electrode. Inversely, the first accelerated electron occurs in the region around 0.3 mm below the electrode tip; actually, the corona discharge first diffuses in the radial direction and afterward drifts into the gap space.

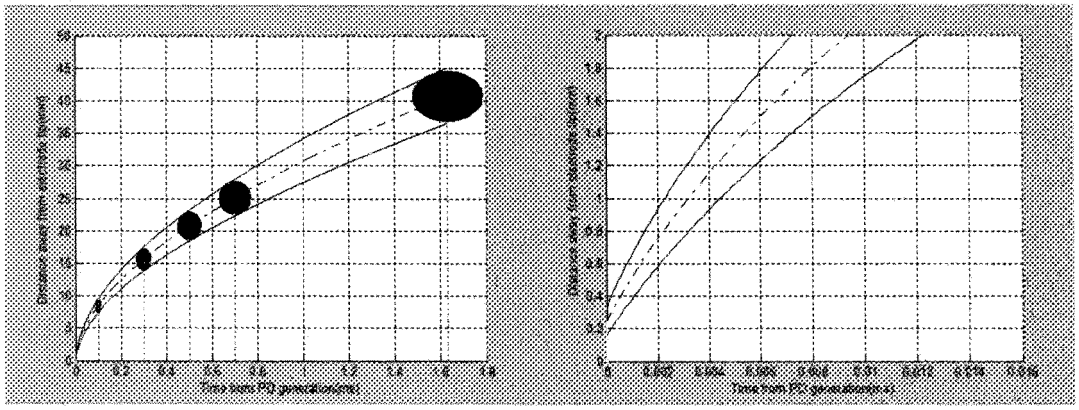

(a). the entire drift process (b). the inception phrase of corona discharge

Figure 8-3 Space time diagram of positive ion drift and the prospective volume of positive ions (d =7 cm, radius of tip=2.5 mm and V_{app}=22.5 kV)

8.6.3 Validation with the Experimental Results

Figure 8-4 compares the entire diffusion and drift process of the space charge sphere with different charge magnitudes. It was found that the time of drift is affected

by the charge magnitude of the space charge sphere. Evidently, the bigger the charge magnitude of the space charge sphere, the longer it drifts.

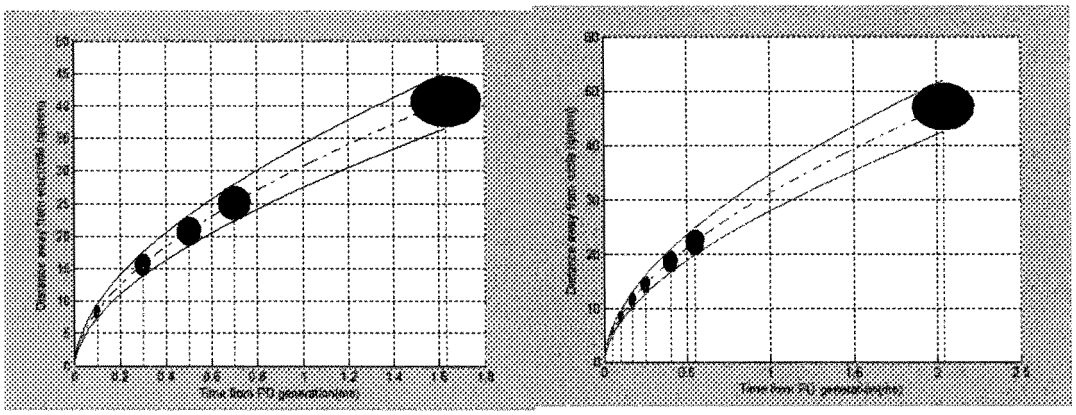

(a).400 pC (b).550 pC

Figure 8-4 Comparison on drift of space charge with different charge magnitude (d=7 cm, radius of tip=2.5 mm and V_{app}=22.5 kV)

Figure 8-5 shows the comparison of critical time intervals between test results and calculated results under DC+ voltage. The calculated critical time intervals decrease with increasing applied voltage and gap distance. For d=5 cm, the test results of critical time interval at 20k.5 kV and 21 kV are 1.61 ms and 1.2 ms, respectively. For d=7 cm, they are 1.42 ms and 1.1 ms at 22.5 kV and 23 kV, respectively. It is observed that these test results are always lower than calculation results, and the difference between test results and calculation results tends to increase. For d=7 cm, the difference and the deviation are 0.18 ms and 11.1% at 22.5 kV, respectively and increase up to approximately 0.5 ms and 31.3% at 23 kV, and a similar result can also be found at d=5 cm.

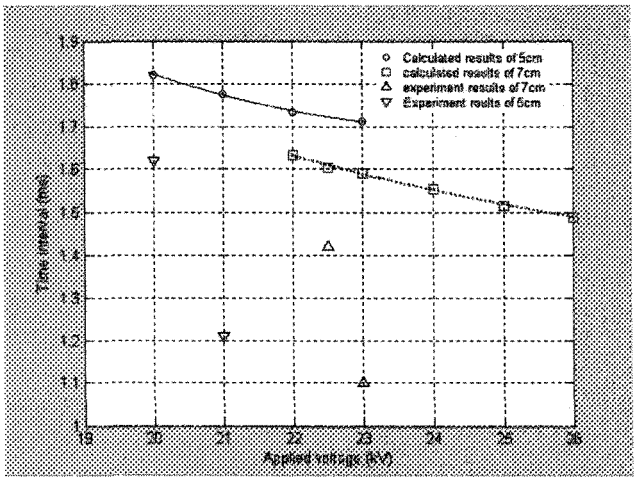

Figure 8-5 Comparison between test and calculated one on the critical time interval

The difference and deviation are caused by the existence of electrons and negative ions in the gap space. Actually, these electrons and negative ions can form initial discharge activities in the whole critical volume by direct desorption induced by photons or positive ions or by indirect desorption through secondary electron emission and sequent electron attachment. The corona discharge will increase the density of electrons and negative ions drastically, and they drift towards the positive electrode and may provide a seed electron to initiate another discharge pulse via collisional detachment [148] in the region where the local electric field is sufficiently high. Test results show that the corona discharge at 7 cm occurs at 22.5 kV. At this moment, the free electrons and negative ions are less; when the discharge activities start, the amount of electrons and negative ions increase radically. This is why the deviation increases at high voltage. Meanwhile, these calculation results and test results verify that the space charge ions with positive and negative charges have different functions during corona discharge activities. The positive space charge ions tend to decrease the electric field and suppress discharge development; however, the negative space charge ions tend to

support initial electrons for motivating discharge development.

8.7 POSSIBLE EFFECTS OF SPACE CHARGE ON THE FLASHOVER OF ICE-COVERED INSULATORS

Generally, it is well known to us that there are several discharge phases before the flashover happen on ice-covered insulators. The corona discharge is the first discharge phase. Corona discharge means the existence of insulation defect; meanwhile, the corona discharge will cause the occurrence of space charge: positive and negative space charge ions. The net charge density in the streamer head remains relatively constant as the streamer propagates, decreasing slowly only with time. The electrical field in the streamer head changes more significantly because it depends on the integrated charge in the streamer head. The various types of space charge have different roles in the discharge activities.

While the positive space charge ions are drifting, the electric field near the anode falls at first due to the shielding effect of the net positive space charge ions, but then the electric field tends to rise toward the anode for two different reasons [149].

- A negative space charge layer at the anode leads to a negative gradient of the electric field, hence a rising electric field towards the anode.
- Later, when only positive space charge remains but is moving away from the anode, the electric field raises at the anode as the electric field approaches the Laplacian distribution.

If the negative space charge does not have adequately high density, the negative ions will become neutralized at the anode. Meanwhile, some negative ions will supply

the initially free electrons for a new streamer to develop. If the negative space charge is high enough, the locally confined field is a quasi-uniform field and will be high enough to lead to a breakdown in this gap as glow discharge. The negative ions drift toward the anode and compensate for the loss in the density of negative ions in the space charge, which is due to recombination with positive ions created in the glow sheath as well as to diffusion.

In addition, the negative space charge ions also supply initially free electrons to form an avalanche. Generally, the negative space charge ions do not dominate the streamer propagation compared to the positive space charge ions.

Therefore, the space charge ions have a significant effect on the corona discharge and the streamer propagation on an ice-covered insulator, and this influence can be concluded as follows:

The space charge cloud suppresses or activates corona discharge, and this will cause a large amount of energy loss and ice melting during ice accretion, and consequently the formation of air gaps. This is also a potential loss to power system. After the existence of air gaps occurs along the ice-covered insulators, almost all applied voltage applies on the air gap, and thus the electric field become less uniform. The streamer propagates ahead in the air gap. The existence of space charge will drive the flashover track along the air gap away, which will increase the arc distance of the air gap and consequently its breakdown voltage. This phenomenon has been verified in this test and by other investigations [54] [150], as shown in **Figure 8-6**. The flashover track is not a straight line along the air gap, and the schematic illustrations of comprehensive direction of the electric field are also presented in **Figure 8-6**(c).

When the air gap is broken down, the partial arc could propagate over the ice

surface. The propagation of the partial arc along the ice surface is determined by the streamer inception electric field, and the space charge left behind the streamer head along the insulator has an effect on streamer propagation just as it does in the air gap. An evident discharge phenomenon that has been observed is the arc float as shown in **Figure 8-7**, which is also driven from the electric field by other factors, mainly the space charge presented in **Figure 8-8**, because the surface charge on the wet ice surface flows toward the opposite electrode. The relationship between the voltage drop and the arc length has been verified in [54] and expressed as: $V_{arc} = E_{arc} x_{arc}$. Therein, when the arc propagates through the air, an increase in the arc length and flashover distance will result in a higher flashover voltage of the ice-covered insulator.

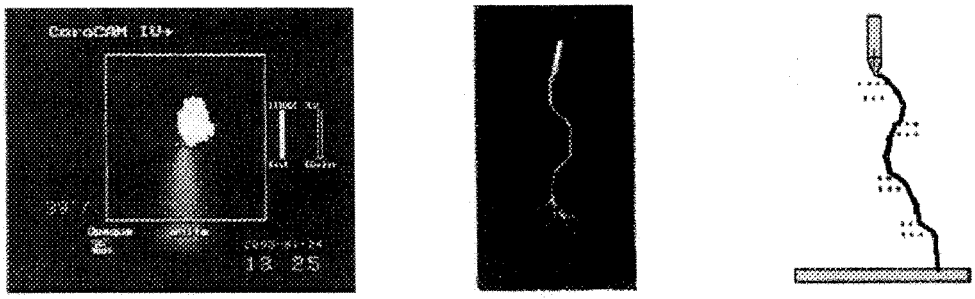

(a) (b) (c)

(a). Breakdown captured by CoroCAM IV+; (b). Breakdown captured by high speed camera under DC+ condition; (c).Flashover track under space charge effect

Figure 8-6 Breakdown track along the air gap

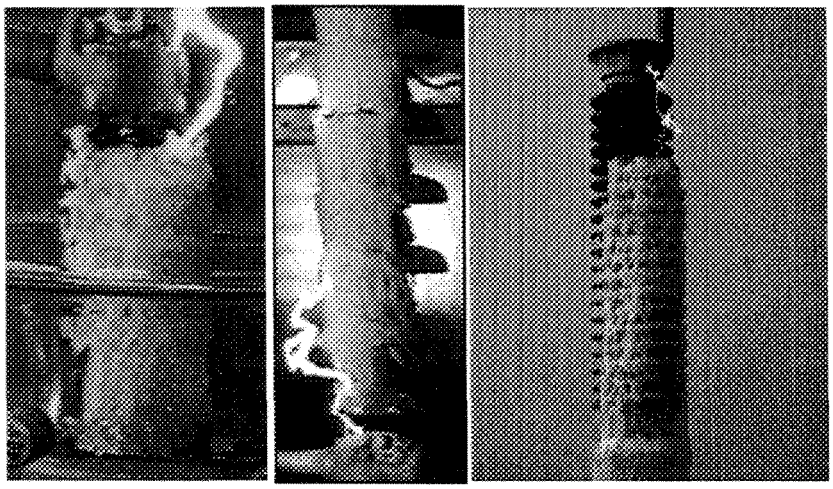

Figure 8-7 Arc float on the ice-covered insulators

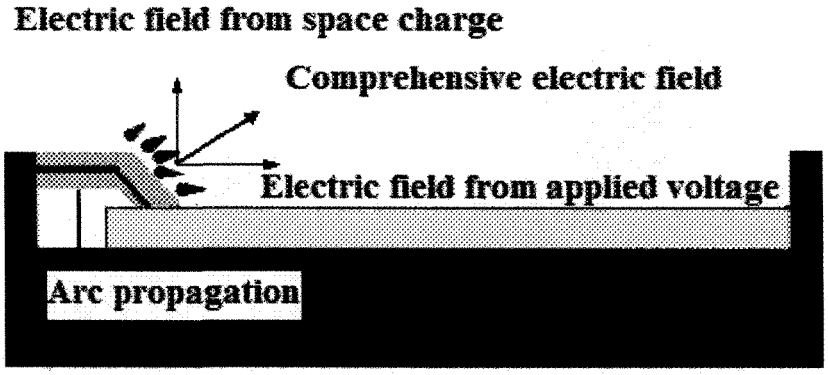

Figure 8-8 Effect of space charge on arc propagation on the ice surface

8.8 CONCLUSIONS

1) A model for calculating the drift and diffusion of the space charge cloud is presented. Due to the electric field and the ion thermal movements, the distance between the space charge cloud center and the electrode tip as well as the radius of the space charge cloud increase with the time. The critical time interval increases

with an increase in the charge magnitude of the space charge sphere and decreases with an increase in the applied voltage.

2) There is a difference between the experiment results and the calculated ones of the critical time interval due to the existence of free electrons or/and negative ions in the gap space, and this difference increases with an increase in the applied voltage because of the existence of more free electrons and negative ions at higher voltage level. Therefore, further study is needed to improve the accuracy of the calculations.

3) Space charge has the following effects on the flashover processes of ice-covered insulators:

   - It suppresses or activates the corona discharge continuously, which cause energy loss and ice melting, as well as consequently the formation of air gaps;
   - It drives the flashover track along the air gap away and increases the discharge distance crossing the air gap;
   - It drives the arc float during the arc propagation on the ice surface and increases the arc length, which results in a higher flashover voltage.

CHAPTER 9

CONCLUSIONS AND RECOMMNEDATIONS

CHAPTER 9

CONCLUSIONS AND RECOMMNEDATIONS

9.1 GENERALLY CONCLUSIONS

In this thesis, the corona discharge phenomenon and influence of space charge on sequential discharge activities were systematically studied for the first time using an icicle/ice-covered plate air gap system. The work presented in this thesis can be roughly divided into five components as follows:

- Corona inception voltage and discharge volume at V_{inc};
- Characteristics of corona current pulses;
- Statistical analysis of discharge pulse magnitude;
- Influence of space charge on sequential discharge processes;
- Modeling of diffusion and drift of space charge.

Based on the experimental results and the subsequent theoretical analysis presented in previous chapters, the general conclusions are summarized as follows:

1. **Corona Inception Voltage and Discharge volume at V_{inc}**

1.1. The corona inception voltage, V_{inc}, increases with an increase in air gap distance

in a logarithmic function. The influence of gap distance on V_{inc} is more evident under AC conditions than under DC conditions. At T=0°C, the logarithmic function of V_{inc} with the gap distance can be expressed as follows:

$$\begin{cases} V_{inc}=4.5\ln(d)+14.07 & \text{for DC+ voltage} \\ V_{inc}=4.49\ln(d)+13.76 & \text{for DC- voltage} \\ V_{inc}=5.90\ln(d)+9.49 & \text{for AC voltage} \end{cases}$$

1.2. The influence of temperature on V_{inc} is significant. V_{inc} at T=0 °C is lower than that at T=-5 °C. However, the influence of freezing water conductivity on V_{inc} is slight.

1.3. V_{inc} under AC voltage is lower than that under DC voltage. Under DC voltage, the influence of voltage polarity on V_{inc} is different at different temperatures. When T=0 °C, V_{inc} under DC+ voltage is always higher than that under DC- voltage; when T=-5 °C, V_{inc} under DC+ voltage is lower than that under DC- voltage.

1.4.The atmospheric pressure has an obvious influence on V_{inc}, and V_{inc} decreases with a decrease in atmospheric pressure. The value of exponent m decreases with an increase in the gap distance, which means that the influence of the atmospheric pressure on m becomes weak at long gap distance. The relationship between them can be expressed as: $m = -0.033 \times d + 0.938$.

1.5.The discharge volume at V_{inc} increases with an increase in the temperature and decreases with an increase in the gap distance. In addition, the discharge volume

at V_{inc} decreases with a decrease in air pressure. At low pressure, the corona discharge occurs directly as the glow discharge under DC+ and AC voltage.

2. Characteristics of Corona Current Pulses

2.1. The development of the corona discharge is different under DC+ voltage and DC- voltage. Under DC+ conditions, when the voltage reaches a certain value, the corona discharge is transited into the glow. However, under DC- voltage, when the voltage is high enough, another discharge volume occurs close to the iced plate.

2.2. The corona discharge under AC voltage is more complex than that under DC voltage due to the switch of voltage polarity. It has some comprehensive characteristics similar to DC+ and DC- voltages. One of the major differences between them is that the discharge current pulse occurs cyclically under AC voltage.

2.3. The repetition rate of the discharge current pulses is affected by the applied voltage, temperature, gap distance, and voltage type. It increases first and then decreases with an increase in applied voltage under DC+ voltage. However, under DC-, it increases with an increase in voltage at -5 °C and it increases first and then decreases with an increase in voltage at 0 °C. The maximum value of the repetition rate increases with an increase in the gap distance, and it is evidently higher under DC voltage than that under AC voltage.

2.4. The waveform of the current pulse is influenced by the environment temperature, the voltage polarity and the atmospheric pressure, but not by the voltage type. The duration of the pulse current at 0 °C is longer than that at -5 °C. The waveform of the current pulse is smoother under DC+ voltage than that under DC- voltage. Under the DC+ and the positive half-cycle of AC, the rising time of current pulse increases proportionally with a decrease in the atmospheric pressure. Under DC- and the negative half-cycle of AC, the falling time of current pulse increases with a decrease in the atmospheric pressure.

2.5. Corona discharge activities have a different influence on icicle shape. Under DC- voltage and AC voltage, the icicle shape is damaged and flattened, but this change is not evident under DC+ voltage.

3. Statistical Analysis of Discharge Pulses

3.1. The distributions of discharge magnitudes under DC and AC voltage follow Gaussian distribution. However, the shapes of the distribution curves are affected by voltage polarities of DC or AC voltages. The distribution may be expressed as follows:

$$P = \frac{1}{\sigma\sqrt{2\pi}} e^{\frac{(q-\mu)^2}{2\sigma^2}}$$ for DC+ and positive half-cycle of AC voltage

$$P = \frac{1}{\sigma_1\sqrt{2\pi}} e^{\frac{(q-\mu_1)^2}{2\sigma_1^2}} + \frac{1}{\sigma_2\sqrt{2\pi}} e^{\frac{(q-\mu_2)^2}{2\sigma_2^2}}$$ for DC- and negative half cycle of AC voltage

3.2. The discharge magnitude and the standard deviation decrease with an increase in gap distance. The gap distance has more evident influence on discharge magnitude under DC+ and positive half-cycle of AC voltage than under DC- and negative half-cycle of AC voltage.

3.3. The discharge magnitude at 0 °C is evidently larger than that at -5 °C. However, the change of conductivity slightly affects the discharge magnitude when the temperature remains constant.

3.4. The voltage polarity and type both have an influence on the discharge magnitude and the standard deviation. The discharge magnitude under DC+ voltage is higher than that under DC- voltage. In addition, the discharge magnitude under DC+ voltage is slightly lower than under the positive half-cycle of AC, but it is higher under DC- voltage than under the negative half-cycle of AC voltage.

3.5. Atmospheric pressure has an obvious effect on the discharge magnitude. The discharge magnitude first increases and then decreases with a decrease in pressure. The maximum discharge magnitude appears at 80 kPa, corresponding to 2 km in altitude.

4. Space Charge Behavior and Corona Stabilization

4.1. At different applied voltage levels, both the magnitude and repetition rates of the corona discharge pulses are different. At a voltage slightly higher than V_{inc},

each corona discharge pulse with larger magnitude is consistently followed by another pulse with lower discharge magnitude. At a high voltage, this phenomenon disappears. In this case, the repetition rates of the corona discharge pulses increase and the discharge pulse magnitudes become uniform.

4.2. The time interval before the "first" pulse discharge is generally larger than that before the "second" pulse discharge. Although the maximum time interval and the mean time intervals both decrease with an increase in applied voltage, the minimum time interval under DC voltage does not decrease strictly with an increase in applied voltage. The minimum time interval under AC voltage is slightly smaller than the mean time interval under DC voltage. Therefore, under AC voltage the influence of the previous discharge pulse on the sequential discharge pulse is not as evident as that under DC voltage.

4.3. The discharge pulse's magnitude is influenced by the time interval between them. At voltages slightly higher than V_{inc}, the discharge magnitude, Q, increases with an increase in the time interval Δt, when Δt is small. However, when Δt reaches a certain critical time interval, this increase in Q is no longer significant. At high voltages, the above relationship between Q and Δt does not exist.

4.4. The space charge will distort the electric field distribution and consequently affect the next discharge. Depending on the applied voltage and other conditions, if the electric field stress produced by the space charge cloud is not strong

enough to suppress the corona discharge, the next discharge will occur and a discharge pulse will be formed after a short time interval. If the electric field stress produced by the space charge cloud is strong enough to suppress the corona discharge, the next discharge will occur when the space charge cloud drifts away from the anode, as the discharge magnitude is dependent on the time interval. If the time interval is longer than the critical time interval, the space charge cloud will drift far away from the anode and will have no effects on the next discharge. Therefore, another "first" pulse discharge will occur.

4.5. The influence of space charge on the sequential discharge pulse is more complicated under AC voltage than under DC voltage due to the switch of voltage polarity. Under AC voltage, the residual ions suppressing the sequential discharge occurrence in the previous half-cycle may contribute to the generation of discharge activities in a sequential half-cycle.

5. Space Charge Diffusion and Drift

5.1. A model for calculating the drift and diffusion of the space charge cloud is presented. Due to electric field and ion thermal movements, the distance between the space charge cloud center and the electrode tip as well as the radius of the space charge cloud increases with time. The critical time interval increases with an increase in the charge magnitude of the space charge sphere and decreases with an increase in the applied voltage.

5.2. There is a difference between the experiment results and the calculated ones of the critical time interval due to the existence of free electrons or/and negative ions in the gap space, and this difference increases with an increase in the applied voltage because of the existence of more free electrons and negative ions at higher voltage levels. Therefore, further study is needed to improve the accuracy of the calculations.

5.3. Space charge has the following effects on the flashover processes of ice-covered insulators:

- It suppresses or activates the corona discharge continuously, which causes energy loss and ice melting, as well as the consequent formation of air gaps;
- It drives the flashover track along the air gap away and increases the discharge distance crossing the air gap;
- It drives the arc float during the arc propagation on the ice surface and increases the arc length, which results in a higher flashover voltage.

9.2 RECOMMENDATIONS

To the best of our knowledge, this is the first time that the mechanisms underlying the corona discharge at icicle tip have been systematically investigated. The results and conclusions of this study will contribute to the understanding of corona discharge phenomena and produced space charge during the whole discharge processes.

However, due to the limit of time for this Ph.D project, several aspects still remain unexplained. It is recommended that the related studies should be carried out, as follows. They include:

1. In the present study, due to the limitation in CoroCAM IV+'s operation temperatures, the simulating temperature of dry ice was set at -5 °C. Hence, it is proposed that a further study should be carried out at -12 °C. In addition, the influence of the humidity and the wind on the characteristics of corona discharge has not yet been investigated.
2. Under negative polarity, because electrons are ejected directly from icicle electrode surface, the shape of the icicle tip was changed by electron emission. Therefore, more experimental and theoretical research are necessary using the undamaged icicle tip to confirm the discharge under DC- voltage.
3. In order to understand the potential effect of corona discharge on the ice-covered insulators, the relationship between the leakage current and the PD magnitude should be investigated as well.
4. Influence of space charge exists not only in the first step of flashover, but also in all arc propagation process on ice surface. Therefore, further research should be carried out to study the space charge behavior in the entire flashover development process.
5. There is a significant difference between the experiment results and the calculated ones of the critical time interval due to the existence of free electrons

or/and negative ions in the gap space. Therefore, further study on the model is needed to improve the accuracy of the calculations.

6. Based on the obtained results, the space charge produced by the corona discharges exists and can not be neglected. Therefore, the electric field distribution along the ice-covered insulators with some air gaps should be simulated dynamically.

REFERENCE

REFERENCE

[1] Farzaneh M., and Drapeau J.F., "AC Flashover Performance of Insulators Covered with Artificial Ice", IEEE, Trans. on power Delivery, Vol.10, pp1038-1051, April 1995.

[2] Farzaneh M., "Ice Accretion on High-voltage Conductors and Insulators and Related Phenomena", Philos. Trans. Roy. Soc., vol. 358, No. 1776, pp. 2971–3005, Nov. 2000.

[3] CIGERE Task Force 33.04.09 2000, "Influence of Ice and Snow on Flashover Performance of Outdoor Insulators Part II", Affects of ice Electra 185, pp.55-69, 2000.

[4] Hara M. and Luan Phan C. "A Study of Leakage Current of HV Insulators under Glaze and Rime", Can.Elelc. Eng. J.Vol.3, pp.15-22, 1978.

[5] Boyer, A. E. and Meale, J. R., "Insulation Flashover under Icing Conditions on the Ontario-Hydro 500 kV Transmission Line System", Proceedings of CEA Spring Meeting, Montreal, Canada, March 1988.

[6] Chisholm, W. A., Ringler, K. G., Erven, C. C, Green, M. A., Melo, O., Tarn, Y., Nigol, O., Kuffel, J., Boyer, A., Pavasars, I. K., Macedo, F. X., Sabiston, J. K. and Caputo, R. B., "The Cold-Fog Test", Proceedings of IEEE/PES Winter Meeting, Baltimore, USA, Paper No. 96 WM 099-2 PWRD, 1996.

[7] Hydro-Québec, "Analysis of the Hydro-Québec System Blackout on April 1988", Official Hydro-Québec Report, Montreal, July 1988.

[8] Melo, O. T., Tarn, Y. T. and Farzaneh, M., " Freezing Rain and Fog Events in Southern Ontario: Properties and Effect on EHV Transmission Systems", Proceedings of 4th

International Workshop on Atmospheric Icing of Structures, Paris, France, pp.70-75, 1988.

[9] Charneski, M. D., Gaibrois, G. L. and Whitney, B. F., "Flashover Tests on Artificially Iced Insulators," IEEE Transactions on Power Apparatus & Systems, Vol. Pas-101, No. 8, pp.2429-2433, 1982.

[10] Kawai, M., "AC Flashover Tests at Project UHV on Ice-covered Insulators", IEEE Transactions on Power Apparatus & Systems, Vol. Pas-89, No. 8, pp.1800-1805, Dec. 1970.

[11] Khalifa, M. M. and Morris, R. M., "Performance of Line Insulators under Rime Ice", IEEE Trans. on Power Application and Systems, Vol. Pas-86, pp. 692-698, 1967.

[12] Matsuda, H., Komuro, H. and Takasu, K., "Withstand Voltage Characteristics of Insulator String Covered with Snow and Ice", IEEE Trans. on Power Delivery, Vol. 6, No. 3, pp. 1243-1250, July 1991.

[13] Fikke, S. M., Hanssen, J. E. and Rolfseng, L, "Long Range Transported Pollution and Conductivity on Atmospheric Ice on Insulators", IEEE Trans. on Power Delivery, Vol. 8, No. 3, pp. 13411-1321, July 1993.

[14] Watanabe, Y., "Flashover Tests of Insulators Covered with Ice or Snow", IEEE Trans. on Power Apparatus and Systems, Vol. Pas-97, No. 5, pp. 1788-1794, 1978.

[15] Forest, J. S., "The Performance of High Voltage Insulators in Polluted Atmospheres", Proceedings of IEEE Winter Meeting, New York, 1969.

[16] Kannus, K., Lahti, K. and Nousiainen, K., "Comparisons between Experiments and Calculations of the Electrical Behavior of Ice-Covered High Voltage Insulators",

Proceedings of International Workshop on Atmospheric Icing of Structures, Iceland, pp. 325-331, 1998.

[17] Farzaneh, M., and Kiernicki, J., "Flashover Performance of Ice-covered Insulators", Canadian Journal of Electrical and Computer Engineering, Vol. 22, No. 3, pp. 95 - 109, July 1997.

[18] Farzaneh, M., Volat, C., and Gakwaya A., "Electric Field Calculation around Ice-covered Insulators Using Boundary Element Method", IEEE Int. Symp. Elect. Insulation, Anaheim, CA, pp. 349-355 Apr. 2000.

[19] CIGRE Task Force 33.04.09. "Influence of Ice and Snow on the Flashover Performance of Outdoor Insulators", Part I: Effects of Ice. ÉLECTRA, No. 187, pp. 90-111, 1999.

[20] Van Brunt, R.J.: "Stochastic Properties of Partial discharge Phenomena", IEEE Trans, Diele. Elect. Insul, 26, (5). pp. 902-948 1991

[21] Starr, W.T.: "Corona Measurement', in Bartniks, R. and McMahon, E.J. (Eds.) 'Engineering Dielectrics and Interpretation", Vol. 1STP669. ASTM Press, Philadelphia, 1979

[22] Hoof, M., Freisleben, B., and Patsch, R. "PD Source Identification with Novel Discharge Parameters Using Counter Propagation Neural Networks", IEEE Trans. Diele. Elect. Insul., 4, (I), pp.17-35, 1997.

[23] IEEE Standard Corona Tests Supplement to ANSI/IEEE C37.34-1971, Test Code for High-voltage Air-Switches ANSI/IEEE Std C37.34a-1978 Volume, Issue, 1978.

[24] Chang, C. and Su, Q., "Memory Propagation of Negative Point-to-Plane Corona under AC Voltage", IEE Proc.-Sic Meas. Techno, Vol. 149, No, 3, pp.117-126, May 2002.

[25] Baden,R. T, "Hochspannungs technik I+II", Course Notes, 1995/96.

[26] Pounder, E.R., "Physics of Ice", Pergamon Press .Oxford, 1965

[27] Rupp, R. "Electrical Properties of Ice Ih Single Crystals", Proceedings of the International Symposium on Physics and Chemistry of Ice, Ottawa, Canada, Aug. 1972

[28] Buchan, P.G., "Electrical Conductivity of Insulator Surface Ices", Ontario Hydro Internal Report, May, 1989.

[29] Farzaneh, M., Chen, X., and Zhang, J., "A Study of Surface Conductivity and Flashover Voltage of Ice Samples Formed under Various Freezing Conditions", International Journal of Offshore and Polar Engineering, Vol.6, No.4, pp.298-303, Dec. 1996.

[30] Farzaneh, M., and Melo, O.T., "Properties and Effect of Freezing Rain and Winter Fog on Outline Insulators," Cold Regions Science and Technology, Vol.19, pp. 33-46, 1990.

[31] Farzaneh, M., Li, S.Y., and Srivastave, K.D., "Flashover on Ice Surface", Atmospheric Research, Vol.46, pp.37-47, 1998.

[32] Maeno, N., "Measurements of Surface and Volume Conductivities of Single Ice Crystals," Proceedings of the International Symposium on Physics and Chemistry of Ice, Ottawa, Canada, pp. 140-143, Aug. 1972.

[33] Fletcher, N.H., "The Surface of Ice", Proceedings of the International Symposium on Physics and Chemistry of Ice, Ottawa, Canada, pp. 132-136, Aug. 1972.

[34] Ibbercht, K.L. "Snow Crystals Ice Crystal Surface Physics", California Institute of Technology, http://www.its.caltech.edu/~atomic/snowcrystals/surface/surface.htm.

[35] Max Planck Socity, "Why is Ice so Slippery? Mysteries of the Invisible Ice Surface", http://www.mpg.de/ice2.htm.

[36] Mcnamara J., "The Structure of Ice and Its Role in Stratospheric", University of Manchester, http://mchhpi.ch.man.ac.uk/~mbdtsma/poster.ice.html.

[37] Yarris L., "Theory on Antarctic Ozone Hole Boosted by New Observations Confirming Wet Surface of Ice", Berkley Lab, http://www.lbl.gov/Science- Articles/Archive/ice ozone-link.html.

[38] Seelig T., Pilling, J. and Berndt L., "Physikalische Zusammenhange Beim Gefrieren und Schmelzen wâBriger Elektrolytlôsungen a Freiluftisolatoren", Wiss. Berichte THZ 1234, pp.34-38, 1990.

[39] E.Kuffel, W.S.Zaengl and J.Kuffel. *High Voltage Engineering Fundamentals*, Butterwoth Press, 2000 (second edition).

[40] Anibal de la O L. and Jorge Glez. De la Vega, "Performance of AC Insulators under Low Pressure Fog Chamber Tests", Proceedings of 7th International Symposium on High Voltage Engineering, Dresden, German, Paper No. 44.19, Aug. 1991.

[41] Drapeau, J.F., and Farzaneh, M., "Ice Accumulation Characteristics on Hydro-Quebec HV Insulators", Proceedings of 6th International Workshop on Atmospheric Icing of Structures, Budapest, Hungary, pp.225-230, Sept. 1993.

[42] Bueckert, D., "Ice Storm Damage Tallied", Report of Canada News on Ice Storm '98, Dec. 15, 1998.

[43] Volât C, "Calcul de la Distribution du Potentiel du Champ électrique le Long des Surfaces de Glace Recouvrant les Isolateurs Haute-tension et dans les Intervalles d'air entre celles-ci," Thesis of Ph.D. in Engineering, UQAC, 2002.

[44] Brettschneider, Farzaneh, S., M., Srivastava, K.D., and Volat, C., "Electrical Discharge Initiation at the Tip of an Icicle-an Experimental Approach", ISH-14, Beijing, China, August 25-29, D-20, 2005.

[45] Bandel, H.W., "Corona from Ice Points," Journal of Applied Physics, Vol.22, pp.984-985, 1951.

[46] Feser, K., and Pigini, A., "Influence of Atmospheric Conditions on the Dielectric Strength of External Insulation," Electra, Vol.112, pp.83-95, 1987.

[47] Farzaneh M., LaForte J.L., "Effect of Voltage Polarity on Icicles Grown on Line Insulators", International Journal of Offshore and Polar Engineering, Vol.2, No.4, pp.298-302, Dec. 1992.

[48] Sugawara N. and Hokari K., "DC Discharge Performance at the Tip of an Icicle", Conference on Electrical Insulation and Dielectric Phenomena, Leesburg, USA, pp.137-142, 1989.

[49] Jordan, I.B., Huu, T. Le, and Saint-Arnaud, R., "Décharge Couronne sur des Pointes de Glace à la Surface de Conducteurs", IEEE Conference Canadienne sur les Communications et l'Energie, Montreal, Publ.No.78 CH1373-0, pp.184-187, Nov.1987.

[50] Teisseyre, Y. and Farzaneh, M., "On the Mechanisms of the Ice Accretion on H.V. Conductors", Cold Regions Science and Technology, 18, pp.1-8, 1990.

[51] Farzaneh, M. and Teisseyre, Y., "Effects of the Temperature and Voltage Polarity on the Ionic Wind Velocity", Proceedings of 7th International Symposium on HV Engineering (ISH), Dresden, Germany, Vol. 4, Article 41.08, pp.39-42, August 1991.

[52] Meier, A., Niggli, W.M., "The Influence of Snow and Ice Deposit on Super tension Transmission Line Insulator Strings with Special Reference to High Altitude Operation," IEEE Conference Publ.44, London, England, pp.386-395, September 1968.

[53] Volat, C., Farzaneh, M. and Gakwaya, A., "Dynamic Variations of Potential and Electric Field Distributions Around an Ice-covered Insulator during ice accretion", Comptes rendus de la 10th International Workshop on Atmospheric Icing of Structures, IWAIS Brno, Czech Republic, juin 2002, 6-8, pp. 85-90, 2002.

[54] Farzaneh, M., Volat, C, and Zhang, J., "Role of Air Gaps on AC Withstand Voltage of an Ice-covered Insulator String", IEEE Transactions on Dielectrics and Electrical Insulation, vol.13, No.6, pp. 1350-1357, December 2006.

[55] Chen, X., Farzaneh, M. and Zhang, J., "Factors Influencing Flashover Characteristics along Ice Surface". 7th international workshop on atmospheric Icing of structures, pp.77-81, 1996.

[56] Swift, D.A., "Water-triggered Breakdown of an Atmospheric Air-gap", 4th Int. Symp. On High Voltage Engineering, Athens, Greece, paper 44.07, Sept. 1983.

[57] Avakoli Zaniani, C. T., "Dynamic Modeling of AC Arc Development on Ice Surfaces", Ph.D thesis in UQAC, 2004.

[58] Fujimura, T., Naito, K., Hasegawa, Y. and Kawaguchi, T., "Performance of Insulators Covered with Snow or Ice", IEEE Transactions on Power Apparatus & Systems, Vol. Pas-98, No. 5 pp. 1621-1631, Sept., 1979.

[59] Matsuda, H., Komuro, H. and Takasu, K., "Withstand Voltage Characteristics of Insulator String Covered with Snow and Ice", IEEE Transactions on Power Delivery, Vol. 6, No. 3, pp. 1243-1250, July 1991.

[60] Kannus, K., Verkonnen, K. and Lakervi, E. "Effect of Ice Coating on the Dielectric Strength of High Voltage Insulators", 4th IWASI, Sept., Paris, pp.296-300, 1988.

[61] Li, Y., "Study of the Influence of Altitude on the Characteristics of the Electrical Arc on Polluted Ice Surface", Doctoral thesis of Université du Québec, 2002.

[62] Farzaneh, M. and Kiernicki, J., "Flashover Problems Caused by Ice Build-up on Insulators", IEEE Transactions on Electrical Insulation, Vol. EI-11, No. 2, pp. 5-17, March/April 1995.

[63] Farzaneh, M. and Zhang, J., "Behavior of DC Arc Discharge on Ice Surfaces", Proceedings of 7th International Workshop on the Atmospheric Icing of Structures, Iceland, pp. 193-197, 1998.

[64] Phan-cong,J.L., Pirotte, P., Brunelle, R., Trinh, N.G., "A Study of Corona Discharge at Water Drops over the Freezing Temperature Range," IEEE Trans. on Power apparatus and system, Vol.Pas-93, No.2,pp. 727–735, March/April 1974.

[65] Brettschneider, S., "Contribution to Study of Visible Discharge Initiation and Development on the Ice Surface," 2000 Ph.D thesis of UQAC.

[66] Trinh, N. G., "Partial Discharge in Air II: Selection of Line Conductors", IEEE, Elect.

Insul. Vol.11, pp. 5-11, May-June, 1995.

[67] Ward, B.H., "Digital Techniques for Partial Discharge Measurements--A Report on the Activities of the Working Group on Digital Analysis of Partial Discharges", IEEE Trans. Power Delivery, Vol. 7, pp. 469-479, 1992.

[68] Bartnikas, R. and Novak, J.P., "On the Character of Different Forms of Partial Discharge andTheir Related Terminologies", IEEE Trans. Elec. Insul., Vol. 28, pp. 956-968, 1993.

[69] Blalock, T.V., Wintenberg, A.L., and Pace, M.O., "Low Noise Wide-Band Amplification System for Acquiring Pre-breakdown Current Pulses in Liquid Dielectrics", IEEE Trans. Elec. Insul., Vol. 24, pp.641-647, 1989.

[70] Okamoto, T., and Tanaka, T., "Novel Partial Discharge Measurement Computer-aided measurement Systems," IEEE Trans. Elec. Insul. Vol. 21, pp. 1015-1016, 1986.

[71] Soucy, L. "Effect de la Fonte et de la Pollution sur la Tension de Tenue Maximale des Isolateurs Recouverts de Glace," Mèmoire de maîtrise, Universitè de Quebec à Chicoutimi, 1997.

[72] Kreuger, F.H., Gulski, E., and Krivda, A., "Classification of Partial Discharges", IEEE Trans. Elec. Insul., Vol. 28, pp. 917-931, 1993.

[73] Van Brunt, R.J. and Kulkarni, S.V., "Method for Measuring the Stochastic Properties of Corona and Partial-Discharge Pulses", Rev. Sci. Instrum., Vol. 60, pp. 3012-3023, 1989.

[74] Kopf, V. and Feser, K., "Possibilities to Improve the Sensitivity of PD Measurements by Using Digital Filters", Proc. Int. Symp. On Digital Techniques in High-Voltage Measurements, Toronto, Canada, pp. 2-27-2-31, 1991.

[75] Meek, J. M., Craggs, S. D., *Electrical Breakdown of Gases*, Chap. 2, Oxford, at the Clarendon Press, 1978.

[76] Feser, K., and Pigini, A., "Influence of Atmospheric Conditions on the Dielectric Strength of External Insulation", Electra, Vol.112, pp.83-95, 1987.

[77] Giao, T.R. and Jordan, J.B., "Modes of Corona Discharges in Air", IEEE Trans.Pas-87, pp.1207, 1968.

[78] Akazaki,.M., "Corona Phenomena from Water Drops on Smooth Conductors Under High Direct Voltage", IEEE Trans., Pas-84, pp1, 1965.

[79] Vuku, Q. and Comsa, R.P., "Influence of Gap Length on Wire-plane Corona", IEEE Trans. Pas.88, pp.1462, 1969.

[80] Morris, R.M. and Rakoshdas, B., "An Investigation of Corona loss and Radio Interference from Transmission Line Conductors at High Direct Voltages", IEEE Trans., Pas-83, pp.5, 1964.

[81] Mason, J. W. and Young, B., "Some Physical Mechanisms Affecting the Distribution of Corona Pulse Intervals", Proc. 7th Int. Conf. on Gas Discharges and Their Applications", Peter Peregrinus, London, pp. 196-199, 1982.

[82] Malik, N. H. and Alrainy, A. A., "Statistical Variation of DC Corona Pulse Amplitudes in Point-to-Plane Gaps", IEEE Trans. Elec. Insul., Vol. 22, pp.825-829, 1987.

[83] Takahashi, T., Yamada, T., Hayakawa, N. and Okubo, H., "Space Charge Behavior in SF_6 Gas and Sequential Generation of PD Pulses", IEEE Transactions on Dielectrics and Electrical Insulation Vol. 7 No. 1, pp.151-155, February 2000.

[84] Al-Arainy,,A. A. Malik, N. H., and Al-Bahoul, M. K., "Statistical Variation of AC Corona Pulse Amplitudes in Point-to-plane Air Gaps", IEEE Trans. Elec. Insul., Vol. 24, pp. 681-697, 1989.

[85] Florkowska, B. and Wlodek, R., "Pulse Height Analysis of Partial Discharges in Air", IEEE Transactions on Electrical Insulation Vol. 28 No. 6, pp.932-940, December 1993.

[86] Steiner, J. P., "Digital Measurement of Partial Discharge", Ph. D. Thesis, Purdue University, May 1988.

[87] Van Brunt, R.J. and Kulkarni, S.V., "New Method for Measuring the Stochastic Properties of Corona on Partial-Discharge Pulses", Conference Record 1988 Int. Symp. on Elec. Insul., IEEE publication CH2594-0/88, pp. 233-237, 1988.

[88] Mason, J. W. and Young, B., "Some Physical Mechanisms Affecting the Distribution of Corona Pulse Intervals", Proc. 7^{th} Int. Conf. on Gas Discharges and Their Applications", Peter Peregrinus, London, pp. 196-199, 1982.

[89] Lama, W. L. and Gallo,C. F., "Systematic Study of the Electrical Characteristics of the Trichel Current Pulses from Negative Needle-to-Plane Coronas", J. Appl. Phys., Vol. 45, pp. 103-113, 1974.

[90] Stever, H. G., "The Discharge Mechanism of Fast GM Counters from the Dead time Experiment", Phys. Rev., Vol. 61, pp. 38-52, 1942.

[91] Kulkarni, S. V., Van Brunt, R. J., and Lak dawala, V. K., "Transition from Trichel-Pulse Corona to Dielectric Barrier Discharge", 1990 Annual Report Conference on Electrical Insulation and Dielectric Phenomena, IEEE public 90CH 2919-9, pp. 267-274, 1990.

[92] Van Brunt, R.J. and Cernyar, E.W., "Stochastic Analysis of AC-Generated Partial-Discharge Pulses from a Monte-Carlo Simulation", 1992 Annual Report-Conference on Electrical Insulation and Dielectric Phenomena, IEEE, NY, pp. 427-434, 1992.

[93] Tormm, U., "Interpretation of Partial Discharges at DC Voltages", IEEE Trans on Dielectrics and insulation, Vol.2 No.5, Oct. pp. 761-770, 1995.

[94] Dawson, G.A. and Winn, W.P.; "A Model for Streamer Propagation", Z.Physik, Vol.183, pp.159, 1973.

[95] Gallimberti, I., "A Computer Model for Streamer Propagation", J.Phys.D, Vol.5, pp.2179-2189, 1971.

[96] Phelps, C.T., "Field-Enhanced Propagation or Corona Streamer," Journal of Geophysical Research, 76, pp.5709-5806, 1971.

[97] Kaled, M., "New Method for Computing the Inception Voltage of a Positive Rod-Plane Gap in Atmospheric air," ETZ-A Bd.95.H.7, pp.369-373, 1974.

[98] Arima, I., and Watanabe, T., "Study of the Inception Voltage and Length of Positive Corona Streamer in Needle to Plane Electrode Geometry," Trans. IEE of Japan, No12, pp.575-582, Vol.1996, 1976.

[99] Hinterholzer, T. and Boeck, W., "Breakdown Behavior in SF_6 Influenced by Space Charge Stabilization", 8th ISH, Netherlands ISBN 90-77017-79-8, 1986.

[100] Loeb, L.B, "Electrical Coronas: *Their Basic Physical Mechanisms*, University of California press, pp.251-266, 1965.

[101] Farzaneh, M., Li,Y., Zhang, J., Shu, L., Jiang, X., Sima, W. and Sun, C., "Electrical Performance of Ice-covered Insulators at High Altitudes", IEEE Trans. Elect. Insul. Vol.11, No.5, pp.870-880, 2004.

[102] Farzaneh, M., Li, Y., Zhang, J., "Effects of Altitude on AC Flashover on Ice Surface," Proceedings of 10th International Symposium on HV Engineering (ISH), Montreal, pp.73-76, 1997.

[103] IEC Standard 60270 (3rd edition, 2000). "Partial Discharge Measurements", International Electro-technical Commission (IEC), Geneva, Switzerland.

[104] Schneider, H.M., "Artificial Ice Tests on Transmission Line Insulators – A Progress Report", IEEE PES Summer Meeting, San Francisco, USA, Paper A75-491-1, pp.347-353, July 1975.

[105] Nasser, E., *Fundamentals of Gaseous Ionization and Plasma Electronics*, Wiley-Interscience, New York, 1971.

[106] Fikke, S.M., Hanssen, J.E., Rolfseng, L., "Long Range Transported Pollutants and Conductivity of Atmospheric Ice on Insulators," IEEE Transactions on Power Delivery, Vol.PWRD-8, No.3, pp.1311-1321, July 1993.

[107] Chisholm, W.A., Tam, Y.T., Melo, T.O., Pavers, I.K., and Erven, C.C., "60-HZ Performance of 500-kV Insulators under Light Contamination, Ice, Fog and Rising

Temperatures: Operating Experience and Field Studies", IEEE Power Engineering Summer Meeting, pp.1-8, 1993.

[108]Kannus, K., Lahti, K., and Nousiainen, K., "Comparisons between Experiments and Calculations of the Electrical Behaviors of Ice-Covered High Voltage Insulators", Proceedings of the 8th International Workshop on Atmospheric Icing of Structures, Iceland, pp. 325-331, June 1998.

[109]Meier, A., and Niggli, W.M., "The Influence of Snow and Ice Deposit on Super tension Transmission Line Insulator Strings with Special Reference to High Altitude Operation", IEEE Conference Publ.44, London, England, pp.386-395, Sept. 1968.

[110]Isa, H., Sonoi, Y., and Hayashi, M., "Breakdown process of a rod to plane gap in atmospheric air under dc Voltage stress", IEEE Trans. Electrical insulation Vol.26 No.2,April pp.291-299, 1991

[111]Morrow, R. and Lowke, J.J., Streamer propagation in air, D. J Phys D: App. Phys, Vol.30, No. 4, pp. 614—620,1997,

[112]Gallagher, T.J., and Pearmain, A.J., *High Voltage Measurement Testing and Design*, John Wiley &Sons Ltd, New York, 1983.

[113]Teisseyre, Y., e t al., "Effect of Corona Discharge on Ice Accretion", 4th International workshop on Atmosphere Icing of Structure, Paris, 1988.

[114]Farzaneh, M. and Laforte, J.L., "Ice Accretion on Conductors Energized by AC or DC: a Laboratory Investigation of Ice Tree", Int.J.Offshore polar Engineering 4, pp.40-47, 1994.

[115] Golinski, J. and Grudzinski, J., "Some properties of Trichel pulses with AC voltage", J.Phys.D:App.Phys.19, pp.1497-1505, 1986.

[116] Allen, N.L. and Hashem, A.A.R., "The Role of Negative Ions in the propagation of Discharge across Insulating Surface", App. Phys. D: App. Phys. 35, pp.2551-2557, 1973.

[117] Zhong, Z. et al. "Pulse Shape Characteristics Analysis of Partial Discharge Signals", high voltage engineering of China, vol.4, Dec. pp.15-18, 1999.

[118] Rea, M. and Fujii, T., "Pulse Corona Characteristics", IEEE Transactions on Industry Applications, Volume 29, Issue 1, pp.98 – 102, Jan.-Feb. 1993.

[119] Cernak, M., Kaneda, T., and Hosokawa, T., "First Negative Corona Pulses in 70% N_2+30% SF_6 Mixture", Japanese Journal of App. Phys., Vol. 28, pp.1989-1996, 1989.

[120] Scott, D. A. and Haddad, G. N., "Negative Corona in Nitrogen Oxygen Mixtures", J. Phys. D: App. Phys., Vol. 20, pp. 1039-1044, 1987.

[121] Kinsey, E. L. and Sponsler, O. L., "the Molecular Structure of Ice and Liquid Water", Chem. Rev. 546.212: 548.7, PP768-779 F.R.S., July 25, 1933.

[122] Mason, J.W. and Young, B., "Some Physical Mechanism Affecting the Distribution of Corona Pulse Intervals", Proc. 7th International Conference on Gas Discharges and Their Applications, Peter Peregrinus, London,pp.196-199,1982.

[123] Steiner, J.P., "Digital Measurement of Partial Discharge", Ph.D Thesis, Purdue University, May 1988.

[124] Van Brunt, R. J. and Kulkarni, S. V., "Stochastic Properties of Trichel-Pulse Corona: A non Markovian Random Point Process", Phys. Rev. A, Vol. 42, pp. 4908-4932, 1990.

[125] Sugimoto, T., Asano, K. and Higashiyama, Y., "Negative Corona Discharge at a Tip of Water Cone Deformed under DC Field", Journal of electrostatics, Vol.53 pp. 25-38, 2001.

[126] Wang, Y., "New Method for Measuring Statistical Distributions of Partial Discharge Pulses", Journal of Research of the National Institution of Standards and Technology, Vol 102, pp.5-14, Sep-Oct., 1997.

[127] Van Brunt, R.J., "Physics and Chemistry of Partial Discharge and Corona", IEEE Trans. on Dielectric and electric, Vol.1 No.5, pp.761-784, Oct.1991.

[128] Morrow, R., "Theory of Negative Corona in Oxygen", Phys. Rev. A 32, 1799–1809, 1985.

[129] Pinnangudi, B.N., Gorur, R.S., Kroese, A.J., "Energy Quantification of Corona Discharges on Polymer Insulators", IEEE-Conference on electrical insulation and dielectric phenomena, pp.315-318, 2002.

[130] M.Goldman and A.Goldman, "Corona Discharge in Gaseous Electronics", M.Nhirsh abd H.J.Oskam.Eds., Academic press, New York, pp.219-290, 1978.

[131] Champlion,R.L. and Doverspike,L.D. "Electron Detachment Processes, in Electron-Molecule Interactions and Their Applications", L.G.Chirstphorou,ed., Academic Press,Orland, pp.619-681,1984.

[132] Reess T., Paillol J., "The Role of the Field-effect Emission in Trichel Pulse Development in Air at Atmospheric Pressure", J. Phys. D, Vol.30, pp. 3115-22, 1997.

[133] Fabiani, D., Montanari, G.C., Cavallini, A. and Mazzanti, G., "Relation between Space Charge Accumulation and Partial Discharge Activity in Enameled Wires under

PWM-like Voltage Waveforms", IEEE Trans on Diele. Electr.Insul., Vol.3,pp.778-783,1996.

[134]Özisik, M.N., *Heat Conduction*, 2nd ed. New York: Wiley, 1993.

[135]E.W.McDaniel and E.A.Mason, *The Mobility and Diffusion of Ions in Gases*, John wiley & Sons, New York, 1973.

[136]Wang,H.. "Model Research to the Effect of Space Charge on Discharge Processes in Air", North China Electric power University, Ph.D thesis, 1994.

[137]Dale,S.J., "Primary Corona Characteristics and the Dark Period in Long Rod Gap Distance Discharges in Air", 3rd ISH, 53.10, 1979.

[138]Abdel-Salam, M., and Allen, N.L., "Inception of Corona and Rate of Rise of Voltage in Diverging Electric Field", IEE Proc., Vol.137, Pt.A, No.4, pp.217-220, 1990.

[139]Peek, F.W., *Dielectric Phenomena in High Voltage Engineering*, McGraw-Hill, 1929.

[140]Les Renardières Group, Research on Long Air Gap Distance Discharges at Les Renardières, Electra 23, pp.53-157, 1972.

[141]Les Renardières Group, Long Air Gap Distance Discharge at Les Renardières: 1973 results, Electra 35, pp.47-156, 1974.

[142]Marode, E., "The Mechanism of Spark Breakdown in Air at Atmospheric Pressure between a Positive Point to Plane", J.Appl.Phys.46, pp.2005-2020, 1975.

[143]Dhali, S. K. and Pal, A. K., "Numerical Simulation of Streamers in SF_6", J. Appl. Phys. 65 pp. 1355–62, 1988.

[144]Peek, F.W., *Dielectric Phenomena in High Voltage Engineering*, McGraw-Hill,1929.

[145]Farzaneh, M., Yu, D., Zhang, J., Shu, L., Sima, W., and Sun, C., "Measurement of Corona Discharge in an Icicle/Iced-Plate Electrode System under Positive DC Voltage", ISH-14, Beijing, China, Aug 22-28, pp.D-05, 2005.

[146]Morrow, R., "Theory of Positive Onset Corona Pulses in SF_6", IEEE Trans on Electrical Insulation Vol.26 No.3, pp. 97-106, June 1991.

[147]Champion, R.L. and Doverspike, L.D., "Electron Detachment Processes, in Electron-Molecule Interactions and Their Applications", L. G. Christophorou, ed., Academic Press, Orlando, pp. 619–681, 1984.

[148]Morrow, R. and Owke, J.J., "Streamer Propagation in Air", J.Phys.D:Appl.Phys.30, pp.614-627, 1991.

[149]Bwatson,D. Kho, D.K., Samuels, K.A., Ma, L. and Chiu, J.B., "Impulse Flashover Trajectory in Air in Non-uniform Fields", IEEE Trans. Insu., Vol.28 No.2, pp 200-208, Apr. 1993.

[150]Hiromu Isa, Yasuo Sonoi and Muneaki Haysshi, "Breakdown Process of a Rod to Plane Gap in Atmospheric Air under DC Voltage Stress", IEEE Trans. Insul. Vol. 26, No. 2, April,pp. 291-299, 1991.

[151]Sugawara, N., Takayama, K., Hokari, K., Yoshida, K. and Ito, S., "Withstand Voltage and Flashover Performance of Iced Insulators Depending on the Density of Accreted", Proceedings of & International Workshop on the Atmospheric Icing of Structures, Budapest, Hungary, pp. 231-235, 1993.